NASA Contractor Report 195020

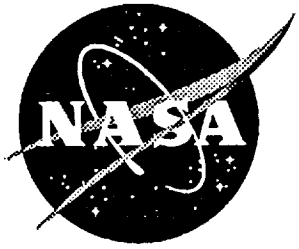

Experimental Verification of a Progressive Damage Model for Composite Laminates Based on Continuum Damage Mechanics

Timothy William Coats
Old Dominion University, Norfolk, Virginia

Contract NAS1-19858

December 1994

National Aeronautics and
Space Administration
Langley Research Center
Hampton, Virginia 23681-0001

EXPERIMENTAL VERIFICATION OF A PROGRESSIVE DAMAGE MODEL FOR COMPOSITE LAMINATES BASED ON CONTINUUM DAMAGE MECHANICS

Timothy William Coats
Old Dominion University

ABSTRACT

Progressive failure is a crucial concern when using laminated composites in structural design. Therefore the ability to model damage and predict the life of laminated composites is vital. The purpose of this research was to experimentally verify the application of the continuum damage model, a progressive failure theory utilizing continuum damage mechanics, to a toughened material system. Damage due to tension-tension fatigue was documented for the IM7/5260 composite laminates. Crack density and delamination surface area were used to calculate matrix cracking and delamination internal state variables, respectively, to predict stiffness loss. A damage dependent finite element code qualitatively predicted trends in transverse matrix cracking, axial splits, and local stress-strain distributions for notched quasi-isotropic laminates. The predictions were similar to the experimental data and it was concluded that the continuum damage model provided a good prediction of stiffness loss while qualitatively predicting damage growth in notched laminates.

INTRODUCTION

Background Information

Because of their light weight and high specific stiffness, laminated continuous fiber-reinforced composite materials are in high demand for use in primary load bearing components in aircraft structures. However, when subjected to high service loads, environmental attack, curing processes, impact, or a combination of any or all of the above, laminated composite materials develop microstructural damage. As service load or the time in service increases, microstructural damage develops into more severe damage and finally into catastrophic failure.

There are four main types of material damage. These are matrix cracking, fiber-matrix interface debonding, delamination, and fiber fracture. Usually, matrix cracking and fiber-matrix interface debonding are the first forms of damage to occur, followed by delamination, and finally fiber fracture resulting in catastrophic failure. While matrix cracking is usually arrested at the fibers or adjacent plies, microstructural damage will result in a redistribution of load to the surrounding regions. As a result, these surrounding regions contain stress fields which are favorable to initiation and propagation of additional damage. During the accumulation of subcritical damage, degradation of material stiffness and strength results from the load redistribution and decrease in load paths until the load paths are unable to support the load, in which case, catastrophic failure occurs.

The initiation and propagation of microstructural damage is one of the problems facing the designer of laminated continuous fiber composite structures. There is a need to model the damage and predict the residual strength and life of composite structures to address durability and damage tolerance requirements. For example, one of the most intriguing and complicated structural configurations is that of laminated composite structures connected by mechanical fasteners such as rivets. These laminates with fastener holes develop stress concentrations that cannot be easily treated using stress concentration factors as is the case with homogeneous metals. As another example, the non-visible damage that develops during foreign object impacts and ground handling accidents must be accounted for in the design. Current methods for treating these local structural details are empirical and very conservative. Therefore, an accurate model of the damage initiation and propagation is necessary to predict the failure of composite structures.

Literature Survey

The occurrence of damage and how it affects the strength and life of laminated composites has been the subject of much research for the past two decades. Many models have been proposed and developed for modelling damage growth and predicting reductions

in strength and stiffness in composite laminates. There are two main topics of this literature survey. The first topic covers general theories and research on the propagation of matrix cracks and delaminations. The models discussed under this topic are studies of the occurrence and effects of damage and include fracture mechanics related studies and mathematical models for predicting damage initiation and growth. The second topic covers various internal state variable approaches. This approach represents the distributed damage as volume averaged quantities. The treatment of a damaged volume of material as a continuous medium and the representation of the damage with averaged quantities was first proposed by Kachanov in 1958 [1] and is referred to as Continuum Damage Mechanics. Fracture mechanics differs from damage mechanics in that fracture mechanics treats a crack as a boundary of the body of interest, whereas damage mechanics includes the effects of cracks in constitutive equations rather than in boundary conditions.

Much research has been done experimentally and analytically to characterize damage in laminated composites. Masters and Reifsnider [2] conducted an investigation of cumulative damage in quasi-isotropic laminates. Highsmith and Reifsnider [3] studied reductions in stiffness due to matrix cracking and interply delaminations., and Garg [4] discussed the state of the art of delamination behavior. A few of the aspects considered in Garg's paper are: causes of delamination and its effect on structural performance, analytical and experimental techniques to predict its behavior, and preventive measures to delay delamination so as to make a structure more damage tolerant. The shear lag model, utilized by Highsmith to predict stiffness reductions in various composite laminates, assumes that the far-field stresses transfer to the cracked layer from the adjacent layers via shear deformation of a thin boundary layer at the layer interface. This particular model is relatively easy to use and provides results that agree with the experimental data. Because some laminates delaminate only in cyclic loading, extensive research has been done to characterize delaminations due to fatigue. Tsai, et al. [5] have investigated the effects of fatigue loading on the life and resulting damage in composite laminates. O'Brien [6] has developed a strain based initiation criterion and strain energy release rate equations for delaminations. Research such as these have provided the tools and insight needed to develop models and damage growth laws to model damage growth and predict reductions in stiffness and strength of laminated composites. In the strain energy method, the displacement fields in a unit cell representing a body with aligned cracks is expanded in Legendre polynomials. Utilizing this model, Aboudi [7] calculated the degraded stiffness tensor from the elastic energy stored in the cracked body. Aboudi's model requires higher order Legendre polynomials to improve accuracy, but overall, the model gives reasonable predictions. Hashin's model [8] is based upon the principle of minimum complimentary

energy. Hashin uses this method to calculate ply level stresses and the reductions in stiffness. Even though his solutions are very accurate when analyzing $[0_a/90_b]_s$ laminates, difficulties arise when the model is applied to multi-layered laminates of the type $[0_a/90_b/0_c/90_d]_s$. A stochastic model for the growth of matrix cracks in composite laminates has been developed by Wang, Chou, and Lei [9]. This model replaces the conventional ply strength criterion with an effective flaws concept. It is also based on the concepts of classical fracture mechanics. The effective flaw concept is a conceptual property of the material ply which enables a gross representation of the actual effects of inherent material flaws. This particular model provides a reasonably reliable method for modelling the static and fatigue growth processes of 90 degree ply transverse cracks in cross-ply laminates loaded in tension. Tan and Nuismer [10] model progressive matrix cracking of composite laminates that contain a cracked 90 degree ply and subjected to uniaxial tensile or shear loading. This theory includes two parts, i.e. an approximate stress analysis using elasticity theory and a failure criterion based on the energy balance consideration. Awerbuch, et al. [11], applied an acoustic emission technique to detect and locate damage initiation, monitor its progression and accumulation, and to identify the major modes of damage associated with the failure process in cross-ply graphite epoxy laminates. Residual degradation models for composites were developed by Yang [12] and Rotem [13]. Yang has developed a fatigue residual strength degradation model to account for the effect of tension-compression fatigue loading. Furthermore, this model can be used to predict the effect of high loads, such as proof loads, on the fatigue behavior of composites as evidenced by a limited amount of test data [14]. Rotem's theory for residual strength is based on cumulative damage theory and it predicts that the static strength of the laminate is maintained almost to the final failure by fatigue.

Other damage theories consist of models using internal state variables. Weitsman [15] proposed a mathematical formulation for the modelling of damage in fiber-reinforced composite materials due to moisture and temperature. Damage was observed to occur as profuse micro-cracking at the fiber/matrix interfaces and as matrix cracking traversing the entire plies. In his work, the moisture-absorbing composite material is treated as a thermodynamically open system and the distributed, micro-mechanical damage is represented as an internal state variable. In addition, general forms of damage growth laws are derived for isotropic and transversely isotropic composites. Talreja [16,17,18] characterized cracks in composite laminates by a set of vectors, each representing an individual cracking mode. The vector components are taken as internal state variables in the elastic strain energy function and the elastic constitutive equations are derived for the in-plane loading condition. For low concentration of cracks in laminates, the residual

stiffness properties are related to the initial elastic constants and the magnitude of the damage vectors. These equations are then used to predict stiffness reductions of composite laminates from the observed crack densities. Other theories utilizing the concept of damage as an internal state variable were developed by Miner [19], Hashin and Rotem [20], Coleman and Gurun [21], Bodner [22], and Krajcinovic [23].

In summary, many methods are currently being studied to model damage and predict life. There are some methods that consider each crack as an internal boundary and the stress or displacement fields are obtained either in closed form or numerically, such as in finite elements. This approach works well as long as there are a relatively small number of flaws. However, as crack density (number of cracks per ply per inch) increases, these methods become quite cumbersome because the finite element solution may require such a high number of elements that it becomes computationally impossible. Other methods, such as phenomenological approaches, have also been used in the analysis of damage evolution in laminated composites. The problem with these approaches is that they are so dependent on stacking sequence, loading history, and component geometry, that such a large amount of experimental data would be needed to be useful. Therefore, these approaches are not very practical either. An alternative to these approaches is the continuum damage model. This model is also phenomenological, however, it is formulated at the ply and sublaminate level and is therefore independent of stacking sequence or geometry.

Once again, it should be kept in mind that Kachanov developed the original concept in the 1950's to model the creep behavior of brittle metals. The continuum damage model has been extended to composites to model the behavior of a brittle epoxy material system to predict stiffness loss due to damage, shear modulus over a period of fatigue, and damage dependent stresses. The model utilized empirical formulations for the damage variables and a damage growth law for transverse matrix cracking [24,25]. Furthermore, a FORTRAN code consisting of constitutive laws, classical laminate theory (CLT), and a damage growth law for transverse matrix cracking was written to perform a fatigue analysis on composite laminates. The program is called FLAMSTR (Fatigue LAMinate STRess) [26]. It is capable of simulating tension-tension fatigue over a number of cycles while quantifying and updating the damage state via internal state variables.

Objectives and Approach

The goal of this research is to experimentally verify the application of the continuum damage model, developed by Allen, Harris, and Groves [27, 28], to a toughened material system, unlike the brittle epoxy material used to develop the model. To achieve this goal several objectives must be met in order to successfully use this model and provide valuable

information to the already existing progressive failure theories. The first objective is to document damage for the IM7/5260 material system. This will allow others to visually inspect the patterns of damage and will aide in verifying the experimental and analytical results of this thesis. The second objective is to document stiffness and strength as a function of fatigue damage. These results are very important because they will not only aide in evaluating the analytical results, but will also provide valuable information about the mechanics and properties of this particular material. The third objective is to determine the growth law parameters which will be used to predict stiffness loss for cross-ply and quasi-isotropic laminates. The fourth objective is to predict stiffness loss in quasi-isotropic laminates with centrally drilled holes and predict residual strength of the quasi-isotropic laminates with and without holes.

MODEL THEORY

Representation of Damage

In previous research [31, 32], internal damage is quantified by degradation of the material stiffness, whereas the continuum damage model measures matrix cracking by the volume averaged dyadic product of the crack face displacement, u_i, and the crack face normal, n_j, as defined by Vakulenko and Kachanov [1],

$$\alpha_{ij}^{M} = \frac{1}{V_L} \int_{S_c} u_i^c n_i^c dS \qquad (1)$$

where α_{ij}^{M} is the second order tensor internal state variable, V_L is the local representative volume, and S_c is the crack surface area. This product can be interpreted as additional strains incurred by the material as a result of the internal damage. Therefore the elemental matrices do not need to be updated as damage accumulates since the effects of the internal damage appears in the equilibrium equations as "damage induced forces". A more detailed description of the internal state variable and its applications can be found in the published literature [24-30, 33, 36].

The internal state variable demonstrates its usefulness in the micromechanics derived ply level (stacking sequence independent) constitutive equations as shown [24],

$$\{\sigma_L\} = [Q] \{\varepsilon_L - \alpha_L^{M}\} \qquad (2)$$

where $\{\sigma_L\}$ are the locally averaged components of stress, [Q] is the ply level transformed stiffness matrix, ε_L are the locally averaged components of strain, and $\overset{M}{\alpha_L}$ are the components of the internal state variable for matrix cracking. The effects of interlaminar delaminations cannot be homogenized at the ply level as can be done for matrix cracks. Detailed descriptions of damage dependent lamination equations can be found in the published literature [25, 26, 34].

The continuum damage model uses damage evolution equations [26, 30] to determine the internal state variables for the matrix cracks and empirical formulas where delaminations are concerned. The predominant type of damage for a uniaxially loaded composite laminate is the mode I opening intraply matrix crack. For this mode of damage only one component of the damage tensor, α_{22}, needs to be utilized for characterizing matrix damage in each ply [25, 26]. Whereas a damage evolutionary relationship has not been developed for delaminations, a damage growth law has been developed for mode I damage where the displacement of the crack face is in a direction parallel to the crack face normal, i.e. perpendicular to the plane formed by the ply. Equation (3) is the proposed [26, 30] damage growth law for uniaxial cyclic loading,

$$d\alpha_{22}^{M} = \frac{d\overset{M}{\alpha_{22}}}{dS}\ \kappa G^{\eta}\ dN \qquad (3)$$

where $\frac{d\overset{M}{\alpha_{22}}}{dS}$ describes the change in the internal state variable for a certain change in crack surface area, κ and η are material dependent parameters, N is the number of load cycles, and G is the damage dependent strain energy release rate for the ply of interest. This strain energy release rate is calculated from the following equation [25, 26],

$$G = V_L\ C_{ijkl}(\varepsilon_{L_{ij}} - \overset{M}{\alpha_{ij}})\frac{d\alpha_{kl}}{dS} \qquad (4)$$

Evolutionary relationships for other matrix cracking internal state variable components and for delamination damage are under development. In developing the continuum damage model up to this point, several assumptions were made and verified in previous research. The first of these assumptions standardizes transverse matrix cracking. It is assumed that a transverse matrix crack appears through the entire width of the laminate instantaneously

[25, 29, 30]. This implies that a crack seen on one edge of a laminate extends to the other edge and appears as an edge crack on the other side of the laminate. Therefore, the crack surface area of one crack could be expressed by [1, 24, 25, 27, 28]

$$s = (2 \text{ crack faces})(\text{ply thickness})(\text{laminate width}) \quad (5)$$

where s is the crack surface area. Without this assumption, a crack seen on the edge of a laminate gives no indication of the crack surface area. Another assumption previously made when developing this model with AS4/3502 was that the material is elastic [27, 28, 30]. Therefore it has no plastic deformation that would hinder or enhance damage growth.

For a uniaxially loaded quasi-isotropic laminate, mode II damage due to shear is considered. The following relationship [25] provides an empirical formula with which to calculate the internal state variable due to shear, α^{M}_{12}

$$\frac{\partial \alpha^{M}_{12}}{\partial \varepsilon_{12}} = 2\left\{1 - \frac{(G_{12})_{exp}}{G_{12o}}\right\}\frac{S_m}{S_{exp}} \quad (6)$$

where $(G_{12})_{exp}$ and S_{exp} refer to the experimental shear modulus and crack density respectively. G_{12o} is the undamaged shear modulus and S_m is the crack density for any given cycle.

In addition, mode I damage due to delamination is also considered for uniaxially loaded quasi-isotropic laminates. The following relationship [25] provides an empirical formula with which to calculate the internal state variable due to delamination

$$\frac{\partial \alpha^{D}_{3}}{\partial \varepsilon_{x}} = -\frac{n}{2}\frac{(E_{xo}-E^{*})}{Q_{15}}\left(\frac{S_D}{S}\right) \quad (7)$$

where E_{xo} is the undamaged experimental stiffness and E^{*} is the moduli of the sublaminates formed by delamination. Furthermore, n is the total number of plies, S_D is the delamination surface area, and S is the total surface area. Q_{15} is defined in the following equation

$$Q15 = \frac{Q_{11}^{T} + Q_{11}^{B}}{2} \qquad (8)$$

where Q_{11}^{T} and Q_{11}^{B} are the stiffnesses of the two sublaminates formed by regions of delamination.

Progressive Failure Scheme

A progressive failure scheme of the continuum damage model is used here to illustrate the application of the internal state variable and list the experimentally obtained inputs needed for the constitutive code. The progressive failure scheme can be thought of as an explanation of how the continuum damage model predicts the following:

1. Matrix crack accumulation in 90 and 45 degree plies of quasi-isotropic laminates.
   (a) Constitutive code for unnotched laminates using classical laminate theory
   (b) Plate code for notched laminates using finite element methods
2. Ex, Ey, Gxy, and n_{xy} as functions of matrix crack damage for unnotched laminates using classical laminate theory.
3. First fiber failure in unnotched and notched quasi-isotropic and cross-ply laminates using classical laminate theory and finite element methods.

The progressive failure scheme is illustrated in Figure 1. The first block briefly describes the information needed as model input. It illustrates that we need to know the loading condition, structural configuration, and the current damage state from impact, curing, environmental induced damage, etc. This damage state is represented by material parameters κ and η of the matrix damage growth law, the change in the i.s.v. with respect to crack surface area, and the change in the i.s.v. with respect to number of cycles. Table 1 lists the input parameters in detail. These are obtained from experimentation and i.s.v. calculations, all of which will be explained in detail within the Model Parameter Calculation section of Analytical Results.

Blocks 2 and 3 in Figure 1 are known as the first constitutive module. This constitutive module performs a damage dependent laminate analysis utilizing equation (2) to produce effective lamina and laminate properties.

Block 4 is a finite element analysis code which utilizes the damage dependent lamina and laminate properties as input for the elemental stiffness matrix for the modified equilibrium equations [34].

$$\begin{bmatrix} K^{11} & K^{12} & 0 \\ K^{21} & K^{22} & 0 \\ 0 & 0 & K^{33} \end{bmatrix} \begin{Bmatrix} u \\ v \\ \delta \end{Bmatrix} = \begin{Bmatrix} F^1 \\ F^2 \\ F^3 \end{Bmatrix}_A + \begin{Bmatrix} F^1 \\ F^2 \\ F^3 \end{Bmatrix}_M + \begin{Bmatrix} F^1 \\ F^2 \\ F^3 \end{Bmatrix}_D \qquad (9)$$

where [K] = element stiffness matrix (input), $\{F\}_A$ = applied force vector (input), $\{F\}_M$ and $\{F\}_D$ = "damage induced" force vectors resulting from matrix cracks and delaminations respectively.

The global structural analysis uses 3 node triangular elements with 5 degrees of freedom at each node; two in-plane displacements (u), one out-of-plane displacement (v), and two out-of-plane rotations (δ). The "damage induced" force vectors provide the continuum damage model with an advantage over other models. As mentioned under Representation of Damage, previous models quantify internal damage by stiffness degradation, thus having to recalculate the stiffness matrix in the finite element code at every change in damage state. However, using the internal state variable as a description of the damage state, the continuum damage model allows the internal damage to appear in the modified equilibrium equations as "damage induced forces". Therefore the elemental stiffness matrix does not have to be recalculated each time damage changes.

Now that the elemental displacements, curvatures, and stresses have been obtained from the first constitutive module and the finite element code, they become input into the second constitutive module, a local material level analysis (ply level elemental stress analysis), which reflects the current damage state. The local strain energy release rate is also computed and is used in block 6, damage evolution calculations, to determine new damage growth. This damage growth is evaluated in block 7 and a failure criterion then determines if the laminate has failed. An excellent guide in using the continuum damage model has been published as a NASA Technical Memorandum [26]. It provides information on the model's development, inputs needed for the model, experimentally determining the internal state variables, and provides sample input and output files for the constitutive code.

EXPERIMENTAL PROCEDURE

Specimen Preparation and Properties

The material system used in this research to verify the life predicting capabilities of the continuum damage model is IM7/5260. The laminates were manufactured, post cured, and machined into ten inch long specimens at NASA Langley Research Center. Table 2 shows the sizes and layups of the specimens and the data to be obtained from each specimen.

The laminate plates were machined into individual specimens and the edges were polished so that edge replicas could be obtained to document matrix crack formation. X-ray radiography and specimen sectioning were also used to determine whether or not cracks extended fully across the specimen width.

Before testing, a classical laminate theory (CLT) code and the Tsai-Wu failure criterion were used to predict engineering properties and failure loads of the IM7/5260 specimens. First ply failure is the load at which the first matrix cracks appear. If we know this load, we can fatigue the specimens at a certain percentage of first ply failure load so that the fatigue tests will run for a moderate number of cycles and generate a representative distribution of matrix cracks over a wide range of fatigue cycles.

Other than non-uniform matrix cracking under static loading, the modulus and failure loads were close to the values predicted by the CLT. The ply level properties used in the CLT code are shown in Table 3 [35]. In Table 4, the components of the stacking sequence independent, ply level transformed stiffness matrix, [Q] from Equation 2, were calculated by applying the ply level properties from Table 3 to the transformed (or reduced) stiffness equations [36]. Tables 5, 6, 7, and 8 are comparisons of CLT predicted values with experimental values for the IM7/5260 specimens.

Testing Equipment And Procedure

The machine used to test the first half of the specimens was an MTS machine with an MTS 436 control unit, an MTS 430 digital indicator, and an MTS 410 Digital Function Generator. The data acquisition unit used was a Nicolet 4094A Digital Oscilloscope with a XF-44 Double Disk Recorder. A bridge amplifier and meter was used to amplify the signal from the Interlaken clip gauge extensometer to the Nicolet. The second half of the specimens were tested using an Instron 8502 machine with an Instron 8500 controller. Furthermore, most of the useful strain data was obtained using the Instron's linear voltage displacement transducer (LVDT).

Initially, a frequency of 1 Hz, a maximum load of 75% first fiber failure, and an R value of 0.1 were chosen for the tension-tension fatigue test. After testing a few practice specimens, it was decided that a frequency of 5 Hz was a better frequency for the tension-

tension fatigue tests. This was decided because any frequency below 5 Hz would require too much time for one test, and frequencies above 5 Hz sometimes developed overshoot and undershoot inaccuracies for the test machine actuator. Furthermore, specimens with 45 degree plies would increase in temperature at frequencies over 5 Hz; this might affect the material properties. Additionally, a maximum load of approximately 30% catastrophic failure (80% of first ply failure) was decided for the $[0/90/0]_s$, $[0/90_2/0]_s$, and $[45/-45]_{2s}$ specimens because any load over that caused crack saturation too early in the fatigue life to obtain a decent development in crack density as a function of fatigue cycles. Other layups were fatigued at approximately 60% catastrophic failure to obtain more extensive damage.

The next step was to conduct the fatigue testing. In general the procedure is to subject the specimen to tension-tension fatigue loading, periodically stopping to take edge replicas and x-rays, and measure stiffness. For the cross-ply laminates special attention is given to accurately obtaining crack density (or crack surface area) since the model parameters are calculated primarily from crack density of the cross-ply laminates. Furthermore, accurate stiffness measurements are needed to evaluate the stiffness loss predictions of the cross-ply laminates. For the $[45/-45]_{2s}$ specimens the main objective here is to calculate shear modulus as a function of damage. Therefore, measuring longitudinal and transverse stiffness as damage increases is high in priority. As for the quasi-isotropic laminates with and without centrally drilled 6.35 mm diameter holes, special attention was given to measuring stiffness loss as well as failure strength at a designated cycle number. This is for the purpose of comparing experimental stiffness loss and residual strength to the model predictions.

Data Acquisition

Most of the stiffness measurements utilized the Interlaken extensometer and bridge amplifier for signal amplification. Once the initial longitudinal modulus known as E_0 was established, the specimen was subject to tension-tension fatigue for about 100 to 1,000 cycles. At this point, several more stiffness measurements were made and averaged as before. This procedure continued until approximately 100,000 cycles where crack density was approximately saturated.

This procedure worked well for most all of the laminates, except the $[0/90/0]_s$ laminates. The stiffness measurements for these laminates showed random fluctuations between decreases and increases in stiffness. One reason for this is that the $[0/90/0]_s$ specimen is two plies thinner than the other laminates. With each ply being only 0.1524 mm thick, it is possible the extensometer, extensometer tabs, and the epoxy used to fasten the tabs to the specimen added additional stiffness to the specimen. Another possibility is

that the extensometer used may not be accurate enough to detect very slight changes in stiffness, and the data that was actually being recorded as fluctuations in stiffness may actually have been within the scatterband of the extensometer. This is not to say that the extensometer is not accurate, but that it is only accurate within its 2.54 cm gauge length. Since the $[0/90/0]_S$ laminates have only two ninety degree plies for every four zero degree plies, and all of the damage happening in the ninety degree plies, these laminates will see a very slight reduction in stiffness anyway. Furthermore, with a gauge length of only 2.54 cm, this is significant because if very little damage occurred in this one inch gauge length, it would be impossible to detect any reductions in stiffness. This was later confirmed in x-rays of specimens used for stiffness measurements. The x-rays showed very little damage within the gauge length and some specimens seemed to have not damaged at all. With these explanations in mind, it seemed reasonable to decide to solve this problem by using the LVDT of the Instron 8502.

Using an LVDT would allow for a gauge length of more than 15.24 cm which is basically the distance from one hydraulic grip to another. Therefore, even if damage isn't evenly distributed along the length of the laminate, if there is damage, reductions in stiffness due to damage is detectable. Furthermore, using the LVDT was accurate to 0.0025 mm and the average displacement of the actuator during a test was approximately 0.7938 mm.

Fortunately, measuring residual strength posed no problems. The procedure was simply to fatigue the specimen to the cycle at which the value of strength is desired and load the laminate in monotonic tension until failure. The failure strength is then calculated by dividing the failure load by the gross cross-sectional area. Measuring crack density, thus measuring crack surface area, seems like a simple, straight-forward, problem-free task. Basically, the procedure here is to periodically take edge replicas at the same number of cycles that stiffness measurements were taken. After fatiguing a laminate for a certain number of cycles, the load was ramped to approximately 80% of its maximum load at which point the edge replica was taken. The cracks in the ninety degree plies showed up very well, and for each replica taken, crack density was calculated. The formulas for the ply level crack density and crack surface area are, respectively,

$$\rho = \#\ \text{of cracks/ply/inch length} \qquad (10)$$

$$s = \rho t w(2\ \text{crack faces}) \qquad (11)$$

where ρ is the crack density, t is the ply thickness, and w is the laminate width. However, the IM7/5260 laminates did not behave such that these simple formulas gave an accurate

computation of the crack surface area determined from cracks shown on the edge replica. It was later found that the cracks did not traverse through the entire width of the specimen as is the case with brittle epoxies. Therefore, another way of obtaining crack surface area had to be devised. Instead of counting cracks on the edge replicas, x-rays magnified at 48x were used to count each crack and note whether or not it traversed 100%, 75%, 50%, or 25% of the specimens entire width, i.e. the laminate width in Equation 11 is now replaced with a percentage of the laminate width. An x-ray radiograph of a cross-ply laminate is represented in Figure 2. Illustrated here is the method by which the percentage of cracks are added together to obtain a total number of cracks. This was a very tedious, but necessary procedure. For only after obtaining a more accurate account of damage could Equations 10 and 11 be used. This should be a warning to all who use this model, that before spending time and effort taking replicas and counting the cracks, x-rays should be used very regularly during a fatigue test to examine how damage initiates and progresses. This problem is discussed in detail in the following section.

EXPERIMENTAL RESULTS

Damage Quantification

Recalling from the previous section, extracting crack density from the cross-ply laminates using edge replicas posed a slight problem. It was noticed that the calculated crack surface areas were rather large and caused some analytical problems when trying to calculate the model parameters. After examining the Figures 3 thru 10, it was concluded that the matrix cracks propagate inward rather than immediately traverse the entire width of the specimen. This matrix crack propagation as the fatigue cycles increase is illustrated in Figures 3, 4, 5, and 9 (a) and (b). The ninety degree matrix cracks starting from the edge of the specimen and progressing inward are illustrated in Figures 3, 4, and 5. Further examination consisted of sectioning several laminates and counting the cracks via edge replicas. The sectioning location for $[0/90_2/0]_s$ laminates that were fatigued to 50,000 and 200,000 cycles are illustrated in Figures 4 and 5. Provided in Figure 6 is the crack count at each section of the laminate fatigued to 50,000 cycles and illustrates the fact that all the cracks do not continue through the width of the specimen. The laminate fatigued to 200,000 cycles in Figure 7 is an example of how the cracks eventually progress through the width and saturate the laminate. However, this particular chart still shows that not all of the cracks are through the entire width of the specimen. As we move from the edge 0.318 cm inward to section BB, the number of cracks decreases. At section CC, 0.584 cm inward from the edge, cracks from the other edge have progressed to this point. Finally, as we travel closer to the center, the cracks from the edges decrease. Provided in Figure 8 are

the crack counts from edge replicas of a $[0/90/0]_s$ laminate that was fatigued and sectioned at 200,000 cycles. It appears that the $[0/90/0]_s$ laminates reach crack saturation at a higher cycle than do the $[0/90_2/0]_s$ laminates. Furthermore, Figure 9 (a) and (b), x-ray radiographs of $[45/-45]_{2s}$ laminates, and Figure 10 again confirm that the cracks slowly propagate inward. Hence, the assumption that the cracks seen on the edge of the specimen via edge replicas are cracks which exist through the entire width of the specimen is not a valid assumption for this material system. Instead, the only way to determine crack density is to use the x-rays and measure crack surface area as discussed in the Data Acquisition section of the previous chapter. However, this is still only an approximation since an x-ray does not verify which ply each crack is in. That is, what may appear as one crack may really be two. Therefore, for the sake of consistency, some assumptions were made to help extract reasonable crack surface areas from the x-rays. For the $[0/90/0]_s$ laminates, it was assumed that for every entire crack or partial crack seen in the x-ray, there exist just that one entire or partial crack. However, as the ninety degree plies increase in number, this assumption becomes invalid, especially when there are consecutive ninety degree plies such as in the $[0/90_2/0]_s$ laminate. The assumption for this particular laminate is that for every entire or partial crack seen in the x-ray, there exist just two entire or partial cracks. It is now obvious how this material system can create a formidable task in obtaining crack density as the number of ninety degree plies in the laminates increase. Illustrated in Figure 11 is the significant difference in calculating crack density from edge replicas to the more accurate approximation of using the x-rays. This method worked well for the $[0/90/0]_s$ laminates, however the number of cracks in the $[0/90_2/0]_s$ laminates became virtually impossible to count after damage increased to a certain level. Cracks started merging and created a blur of damage. Illustrated in Figures 12 (a) and (b) are the transverse matrix cracks in ninety degree plies as seen from the edge. Aside from the matrix cracks progressing from the outer edge of the laminate towards the center, Figure 12 (a) illustrates the anomaly of a crack initiating near the outer edge of the ply and progressing inward.

Cases of non-uniform matrix cracking was seen predominantly in the $[45/-45]_{2s}$ laminates. X-ray radiographs, Figures 9 (a) and (b), of laminates cycled at 5 Hz and 3 Hz respectively, reveal areas of dense and sparse matrix cracking. At a maximum stress level of 119.8 MPa, the [45/-45]s laminates failed anywhere from 100,000 to 600,000 cycles. Specimens cycled at 3 Hz failed closer to 600,000 cycles while a frequency of 5 Hz would see a specimen fail closer to 200,000 cycles. If the damage along the edge of the laminate was extremely concentrated in a few places, the specimen failed early at the point of concentrated damage. Illustrated in Figures 13 (a) and (b) are photographs of the pattern of matrix cracking as seen on the edge of the $[45/-45]_{2s}$ laminates.

Quasi-isotropic laminates were fatigued at stress levels equal to about 60% of fiber failure. The purpose of this was to create delaminations as well as transverse matrix cracking in order to visualize and document the pattern of damage as well as predict stiffness reductions and residual strengths up to the point of delamination onset. The patterns of matrix cracking on the edge of quasi-isotropic laminates are illustrated in Figures 14 (a) and (b), and Figures 15 thru 19 illustrate patterns of delamination as well as matrix cracking. X-rays of damaged $[0/45/-45/90]_S$ specimens subjected to fatigue loading are shown in Figure 15. The two black splotches are just tabs and can be ignored. This figure shows how at 100 cycles the damage is predominantly matrix cracking with the damage initiating at the edge of the specimen and progressing toward the center. By 100,000 cycles, roughly 50% of the specimen is delaminated. At a stress level of 60% fiber failure, it is evident delaminations initiate very early in the test. Laminates of the same layup but with a centrally drilled hole are illustrated in Figure 16. There was axial splitting at the hole within the first 100 cycles during these tests. The damage pattern around the hole becomes recognizable at around 1,000 cycles with dense 90 degree matrix cracking in the vicinity of the hole. At or near 20,000 cycles, edge delamination initiates and matrix cracking only travels through the width of the specimen in the vicinity of the hole. Delamination and matrix cracking continues to progress normally up through 100,000 cycles where the edge delamination becomes more severe, the axial split initiates delamination at the hole, and the matrix cracks away from the hole are still not through the entire width of the specimen. However, at 300,000 cycles, the matrix cracks have progressed through the width of the laminate.

An x-ray of a laminate that has a transverse layup of the previously mentioned laminate is given in Figure 17. Again, the matrix cracking is more dense and progresses further into the width of the specimen at the vicinity of the hole. At 30,000 cycles, edge delamination sets in and the delamination pattern at the hole is axial as well as in the 45 degree direction. X-rays of 5.08 cm wide laminates with central notches and layups identical to the two previously mentioned laminates are given in Figures 18 and 19. As expected, the damage pattern is nearly identical to the previously discussed laminates.

Stiffness Loss

Stiffness measurements were actually more successful using the LVDT of the Instron rather than the extensometer since it provided a gauge length of the entire specimen from grip to grip. The normalized stiffness of the $[0/90/0]_S$ laminates is given in Figure 20. This plot reveals an average reduction in stiffness of approximately 0.5%. Revealed in Figure 21 is an approximate 6% stiffness loss in the $[0/90_2/0]_S$ specimens.

The $[45/-45]_{2s}$ specimens behaved a little more abnormal than the other layups. First of all, as was mentioned in the Damage Quantification section, matrix cracking did not saturate the entire length of the specimen. Instead, just one or two areas would saturate with matrix cracking and then fail catastrophically. Secondly, the stiffness and shear modulus increased until significant damage caused a sharp decrease in both stiffness and shear modulus prior to failure, Figure 22. For the laminates cycled at 5 Hz, significant damage started approximately at 10,000 to 40,000 cycles. A frequency of 3 Hz would slow the damage initiation so that 50,000 to 100,000 cycles was the point of significant damage. Furthermore, slight plastic deformation probably stretched the 45 degree plies such that the 45 degree ply orientation slowly shifted a few degrees toward the zero degree direction. This shifting of plies, along with damage initiation at about 20,000 cycles could be a possible explanation as to why the stiffness and shear modulus increased until 20,000 cycles.

The percentage drop in stiffness for the quasi-isotropics, with or without notches, were generally higher. This is not only due to their layup but also because the more severe loading conditions caused damage to increase more rapidly. Furthermore, at the onset of edge delamination, stiffness values really plunged. The laminates with centrally drilled 6.35 mm holes also experienced fairly steep reductions in stiffness, however, they were more gradual since the delamination at the hole allowed for a less severe reduction in stiffness at edge delamination onset. The stiffness loss for these specimens is illustrated in Figures 23 thru 28. Currently, the model does not have a growth law for delamination. There are empirical equations relating stiffness loss to delamination [12] as was shown in Equation 7. The actual use of such formulations will be discussed in detail in the "Analytical Results".

Residual Strength

The centrally notched quasi-isotropic laminates did not behave very differently compared to the quasi-isotropics without the center drilled hole when measuring strength. The damaged quasi-isotropic laminates appeared to increase in strength up to a certain number of fatigue cycles. It appears that a decrease in strength is initiated by extremely significant delamination, as seen in Figure 15. However, the unnotched laminates' increase in strength prior to strength reduction is unexpected. Appendix A contains the experimental values of the quasi-static strengths and the residual strengths.

The damaged centrally notched laminates fail at a higher stress than undamaged laminates for a reason slightly complicated, but logical. An undamaged centrally notched specimen experiences a high stress concentration around the hole. This stress

concentration decreases with increasing damage around the hole, but for an undamaged specimen being tested quasi-statically, delamination was virtually undetectable just prior to failure. As damage accumulates due to fatigue, and axial splitting and delamination occur around the hole, the stress concentration decreases until the stress distribution across the width of the specimen is characteristic of an unnotched laminate. The residual strengths are illustrated in Figures 29 thru 34.

ANALYTICAL RESULTS

Model Parameter Calculation

Before reviewing the model's computational predictions, an outline containing the procedures used to calculate the model inputs from the experimental data would help keep things in perspective. Figures 35 and 36 would be helpful in understanding this outline. First of all, the internal state variables due to transverse matrix cracking, α_{22}, had to be calculated for each crack density measurement. A FORTRAN program, ALPHAM22, was written using Equation 12 and 13, [25, 22, 26], shown below.

$$\alpha_{22} = \frac{\frac{-\rho}{2t}}{\frac{\pi^4}{64\,\xi} - C_{2222}} \qquad (12)$$

$$\xi = \sum_m \sum_n \frac{1}{C_{2222}(2m-1)^2(2n-1)^2 + C_{1212}\left(\frac{a}{t}\right)^2(2n-1)^4} \qquad (13)$$

where $\rho/2t$ is the far field stress in the 90 degree ply, $1/2a$ is the crack density, C_{2222} is the transverse modulus, and C_{1212} is the shear modulus. However, the far field stress in that equation decreases with increasing transverse matrix cracking, therefore it had to be recalculated for each internal state variable calculation. So what we have is an iterative process between ALPHAM22 and a static version of FLAMSTR called SLAMSTR, Static LAMinate STRess. The static laminate stress program and the α_{22} calculation program were later combined into an iterative program, SLAMALPHA22. This procedure is illustrated in Figure 35.

Secondly, effort was made to determine $d\alpha_{22}/ds$ by plotting α_{22} as a function of crack surface area, Figure 37. The equation of the best fit curve was found, Equation 14,

and its derivative provided the equation for $d\alpha_{22}/ds$ as a function of fatigue cycles, Equation 15,

$$\alpha_{22} = -1.57378\times10^{-6} + (0.0002909)(s) + (1.224915\times10^{-5})(s^2) \qquad (14)$$

$$\frac{d\alpha_{22}}{ds} = 0.0002909 + (2.449830\times10^{-5})(s) \qquad (15)$$

where s is the crack surface area. It was noticed that the fitted curve was very nearly linear, which would result in a constant $d\alpha_{22}/ds$ if a linear curve fit were used. As it turns out, using a constant $d\alpha_{22}/ds$ to find the parameters enhances the results. However, $d\alpha_{22}/ds$ obviously cannot be constant when used to find dpara, since dpara is the average slope of $d\alpha_{22}/ds$ vs the far field stress, SG2. This procedure is described as the third element of parameter calculation. The determination of dpara is illustrated in the plot of Figure 38.

The damage dependent strain energy release rate, G, could be calculated using Equation 16 since $d\alpha_{22}/ds$ and SG2 is known over the given number of cycles. The ply thickness, t, is actually the thickness of the consecutive ninety degree plies, i.e., t is equal to two times the thickness of one ply for a $[0/90_2/0]_s$ laminate, whereas t is equal to the thickness of one ply in a $[0/90/0]_s$ laminate.

$$G = (t)\left(\frac{d\alpha_{22}}{ds}\right)(SG2) \qquad (16)$$

The fourth step was to plot α_{22} as a function of the number of cycles, N, as illustrated in Figure 39. The derivative of the fitted curve, Equation 17, supplied Equation 18 for $d\alpha_{22}/dN$.

$$\alpha_{22} = -4.806625\times10^{-6} + (3.49422\times10^{-9})N - (4.77246\times10^{-15})N^2 \qquad (17)$$

$$\frac{d\alpha_{22}}{dN} = 3.49422\times10^{-9} - (9.54492\times10^{-15})N \qquad (18)$$

Finally, rearranging the damage growth law equation, Equation 3, to the form

$$\frac{d\alpha_{22}/dN}{d\alpha_{22}/ds} = \kappa G^{\eta} \qquad (19)$$

$\frac{d\alpha_{22}/dN}{d\alpha_{22}/ds}$ is plotted as a function of the damage dependent strain energy release rate, G. A power curve fit is assigned to the plot as shown in Figure 40. Thus we now have the parameters dpara, κ, and η. Referring to Appendix B may be helpful in the specifics of the analysis and may further summarize the entire process just described. At this point, all of the necessary parameters for the model are known. A list of all the data needed as model input is in Table 9 . This table is easily defined by Table 1.

Shear and Delamination Variables

To achieve an accurate prediction of stiffness and strength, mode II damage due to shear and mode I damage due to delamination needs to be taken into account. Equation 7 is used to calculate the delamination internal state variables. Classical laminate theory is used to determine the stiffnesses of the sublaminates in order to calculate E^* in Equation 7. From those results the transformed stiffnesses of the sublaminates, Q_{11}^T and Q_{11}^B, were determined. The percentages of delamination area to total surface area, $\frac{S_D}{S}$, are found from the x-ray radiographs of the laminates. Tables 10 and 11 reveal the results of the calculations involved for the unnotched quasi-isotropic laminates. It should be noted here that the $[90/-45/45/0]_s$ laminates had four sites of delamination at the 90/-45 and -45/45 interfaces on both sides of the midplane. Delamination existed only at the 90/-45 interfaces in the $[0/45/-45/90]_s$ laminates. Appendix C should be referred to for any specifics in internal state variable calculations.

The internal state variables due to shear are calculated from Equation 6. Since the relationship between G_{12D}/G_{12o} and the number of cracks per ply is linear, and $G_{12D}/G_{12o} = 0.9182$ for $S_D = 22.5$ cracks/ply, then the resulting equation is

$$\alpha_8^M = (0.0073\ S)\varepsilon_6 \qquad (20)$$

Supplied in Table 12 are the results of calculations used to determine the mode II internal state variables. For further details of the analysis, refer to Appendix D.

Predictions of Stiffness

The three ingredients to predicting reductions in stiffness are the model parameters, a knowledge of using the fatigue damage dependent laminate analysis program, FLAMSTR, and a method by which to incorporate delamination and shear variables into the predictions. Once the model parameters were found, using the model to predict stiffness due to transverse matrix cracking in the 90^o plies was done simply by inputting the parameters into the program FLAMSTR and calculating from the output the reductions in stiffness from the longitudinal midplane strains. This calculation is done by obtaining the initial longitudinal midplane strain from running SLAMSTR with no damage, and dividing it by the longitudinal midplane strain of each consecutive cycle from the output of FLAMSTR. The plots in Figures 41 and 42 show the experimental and analytical comparisons in stiffness for the $[0/90/0]_s$ and $[0/90_2/0]_s$ laminates. The analytical plot for the $[0/90/0]_s$ laminate fit the experimental plot quite well as expected. This is expected not only because of the results of previous research [5], but because the model parameters were calculated from the $[0/90/0]_s$ laminate. Therefore, the output is a direct result of the input.

The analytical plot for the $[0/90_2/0]_s$ laminate did not fit the experimental plot as well as the $[0/90/0]_s$ laminate. This could possibly be due to the following three explanations. First of all, the $[0/90_2/0]_s$ laminates could have experienced more plastic deformation than the $[0/90/0]_s$ laminates from where the prediction came. This plastic deformation would cause a further decrease in stiffness whereas the model does not compensate for plastic deformation. If the model were required to compensate for plastic deformation, the ply level constitutive equations, Equation 2 would have to be modified to the following equation,

$$\{\sigma_L\} = [Q]\ \{\varepsilon_L - \alpha^M_L - \alpha^M_{Def}\} \qquad (21)$$

where α^M_{Def} is the damage variable due to plastic deformation. Another reason for the divergence in Figure 42 could be that since the $[0/90/0]_s$ laminates were several plies thinner, thus suffering a higher degree of warpage, the parameters calculated from the $[0/90/0]_s$ laminates could be causing the predicted reductions in stiffness to be a little low. This could quite possibly happen if the warpage causes some non-uniform matrix cracking where one ply does not suffer as much damage as the other ply because there may be residual compressive stresses in that particular ply. This would decrease the calculated

crack surface area, thus decreasing the damage variable calculations, and as a result, the prediction in stiffness may seem slight. This could explain why the prediction fit the $[0/90/0]_s$ laminate well and only fairly well for the $[0/90_2/0]_s$ laminate. It's because the slight prediction originated from the more warped $[0/90/0]_s$ laminate and since the $[0/90_2/0]_s$ laminate was less warped, the damage could have been more uniform causing a higher reduction in stiffness. Finally, parameters were not calculated separately from the $[0/90_2/0]_s$ laminate data. These parameters could have been used to cross-check the parameters calculated from the $[0/90/0]_s$ laminates. If this had been done, there might have been a slight difference in the parameters, and averaging them could have brought the analytical and experimental plots of the $[0/90_2/0]_s$ laminates closer together. The reason this was not done was because as was mentioned in the Damage Quantification section, the damage shown in the x-rays became saturated to the point that it was impossible to detect one crack from another.

The parameters and FLAMSTR were used to predict stiffness reductions due to transverse matrix cracking in the 90^o plies for the unnotched quasi-isotropic laminates as well, Figures 43 and 44. However, the experimental stiffness decreased significantly due to the damage in the 45^o plies and at the onset of delamination. The model has empirical formulations for damage variables due to delamination and shear. However these delamination and shear internal state variables have not yet been incorporated into FLAMSTR. Therefore, the following equations, Equations 22 thru 25 were used to predict reductions in stiffness due to transverse matrix cracking, delamination, and shear.

$$\frac{E_x}{E_o} = 1 - \frac{\Delta E^M}{E_o} - \frac{\Delta E^D}{E_o} - \frac{\Delta E^S}{E_o} \qquad (22)$$

where $\frac{\Delta E^D}{E_o}$ is defined by the following equation for any number of delamination sites as [25]

$$\frac{\Delta E_x^D}{E_o} = \frac{1}{TE_o} \sum_{i=1}^{d} [Q_{15}]_i t_i \left\langle \frac{\partial \alpha_{3i}^D}{\partial e_{xx}} \right\rangle \qquad (23)$$

which can be reduced for two delamination sites by substituting Equation 7 into Equation 23 as

$$\frac{\Delta E^D}{E_o} = \frac{1}{2}\left(1 - \frac{E^*}{E_{xo}}\left(\frac{S_D}{S}\right)\right) \qquad (24).$$

Stiffness loss due to shear is defined as [25]

$$\frac{\Delta E_x^s}{E_o} = \frac{1}{n}\sum_{k=1}^{n} [Q_{11}]_k \left\{\frac{\partial \alpha_8}{\partial e_6}\right\} \qquad (25)$$

Illustrated in Figures 43 and 44 are the analytical reductions in stiffness compared to the experimental stiffness loss for the quasi-isotropic laminates. It should be pointed out that the x-rays and replicas that helped determine the delamination and shear damage variables are from laminates other than the laminates actually used to measure stiffness and shear modulus. Because the laminates have the same geometry, layup, and loading history, the damage recorded is indicative of the damage causing the reductions in stiffness in the laminates used only for measuring stiffness and shear modulus. The stiffness predictions are shown in Appendix E.

Strength Predictions

The use of internal state variables provides a tool to homogenize the damage and express it as an average of strain like quantities. Therefore, the result is a global strain distribution which will not reach the ultimate failure strain as would a local strain distribution. However, a qualitative analysis using only mode I matrix cracking did reveal trends in damage, stress, and strain that are similar to the trends seen in the experimental laminates.

A damage dependent finite element analysis code was used to predict local strains, stresses, and mode I matrix cracking internal state variables in centrally notched laminates. The finite element code utilized 3-node triangular elements, Figure 45, and the analysis considered only mode I matrix cracking. The code will not be able to accurately simulate fiber failure or mode I delamination until damage growth laws for these modes of failure are developed. The analysis was attempted using a fiber failure routine (ply discount) where an element's stress was set to zero if the strain in the 0 degree ply of that element

exceeded the fiber failure strain. This analysis yielded extremely conservative results. Since there is no fiber failure growth law, the strains and stresses in the 0 degree plies will continue to increase.

Further results of the model reveal trends in damage growth that are similar to experimental results. Figure 46 illustrates the transverse matrix crack growth in the 90 degree plies up to 100,000 cycles. Note the high density of matrix cracks near the hole. Furthermore, the crack density at the hole appears to have reached a saturation level early in the loading history, while away from the hole the crack density continues to increase. It should be made clear here that the model is not capable of interpreting internal state variable values into a numerical estimate of the number of cracks. The results in Figure 46 should be interpreted simply as the number of cracks at the hole are larger than the amount away from the hole, and the crack face displacements are more severe at the hole.

Illustrations of the model predictions are given in Figures 47, 48, and 49 for the 90 degree ply transverse crack growth shown in Figure 46. These figures are a visual interpretation of the graph. They illustrate the decrease in crack density as the distance away from the cut-out increases as well as the increase in crack growth with increasing fatigue cycles. Here again, we have no indication as to how many cracks are in each element, but we do know the number of cracks and the crack face displacements are more severe at the hole.

Mode I matrix cracking in the 0 degree plies was less severe than in the 90 degree plies. Illustrated in Figure 50 is an increase in crack density at the hole with an increase in fatigue cycles. However, as the transverse distance away from the hole increases, the amount of matrix cracking in the 0 degree plies quickly approaches zero. Similarly, Figure 51 is a graph of matrix crack growth in the axial direction. This damage, known as axial splitting, is more severe at the cut-out and quickly approaches zero as distance away from the cut-out increases. The level of damage in the 0 degree plies at the cut-out is less severe than in the 90 degree plies because the crack face displacements are smaller in the 0 degree plies. However, the graph shows the severity of damage increases at the hole as cycling continues. The 0 degree matrix damage in the axial direction extends slightly further than in the transverse direction representing an axial split.

Illustrations of the model predictions are given in Figures 52, 53, and 54 for the 0 degree ply crack growth shown in Figures 50 and 51. The axial split seen in these figures grows more dense as the cycles increase. The length of axial split does not grow nearly to the extent as seen in the experiments, however the damage growth trend is similar. Furthermore, these figures illustrate well the increase in crack face displacement with an increase in fatigue cycles.

DISCUSSION AND CONCLUSIONS

A progressive failure model based upon continuum damage mechanics, the continuum damage model, has been studied and applied in this research to a toughened epoxy material system, IM7/5260. The accomplished objectives for this research have helped develop and verify certain conclusions pertaining to this model as well as to open new areas for investigation to further develop this model toward the long term goal of residual strength and life prediction for composite laminates.

Edge Replication and x-ray radiography were used to document the damage growth in the IM7/5260 laminates. The x-rays and replicas were most helpful in verifying certain patterns of damage growth as well as experimental and analytical results. One particular example is the assumption of 90 degree transverse matrix cracks traversing the entire width of the laminate. The x-rays proved this assumption to be invalid for this material system. The x-rays were used to show which matrix cracks traversed the entire width of the laminate and which cracks were only partially traversing the width of the laminate. So that crack density measurements could still be useful in determining internal state variables, an assumption was made to where the cracks were evaluated as percentages of full length cracks. This may not be a very good assumption, however, the assumption did supply reasonable internal state variables. Furthermore, since we don't really know the effects of partial cracks on stiffness loss, the assumption is satisfactory for this particular instance.

Stiffness loss and residual strength were documented for the IM7/5260 composite laminates. It was obvious in these experiments that the stiffness loss for the $[0/90/0]_s$ laminates was nearly trivial, but increased with an increase in the number of 90 degree plies or a change in the stacking sequence as well as an increase in load. It was mentioned earlier that stiffness was measured in specimens of the same geometry, stacking sequence, and loading history as the specimens used for x-rays, but not the exact same specimen. This is not a grave concern. Circumstances did not permit the use of a materials testing machine located in an x-ray safe area. However, the documented damage is indicative of the damage inducing stiffness loss.

The residual strength plots may seem a little odd. Much more residual strength data should be collected before drawing conclusions. The residual strength data was plotted mainly to document the behavior of the fatigued specimens. Discussed in the chapter titled Experimental Results was the possibility that the specimens' warpage may have had a stress relieving effect, thus affecting the residual strength. This is not necessarily an explanation for the specimens' behavior since residual ply stresses due to warping was not

investigated in this research, but a suggestion that more data should be taken before making conclusions about the residual strength for this material.

The transverse matrix cracking internal state variables were calculated via Equations 12 and 13, from which the damage growth law parameters were numerically determined. Furthermore, the mode II matrix cracking and mode I delamination internal state variables were calculated using empirical Equations 6 and 7. The growth law parameters were input into a damage dependent constitutive code to predict stiffness due to mode I matrix cracking in the 90 degree plies. The damage mode II matrix cracking and mode I delamination variables were used in empirical Equations 22 thru 25 to predict stiffness loss due to shear and delamination. These predictions combined provided a stiffness loss prediction for the unnotched quasi-isotropic laminates.

A damage dependent finite element analysis code was used to provide a qualitative prediction of the mode I matrix cracking, stresses, and strains in each ply of the quasi-isotropic laminates with circular cut-outs. The actual stiffness loss was not predicted since this was a qualitative analysis designed to show the predicted trends in damage growth were similar to the experimental trends. An accurate quantitative prediction was postponed until further development. A quantitative residual strength prediction is not possible for this model at this time.

Several conclusions can be made from this research. First of all, the continuum damage model provides a fairly good prediction of stiffness loss for unnotched, quasi-isotropic, IM7/5260 composite laminates due to mode I matrix cracking, mode II matrix cracking, and mode I delamination. These predictions were shown in Figures 41 thru 44. Secondly, the continuum damage model predicts damage growth, stresses, and strains in all plies due only to mode I matrix cracking for quasi-isotropic, centrally notched, IM7/5260 composite laminates. Granted, only the qualitative trends are comparable to experimental results, but if fiber failure and mode I delamination are considered, the predicted damage would quantitatively be comparable.

Further development is required for this model to eventually be able to predict life of a laminated composite. Following is a brief list of objectives for future work and areas of investigation that are necessary for further development.

- The effect on stiffness loss of transverse matrix cracks, which progress slowly from the edge of the laminate, needs to be investigated for materials that are not brittle enough such that the transverse matrix cracks traverse the entire width of the laminate. Perhaps a correlation between crack density and partial matrix cracking can be developed. If so, a new method by which to measure crack density may need to be developed.

- A linear damage growth law for mode I matrix crack growth should be developed for materials exhibiting linear matrix crack growth. This would significantly simplify the analysis.
- Damage growth laws for mode II matrix cracking, mode I delamination, and fiber failure need to be developed for accurately modelling damage growth and stress redistribution.
- The damage dependent constitutive and finite element analysis codes need to be upgraded to incorporate damage growth laws for fiber failure, mode II matrix cracking, and mode I delamination.

In conclusion, the continuum damage model has the potential to become a useful tool to predict life of laminated composites. If this progressive failure model can develop to the point of actually predicting life using damage growth laws for all the modes of damage, it will be a powerful tool.

Note: This report is the edited version of the Master's thesis written by Tim Coats. This report is intended as a thorough reference for using the continuum damage model. For more accurate data and a concise and professional presentation of the model, refer to Coats,T.W. and Harris, C.E.,"Experimental Verification of a Progressive Damage Model for IM7/5260 Laminates Subjected to Tension-Tension Fatigue," Journal of Composite Materials, 1994 or 1995.

REFERENCES

1. Vakulenko, A. A. and Kachanov, M. L., "Continuum Theory of Cracked Media," *Izv. AN SSR. Mekhaniha Tverdogo Tela*, Vol. 6, p. 159, 1971.

2. Masters, J. E. and Reifsnider, K. L., "An Investigation of Cumulative Damage Development in Quasi-Isotropic Graphite/Epoxy Laminates," *Damage in Composite Materials*, ASTM STP 775, K. L. Reifsnider, Ed., American Society for Testing and Materials, 1982, pp. 40-62.

3. Highsmith, A. L. and Reifsnider, K. L., "Stiffness-Reduction Mechanisms in Composite Laminates," *Damage in Composite Materials*, ASTM STP 775, K. L. Reifsnider, Ed., American Society for Testing and Materials, 1982, pp. 103-117.

4. Garg, A. C., "Delamination-A Damage Mode in Composite Structures," *Engineering Fracture Mechanics*, Vol. 29, No. 5, 1988, pp. 557-584.

5. Tsai, G. C., Doyle, J. F., and Sun, C. T., "Frequency Effects on the Fatigue Life and Damage of Graphite/Epoxy Composites," *Journal of Composite Materials*, Vol. 21, January 1987, pp. 2-13.

6. O'Brien, T. K., "Mixed-Mode Strain-Energy-Release Rate Effects on Edge Delamination on Composites," *Effects of Defects in Composite Materials*, ASTM STP 836, American Society fo Testing and Materials, 1984, pp.125-142.

7. Aboudi, J., "Stiffness Reduction of Cracked Solids," *Engineering Fracture Mechanics*, Vol. 26, No. 5, 1987, pp. 637-650.

8. Hashin, Z., "Analysis of Cracked Laminates: A Variational Approach," *Mechanics of Materials 4*, North Holland, 1985, pp. 121-136.

9. Wang,A.S.D., Chou,P.C., Lei,S.C., "A Stochastic Model for the Growth of Matrix Cracks in Composite Laminates", J. of Composite Materials, Vol. 18, May 1984.

10. Tan,S.C., Nuismer,R.J., "A Theory for Progressive Matrix Cracking in Composite Laminates", *J. Composite Materials*, Vol. 23, October 1989.

11. Awerbuch,J., Eckles,W.F., and Erdman,D.L., "Detection of Failure Progression in Cross-Ply Graphite/Epoxy During Fatigue Through Acoustic Emission", Wright Research and Development Center, WRDC-Tr-89-3087, Vol. 1, 1990.

12. Yang,J.N., "Fatigue and Residual Strength Degradation for Graphite/Epoxy Composites Under Tension-Compression Cyclic Loadings", *Journal of Composite Materials*, Vol. 12, Jan. 1978.

13. Rotem,A., " Fatigue and Residual Strength of Composite Laminates", *Engineering Fracture Mechanics*, Vol. 25, 1986.

14. Yang, J.N. and Liu, M. D., "Residual Strength Degradation Model and Theory of Periodic Proof Tests for Graphite/Epoxy Laminates," *J. Composite Materials*, Vol 11, 1977.

15. Weitsman, Y., "Environmentally Induced Damage in Composites," *5th International Symposium on Continuum Models of Discrete Systems*, Nottingham, July 1985.

16. Talreja, R., "A Continuum Mechanics Characterization of Damage in Composite Materials," *Proc. R. Soc London*, Vol. 399A, 1985, pp. 196-216.

17. Talreja, R., "Residual Stiffness Properties of Cracked Composite Laminnates," *Advances in Fracture Research*, Proc. Sixth Int. Conf. De Fracture, New Delhi, India, Vol. 4, 1985, pp. 3013-3019.

18. Talreja, R., "Transverse Cracking and Stiffness Reduction in Composite Laminates," *J. Composite Materials*, Vol. 19, 1985, pp. 355-375.

19. Miner, M. A., "Cumulative Damage in Fatigue", *J. Applied Mechanics*, Vol. 12, 1945.

20. Hashin, Z. and Rotem, A., "A Cumulative Damage Theory of Fatigue Failure," AFOSR-TR-77-0717, 1977.

21. Coleman, B. D. and Gurun, M. E., "Thermodynamics with Internal State Variables," *J. Chemistry and Physics*, Vol. 47, 1967, pp. 597-613.

22. Bodner, S. R., "A Procedure for Including Damage in Constitutive Equations for elastic-viscoplastic work hardening materials," *Physical Non-linearities in Structural Analysis*, pp. 21-28, 1981.

23. Krajcinovic, D., "Continuum Damage Mechanics," *Applied Mechanics*, January 1984.

24. Lee,J.W., Allen,D.H., Harris,C.E., "Internal State Variable Approach for Predicting Stiffness Reductions in Fibrous Laminated Composites with Matrix Cracks", *J. of Composite Materials*, Vol. 23, Dec. 1989, pp. 1273-1291.

25. Nottorf,Eric W., "An Investigation Into the Effects of Damage on the Stresses in a Composite Laminate", Dissertation, Texas A&M, 1990.

26. Lo, D.C., Allen, D.H., and Harris, C.E., "A Procedure for Utilization of a Damage-Dependent Constitutive Model for Laminated Composites," *NASA Technical Memorandum 104219*, NASA LaRC, February 1992.

27. Allen,D.H., Harris,C.E., Groves,S.E., "A Thermomechanical Constitutive Theory for Elastic Composites with Distributed Damage-I. Theoretical Development", *Int. J. Solids Structures*, Vol. 23, No. 9, 1987.

28. Allen,D.H., Harris,C.E., Groves,S.E., "A Thermomechanical Constitutive Theory for Elastic Composites with Distributed Damage-II. Application to Matrix Cracking in Laminated Composites", *Int. J. Solids Structures,* Vol. 23, No. 9, 1987.

29. Harris,C.E., Allen,D.H, O'Brien,T.K., "Progressive Failure Methodologies for Predicting Residual Strength and Life of Laminated Composites", *1st NASA Advanced Composites Technology Conference*, Oct 30 - Nov 1, 1990

30. Lo,D.C., Allen,D.H., Harris,C.E., "A Continuum Model for Damage Evolution in Laminated Composites", *IUTAM Symposium on Inelastic Deformation of Composite Materials*, 1990

31. de Rouvray, A. and Haug, E., "Failure of Brittle and Composite Materials by Numerical Methods," *Structural Failure*, Tomasz Wierzbicki and Norman Jones, eds., John Wiley & Sons, New York, N.Y., 1989, pp. 193-254.

32. Ladeveze, P., Allix, O., and Daudeville, L., "Mesomodelling of Damage for Laminated Composites Application to Delamination," *Proceedings of the IUTAM Symposium on Anelastic Deformation of Composite Materials*, Troy, N.Y., vol. 29, 1990.

33. Allen,D.H., Lee,J.W., "Matrix Cracking in Laminated Composites Under Monotonic and Cyclic Loadings", Aerospace Engineering Department Texas A&M, 1990.

34. Allen,D.H., "Life Prediction in Laminated Composites Using Continuum Damage Mechanics", Aerospace Engineering Department Texas A&M, 1989.

35. Gates, T.S., "Experimental Characterization of Non-Linear Rate Dependent Behavior in Advanced Polymer Matrix Composites," *Experimental Mechanics SEM Spring Conference*, Milwaukee, Wisconsin, June 1991.

36. Jones, R.M., "Mechanics of Composite Materials," Hemisphere Publishing Corp., New York, 1975.

37. Nuismer,R.J., Whitney, J.M., "Stress Fracture Criteria for Laminated Composites Containing Stress Concentrations", *J. Composite Materials*, Vol. 8, July 1974

Table 1 - Description of Input for the First Constitutive Module

Data	Description of Data
nplies	Number of Plies in Laminate
Q11,Q22,Q33, Q12,Q13,Q66	Transformed Ply Level Stiffness Matrix
iflag	Damage Condition
Nx,Ny,Nxy Mx,My,Mxy	Applied Forces and Moments
t(i), theta(i)	Ply Thickness and Orientation
alpham(i,2), alpham(i,8)	Initial Values of Mode I and Mode II ISV for ply i
dpara, κ, η	Slope of $d\alpha/ds$ vs σ, Growth Law Parameters
nci, ncf, ninc	Initial Cycle Number, Final Cycle Number, Increments
iprnum, nsubic	Increments to Output, Subincrements During Load Change
njump, xfac	Load Change Cycle Number, Load Factor

TABLE 2 - Specimens Used in Experimentation

Layup	No. of Specimens	Width	Type of Notch	Data Collected and/or Calculated
$[0/90/0]_S$	10	1"	unnotched	Crack Density, Stiffness Loss
$[0/902/0]_S$	10	1"	unnotched	Crack Density, Stiffness Loss
$[45/-45]_{2S}$	10	1"	unnotched	Shear Modulus
$[0/45/-45/90]_S$	10	1"	unnotched	Stiffness Loss, Residual Str.
$[0/45/-45/90]_S$	10	1"	1/4" hole	Stiffness Loss, Residual Str.
$[0/45/-45/90]_S$	5	2"	1/4" hole	Stiffness Loss, Residual Str.
$[90/-45/45/0]_S$	10	1"	unnotched	Stiffness Loss, Residual Str.
$[90/-45/45/0]_S$	10	1"	1/4" hole	Stiffness Loss, Residual Str.
$[90/-45/45/0]_S$	5	2"	1/4" hole	Stiffness Loss, Residual Str.

Table 3 - Ply Level Properties of IM7/5260 @ 23 Degrees Celsius

E11=	152.8 GPa	(22.162 Msi)
E22=	8.7 GPa	(1.262 Msi)
G12=	5.2 GPa	(0.754 Msi)

Poisson's Ratio = 0.3

Table 4 - Components of the Transformed Ply Stiffness Matrix

Q11 =	167.9 GPa	(24.354 Msi)
Q22 =	9.6 GPa	(1.392 Msi)
Q12 =	2.9 Gpa	(0.421 Msi)
Q66 =	5.2 GPa	(0.754 Msi)

Table 5 - Initial Data for IM7/5260 $[0/90/0]_S$ Laminates

	Theoretical	Experimental
Longitudinal		
Engineering	15.250 Msi	15.430 Msi
Modulus	105.145 Gpa	106.386 Gpa
First Ply		
Failure Load	4.395 kip	4.000 kip
	19.549 kN	18.126 kN
First Fiber		
Failure Load	9.900 kip	8.325 kip
	44.037 kN	37.031 kN

Table 6 - Initial Data for IM7/5260 $[0/90_2/0]_S$ Laminates

	Theoretical	Experimental
Longitudinal		
Engineering	11.758 Msi	12.305 Msi
Modulus	81.068 GPa	84.840 GPa
First Ply		
Failure Load	4.324 kip	4.000 kip
	19.234 kN	17.882 kN
First Fiber		
Failure Load	9.783 kip	8.000 kip
	43.517 kN	35.586 kN

Table 7 - Intial Data for IM7/5260 $[45/-45]_{2S}$ Laminates

	Theoretical		Experimental
Longitudinal			
Engineering	2.684 Msi		2.949 Msi
Modulus	18.505 GPa		20.333 GPa
First Ply			
Failure Load	.256 kip	1	.155 kip
	5.587 kN		5.138 kN
First Fiber			
Failure Load			2.000 kip
			8.896 kN

Table 8 - Initial Data for IM7/5260 $[0/45/-45/90]_S$ Laminates

	Theoretical	Experimental
Longitudinal		
Engineering	8.426 Msi	8.030 Msi
Modulus	58.095 GPa	55.365 GPa
First Ply		
Failure Load	3.125 kip	2.400 kip
	13.901 kN	10.676 kN
First Fiber		
Failure Load	7.070 kip	3.500 kip
	31.450 kN	15.569 kN

Table 9

$[0/90/0]_s$ Input Data for the Constitutive Model

nplies: 6

Q11	=	167.799 GPa	Q13	=	2.901 GPa
	=	24.354 Msi		=	0.421 Msi
Q22	=	9.591 GPa	Q33	=	9.591 GPa
	=	1.392 Msi		=	1.392 Msi
Q12	=	2.901 GPa	Q66	=	5.195 GPa
	=	0.421 Msi		=	0.754 Msi

iflag: 1

Nx	=	14.240 kN	Mx	=	0
	=	3.200 kip			
Ny	=	0	My	=	0
Nz	=	0	Mz	=	0

Ply Thickness: 0.1524 mm (0.006 inches)

Ply Orientation: $[0/90/0]_s$

alpham(i,2) = 0 alpham(i,8) = 0

dpara = 3.4214×10^{-8} [SI]

= 3.8686×10^{-7} [English]

k	=	7.7746	h =	5.523	[SI]
	=	1.1695	=	5.5109	[English]

nci: 0 iprnum: 10000

ncf: 100000 nsubic: 200

ninc: 100000 njump: 100001

xfac: 1

Table 10

Delamination Internal State Variable Results for

Unnotched $[0/45/-45/90]_S$ Laminates

Cycle	S_d/S (%)	e_x	a_3^D
10000	2.0	0.0086	0.0011
20000	21.0	0.0090	0.0117
40000	40.0	0.0091	0.0224
60000	44.0	0.0092	0.0247
100000	48.0	0.0092	0.0273

Table 11

Delamination Internal State Variable Results for

Unnotched $[90/-45/45/0]_S$ Laminates

Cycle	S_d/S (%)	e_x	a_{31}^D	a_{32}^D
10000	3.13	0.0082	0.0011	0.0002
50000	12.50	0.0089	0.0043	0.0010
100000	20.00	0.0091	0.0068	0.0015

Table 12

Shear Internal State Variable Results

from $[45/-45]_{2S}$ Laminates

Cycle	G_{12} (Msi)	e_6	S	a_8^M
25000	0.966	0.0086	6.416	0.000403
50000	0.957	0.0087	10.667	0.000677
100000	0.887	0.0094	22.500	0.001544

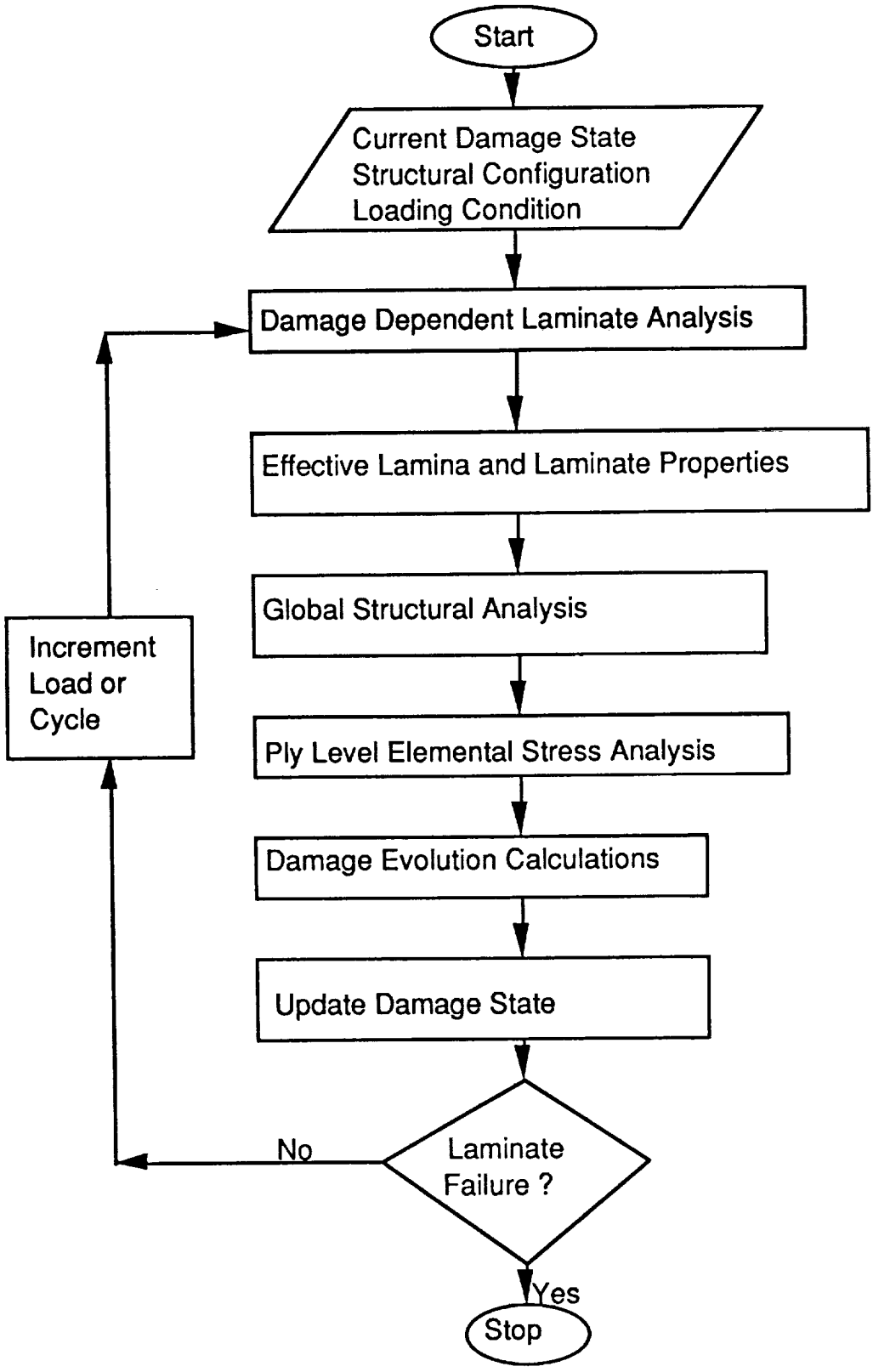

Figure 1 - Progressive Failure Scheme

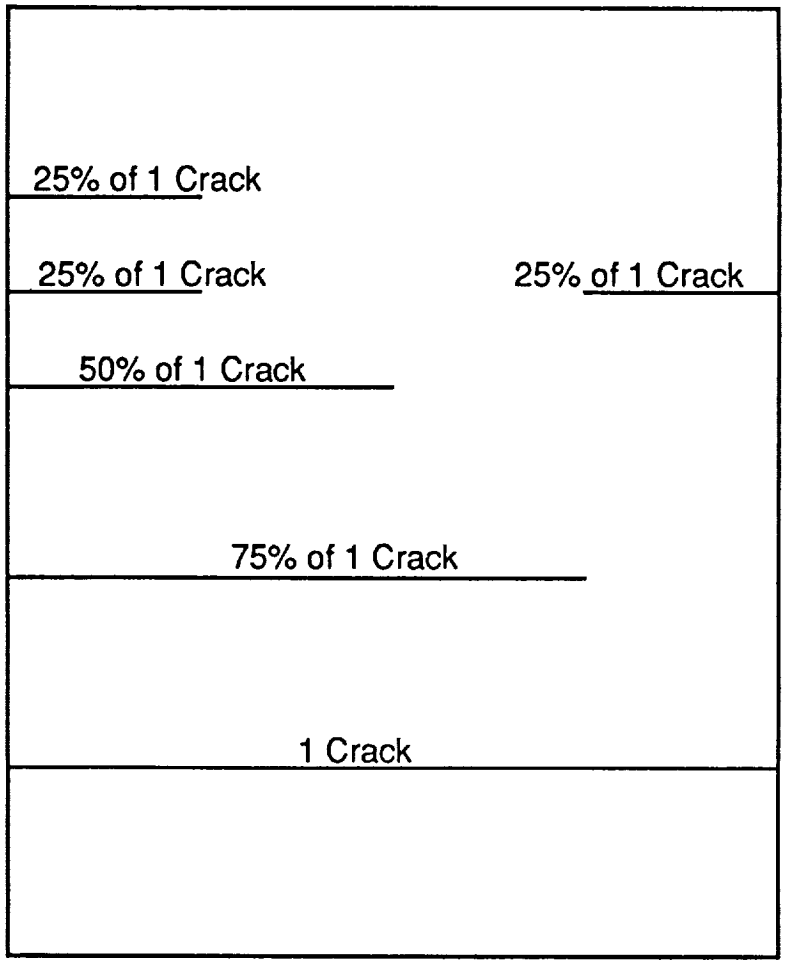

Total number of cracks = 3

Figure 2 - Schematic of Transverse Matrix Cracking

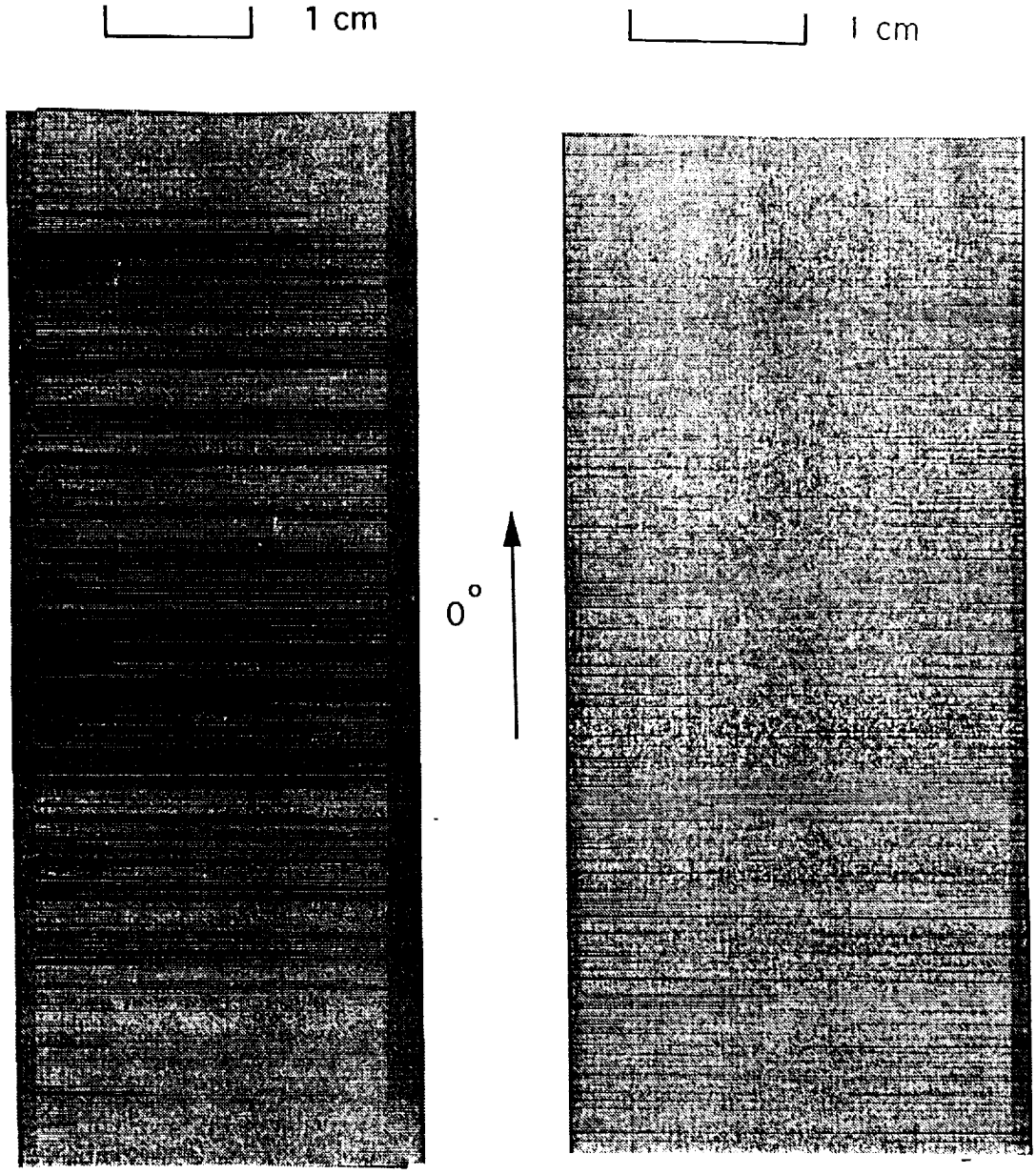

Figure 3 - X-Rays of Damaged [0/90/0]s Specimens Subjected to Fatigue Loading.
Max Stress = 479 MPa, R = 0.1, f = 5 Hz

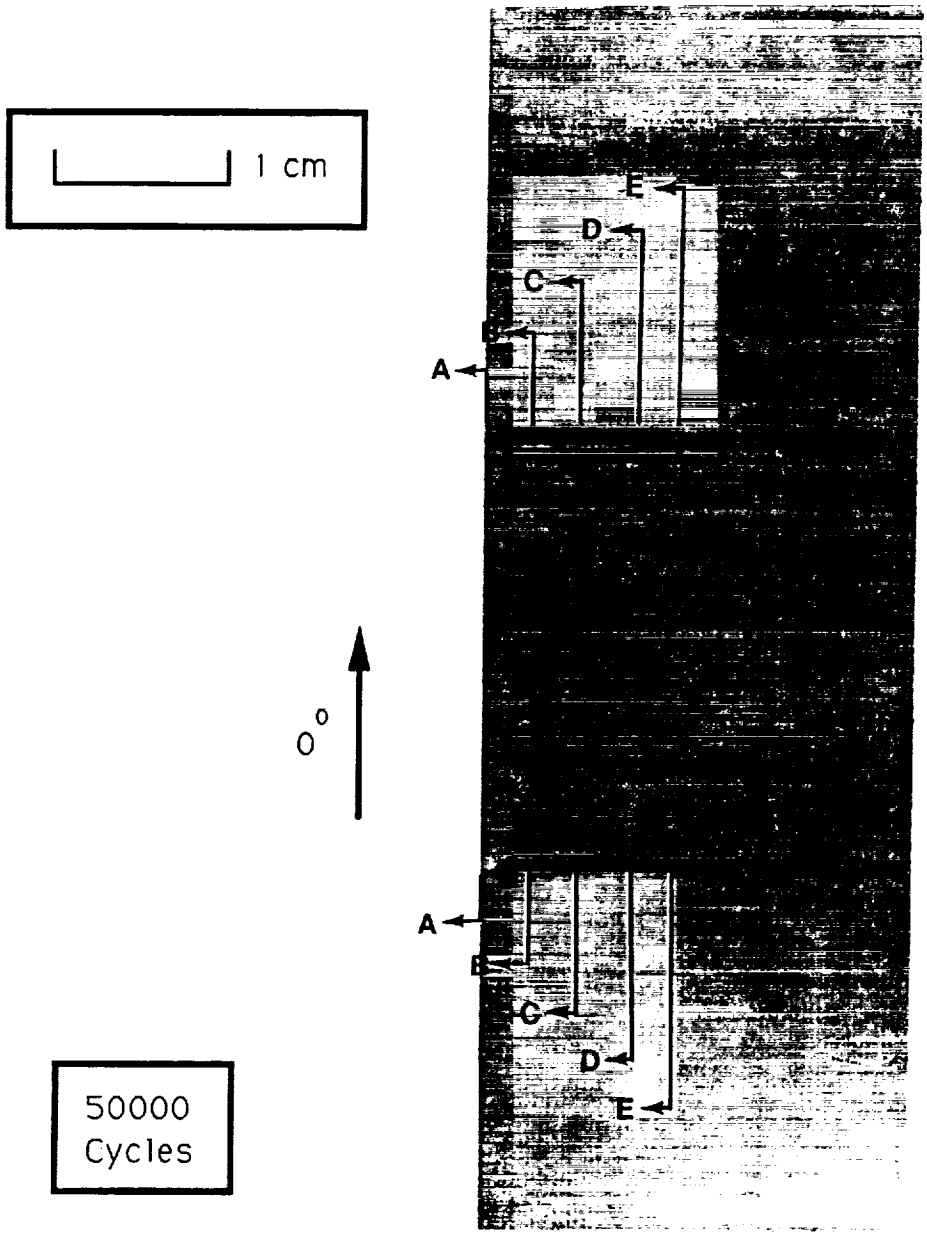

Figure 4 - Sectioning of a $[0/90_2/0]_s$ Laminate Subjected to Tension-Tension Fatigue.
Max Stress = 479 MPa, R=0.1, f=5Hz

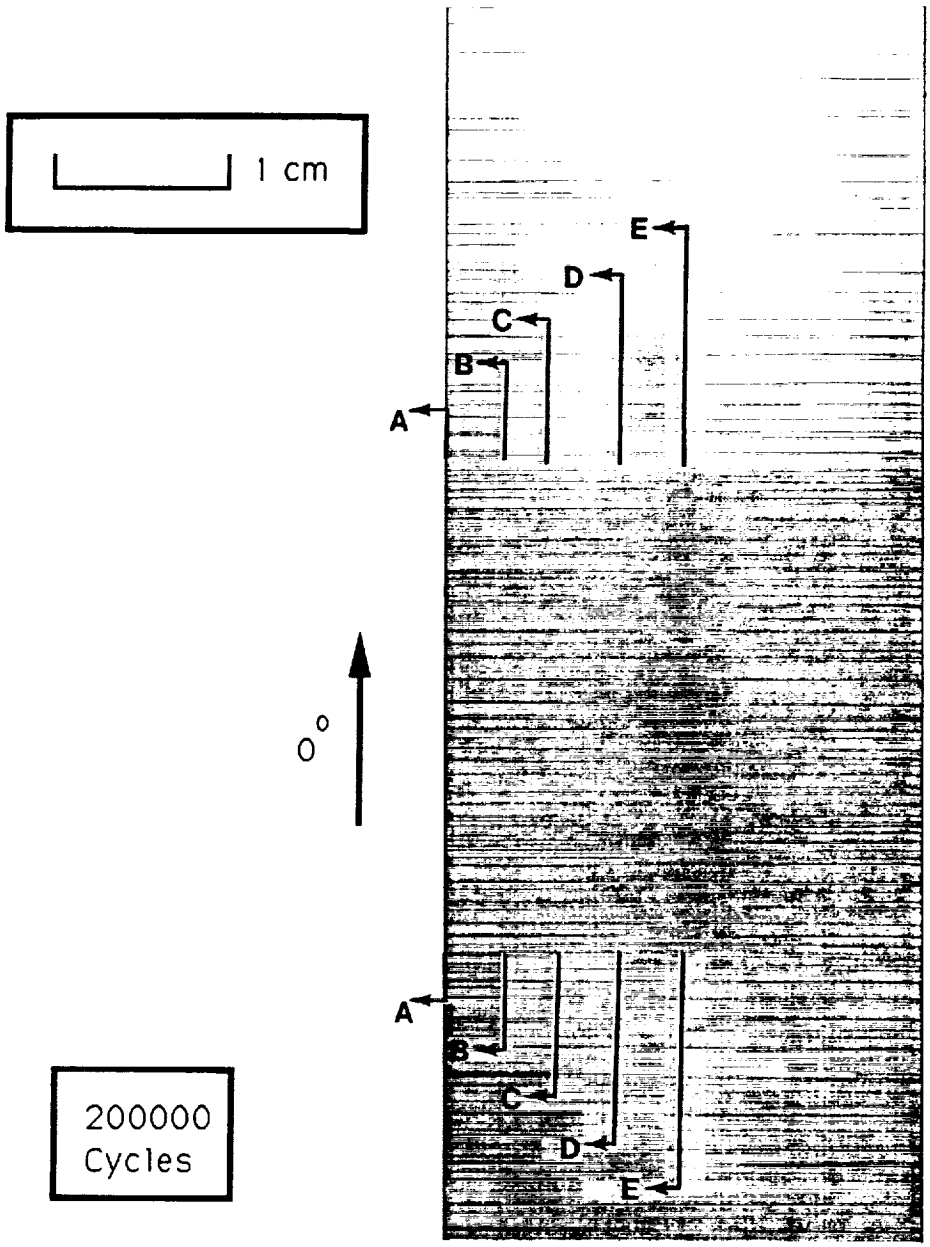

Figure 5 - Sectioning of a $[0/90_2/0]_s$ Laminate Subjected to Tension-Tension Fatigue.
Max Stress = 479 MPa, R=0.1, f=5Hz

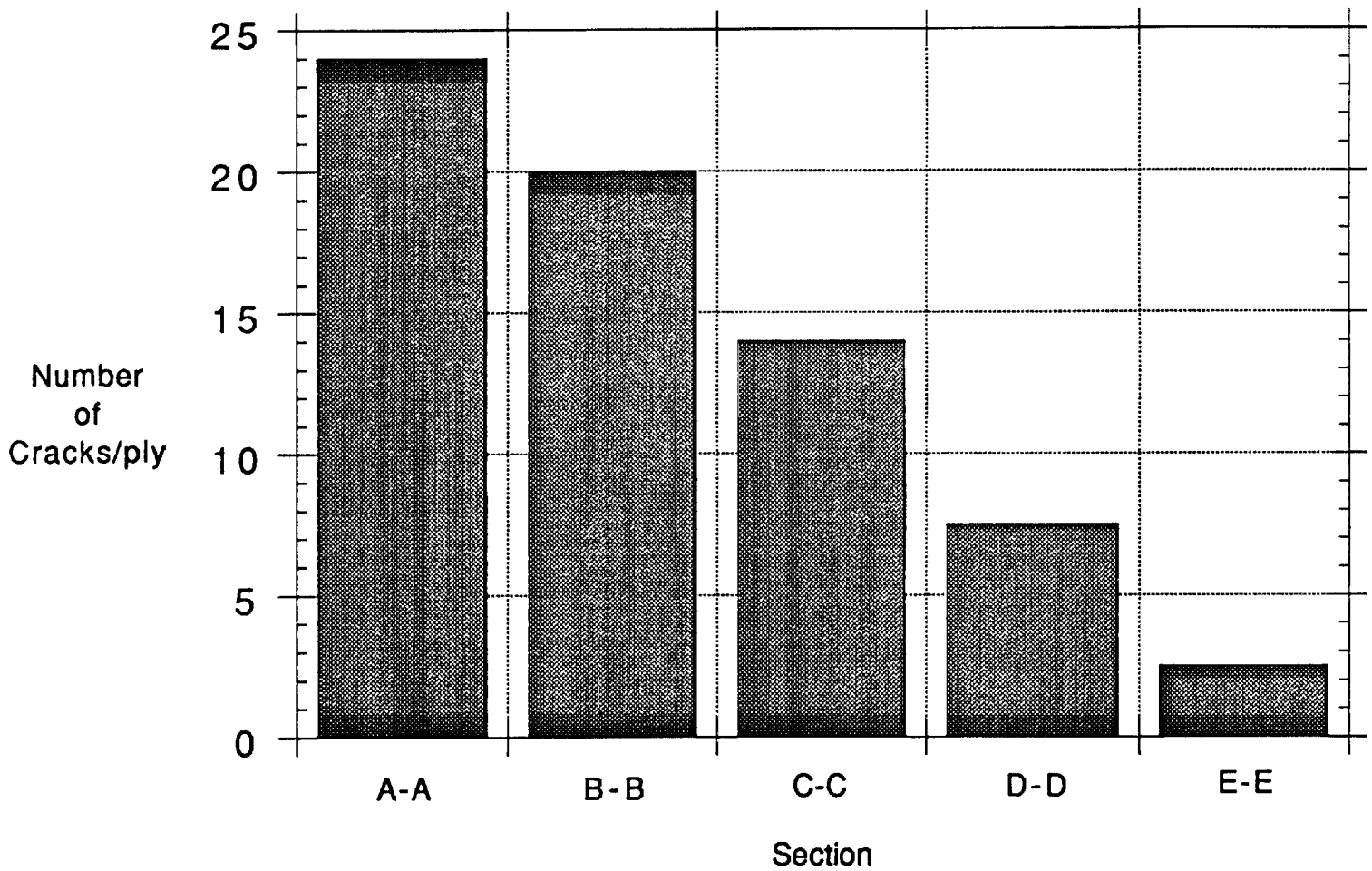

Figure 6 - Crack Count for $[0/90_2/0]_s$ Specimen Sectioning at 50000 Cycles Over a 2.54 cm Edge Length

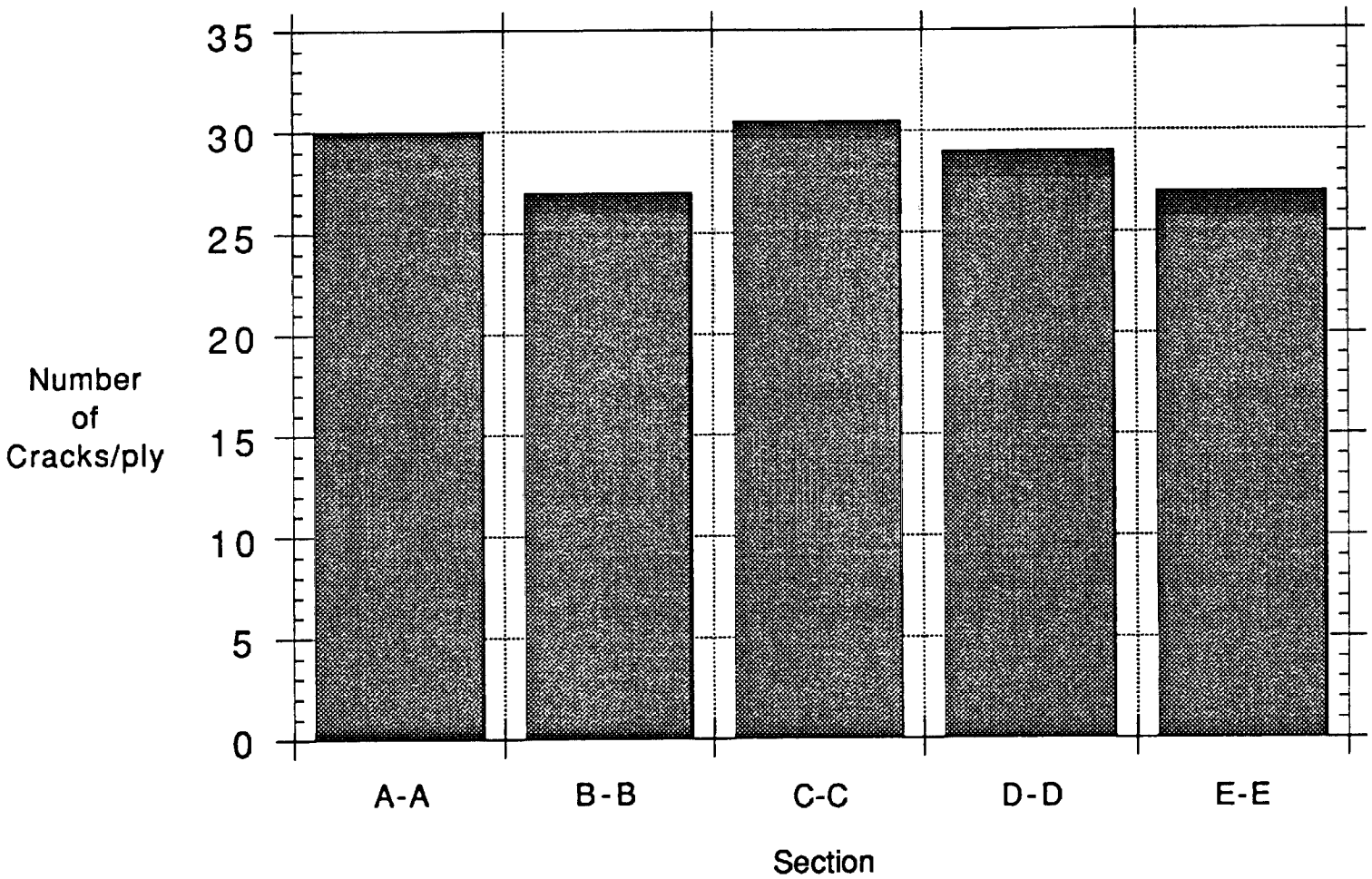

Figure 7 - Crack Count for $[0/90_2/0]_s$ Specimen Sectioning at 200000 Cycles Over a 2.54 cm Edge Length

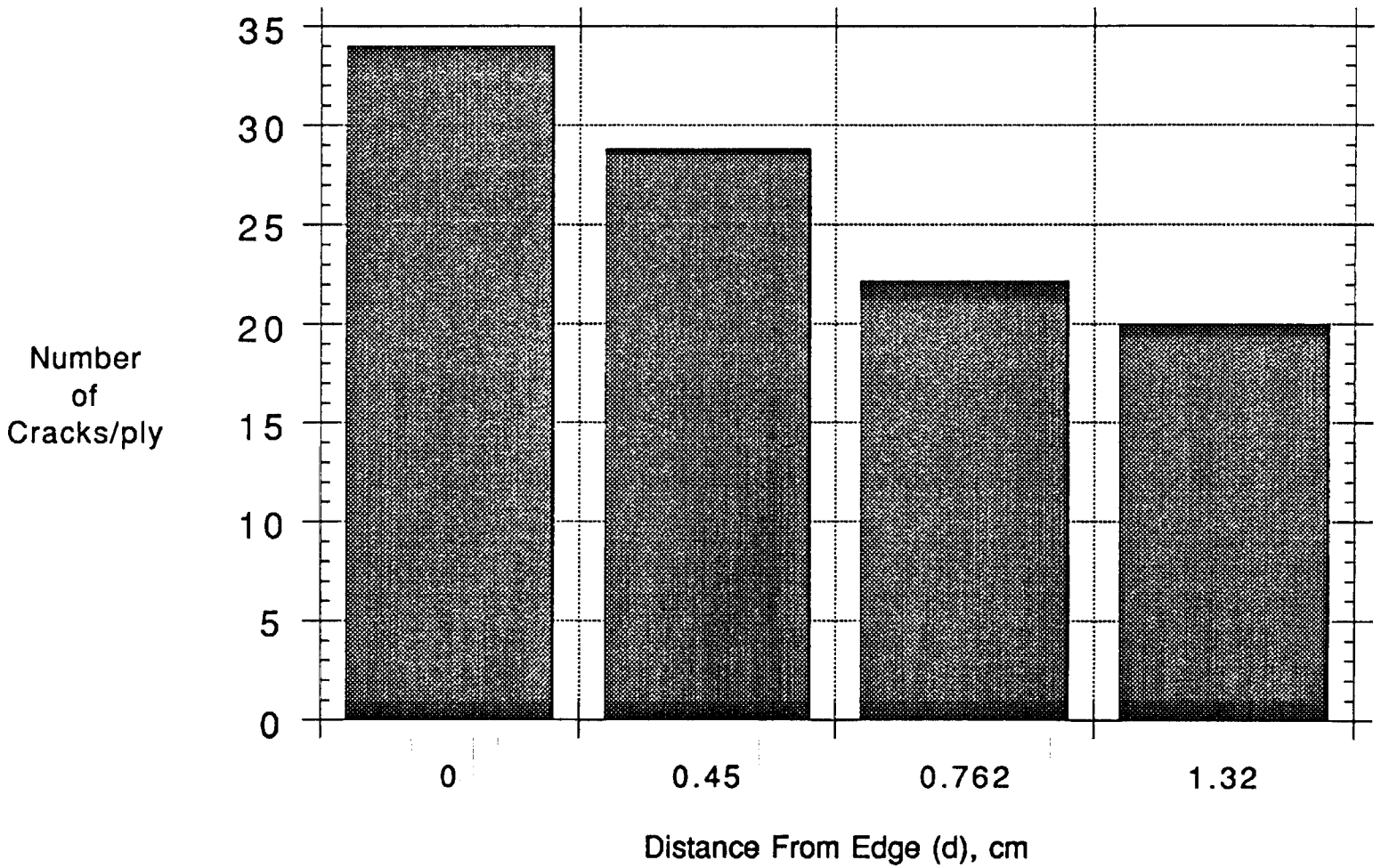

Figure 8 - Crack Count for $[0/90/0]_s$ Specimen Sectioning at 200000 Cycles Over a 2.54 cm Edge Length

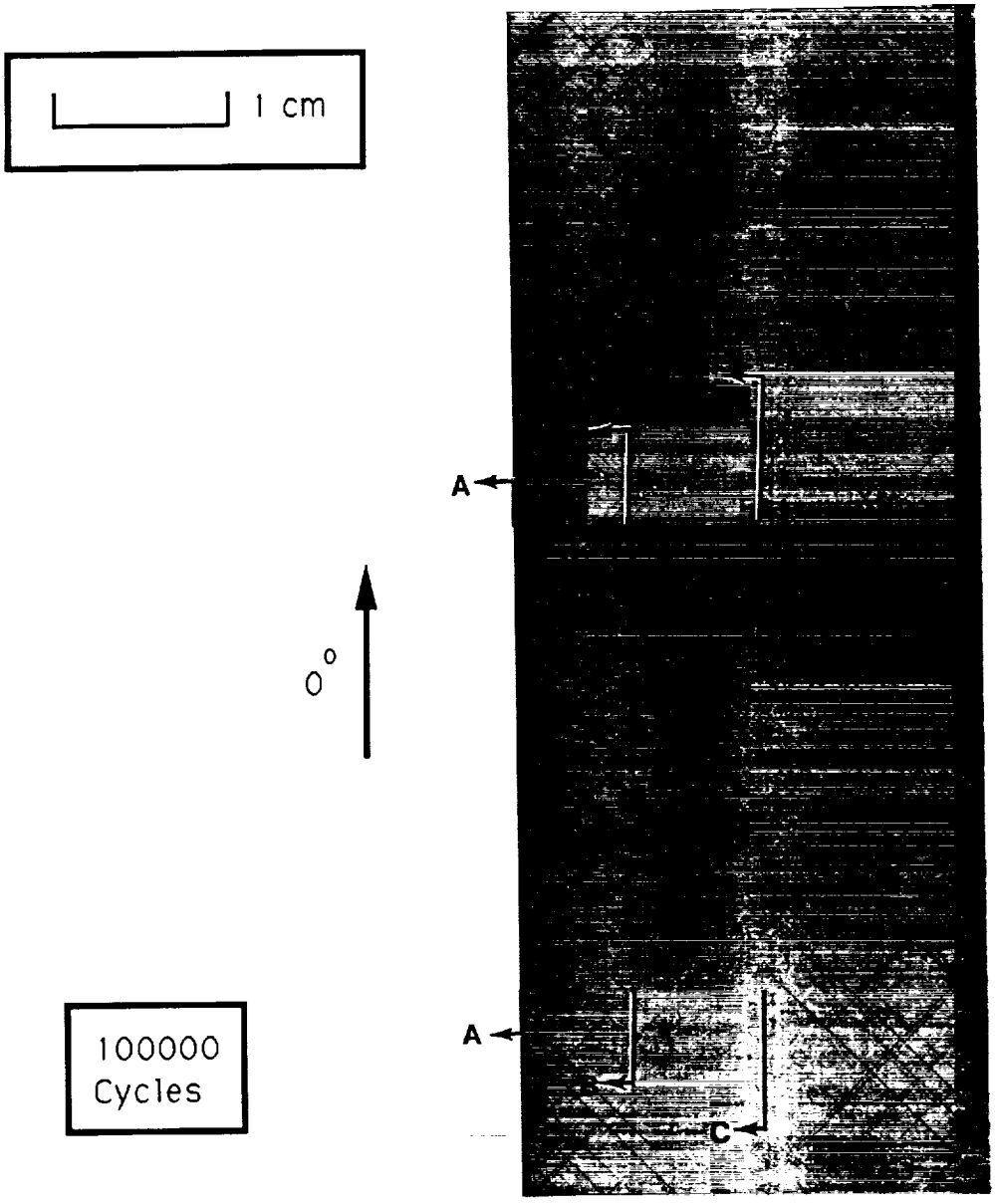

Figure 9 (a) - Sectioning of a $[45/-45]_{2s}$ Laminate Subjected to Fatigue Loading.
Max Stress = 120 MPa, R=0.1, f=5 Hz

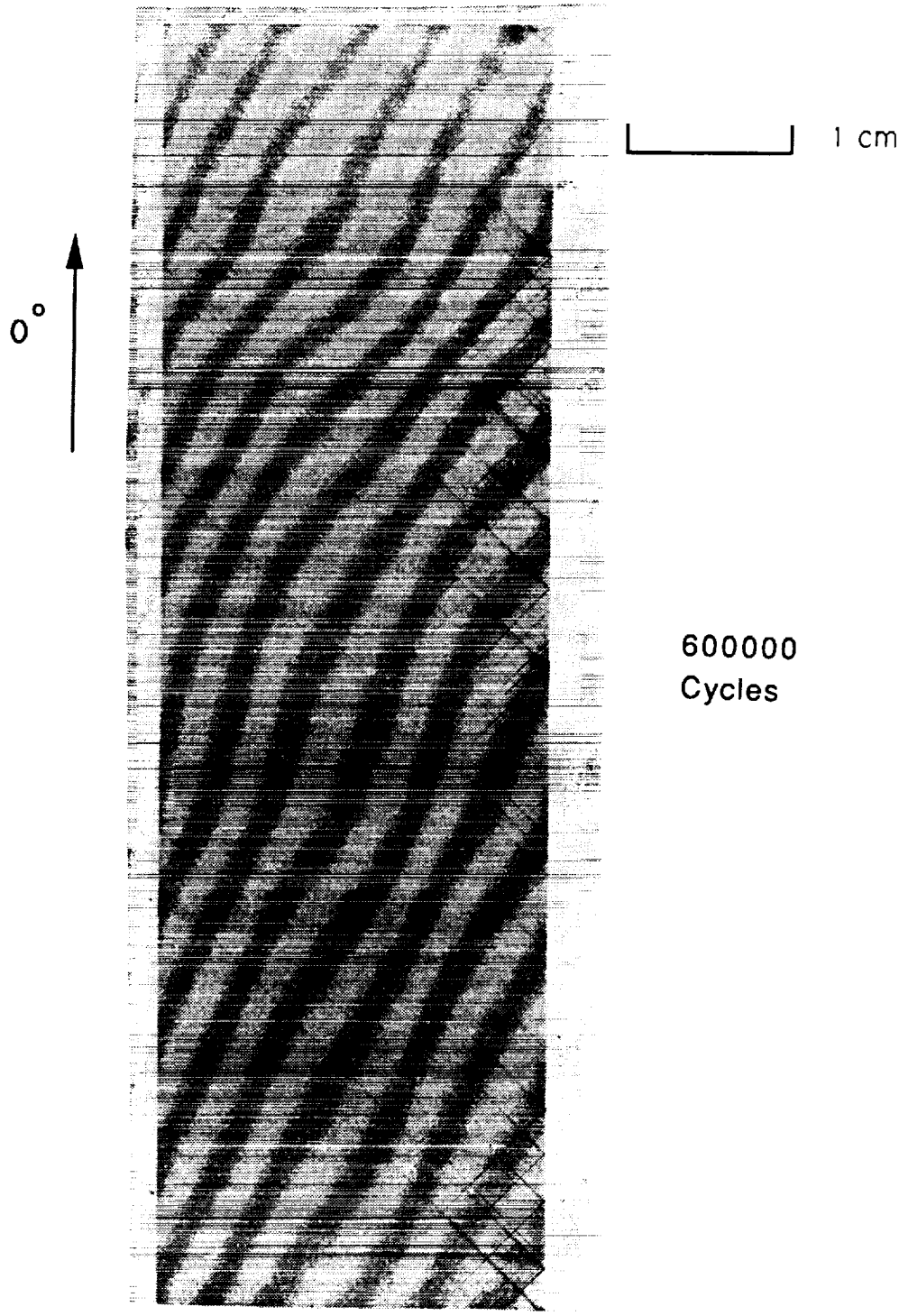

Figure 9 (b) - X-Ray of a Damaged $[45/-45]_{2s}$ Laminate Subjected to Fatigue Loading Just Prior to Catastrophic Failure. Max Stress = 120 MPa, R=0.1, f=3 Hz

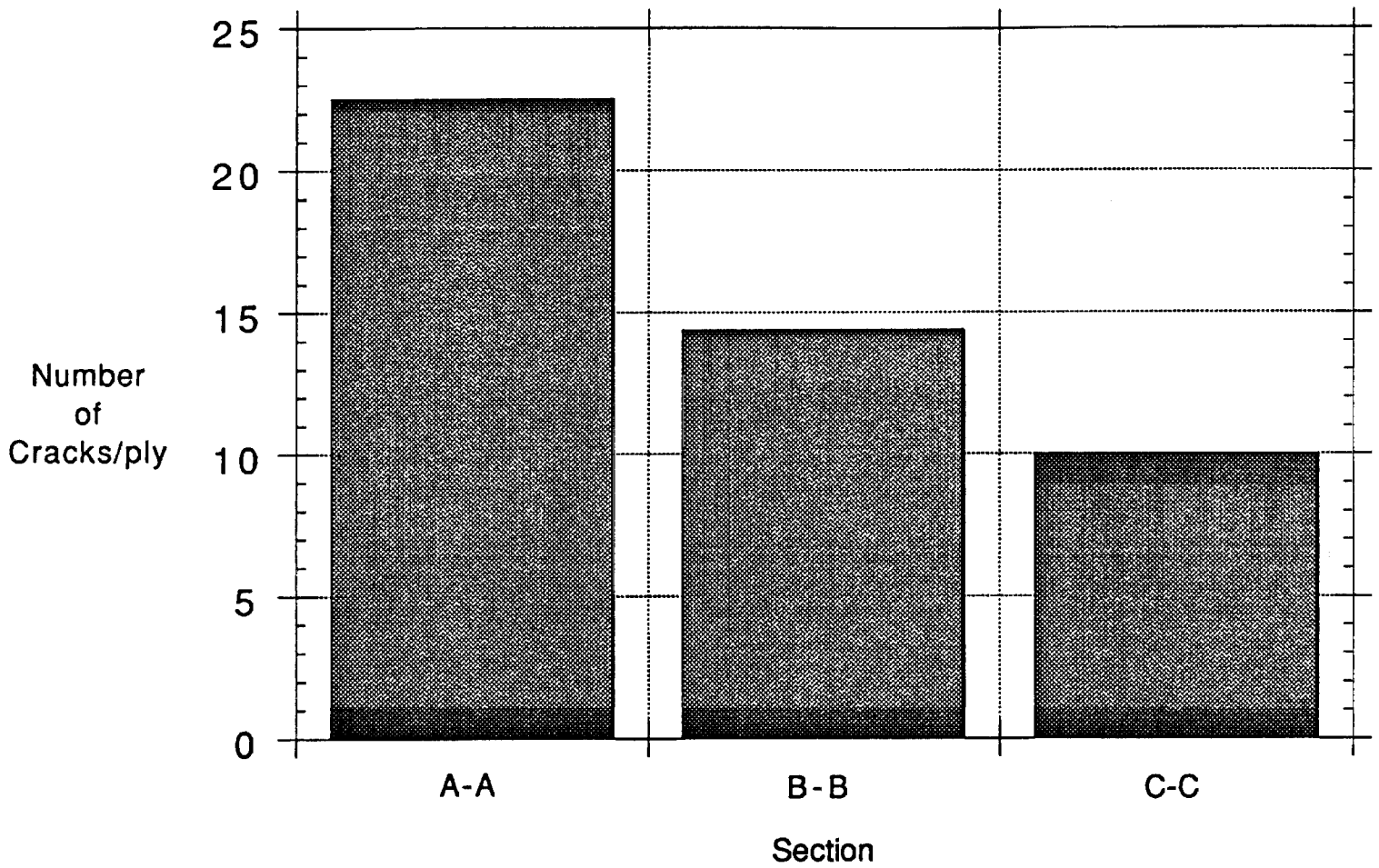

Figure 10 - Crack Count for $[45/-45]_{2s}$ Specimen Sectioning at 100000 Cycles Over a 2.54 cm Edge Length

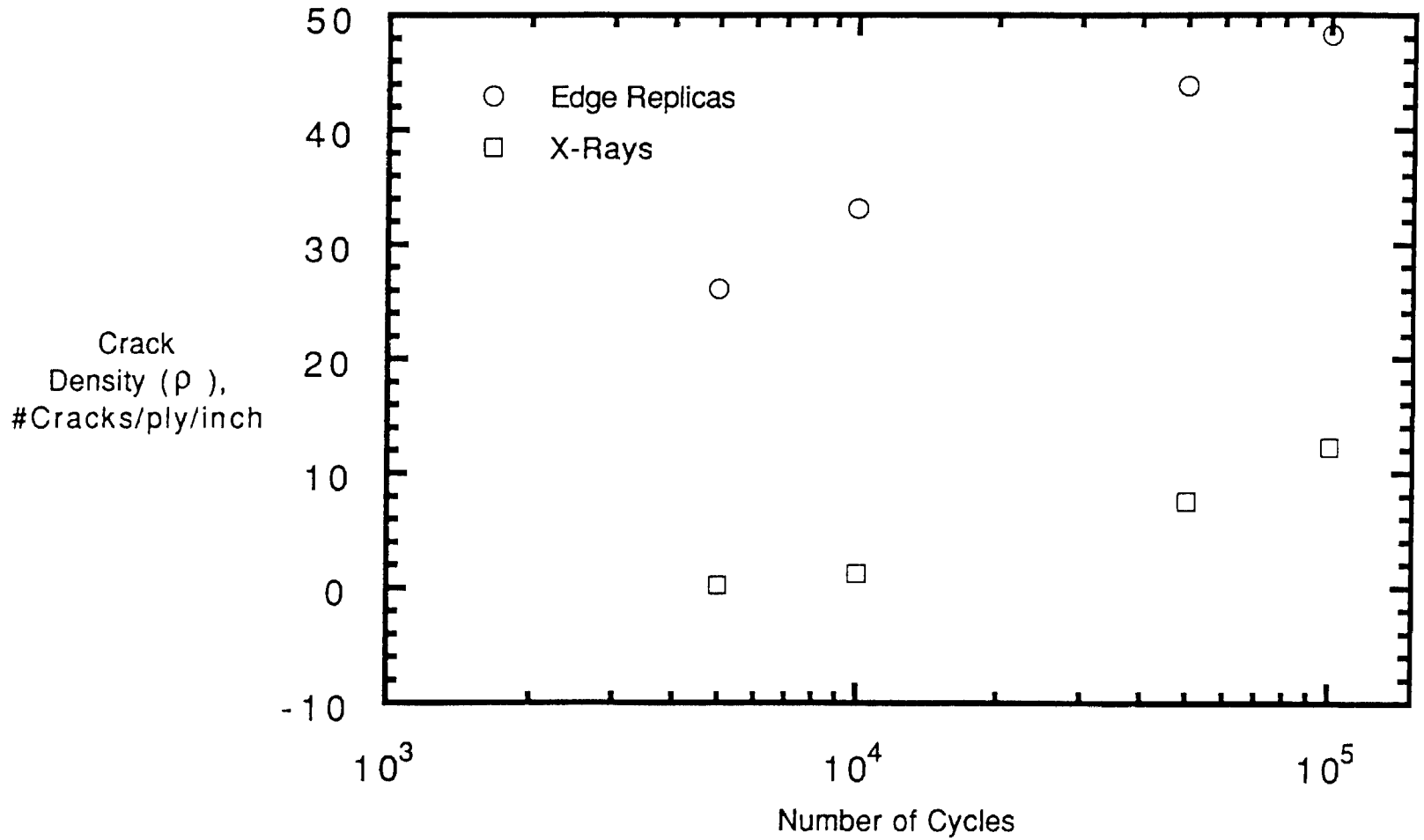

Figure 11 - Crack Density Comparison of Edge Replicas vs X-Rays for IM7/5260 [0/90/0]s Composite Laminates

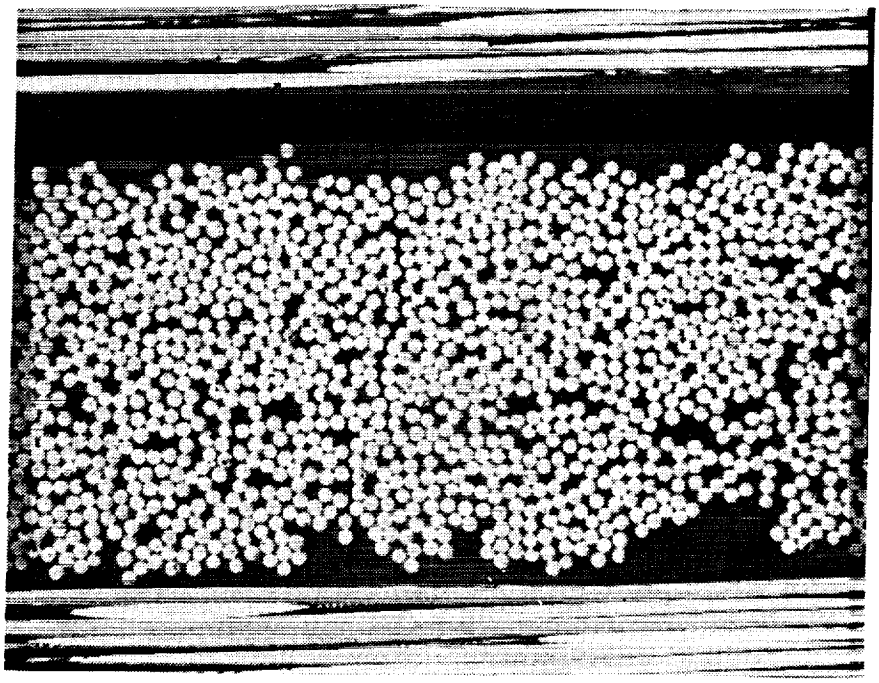

(a)

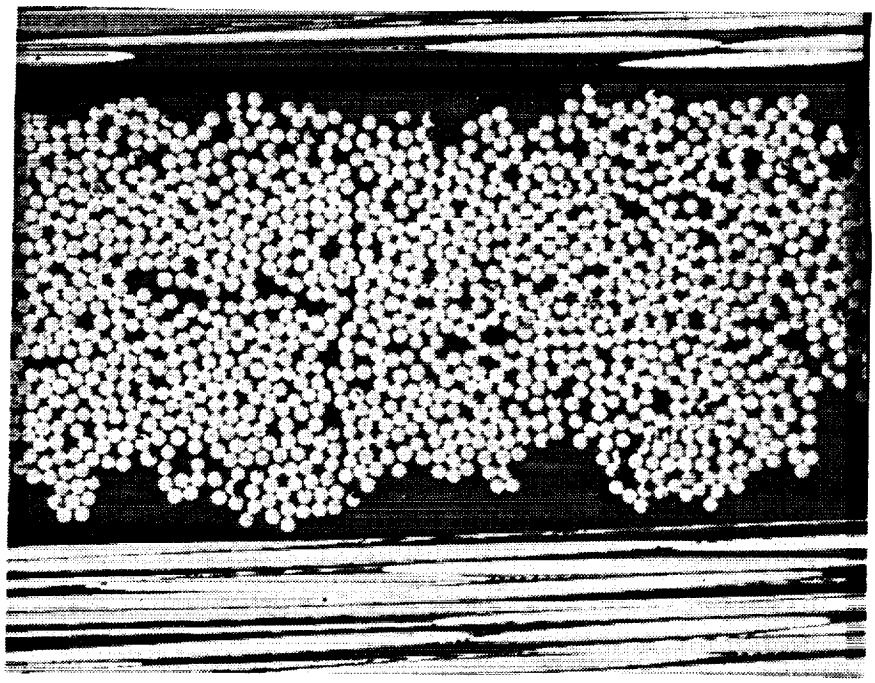

(b)

Figure 12 - Matrix Cracking of Ninety Degree Plies of a $[0/90/0]_s$ IM7/5260 Composite Laminate Magnified 400x

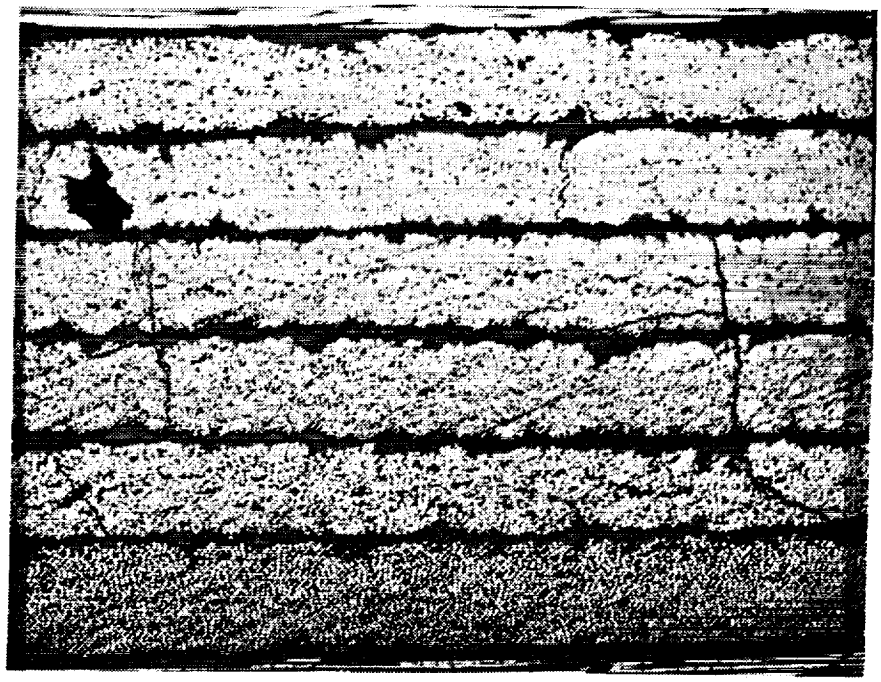

(a)

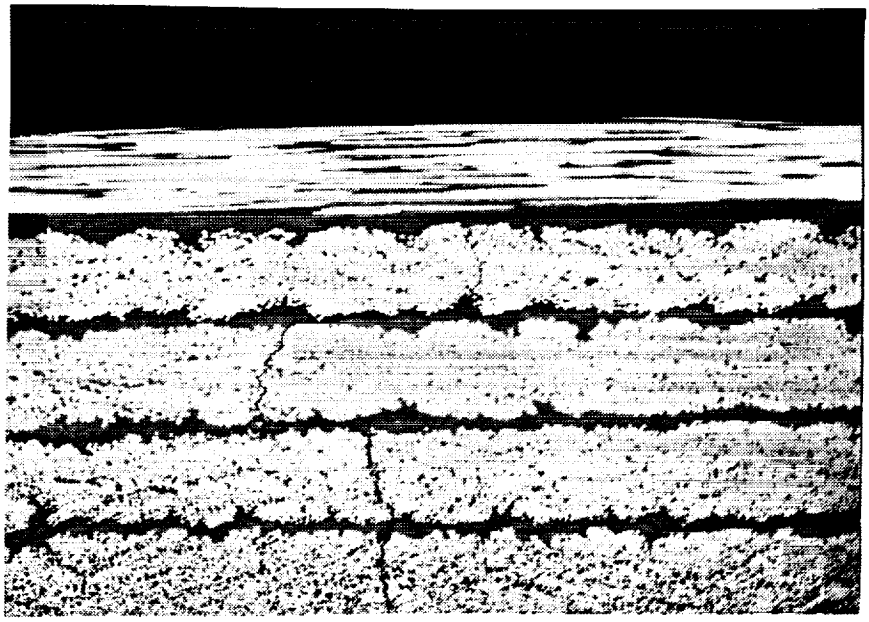

(b)

Figure 13 -Matrix Cracking in the $[0/45/-45/90]_s$ IM7/5260 Composite Laminate Magnified 100x

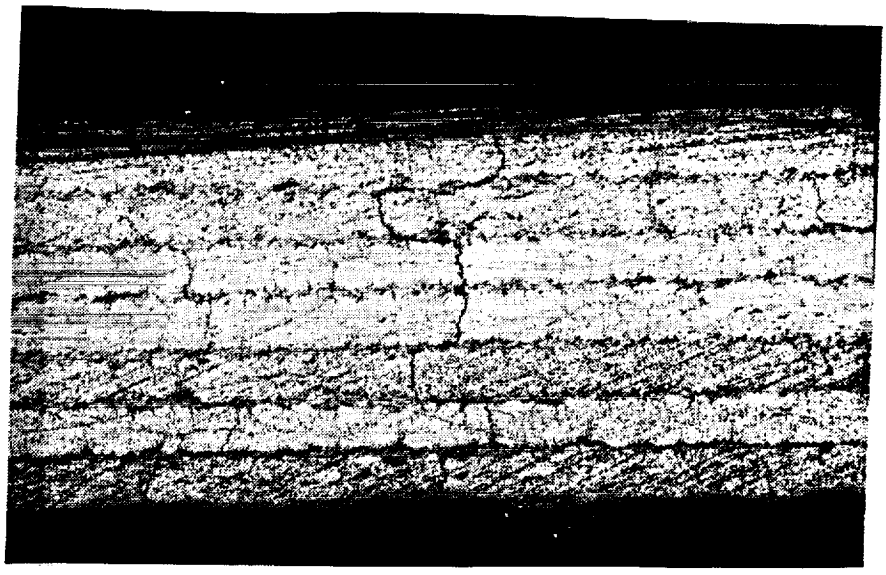

(a)

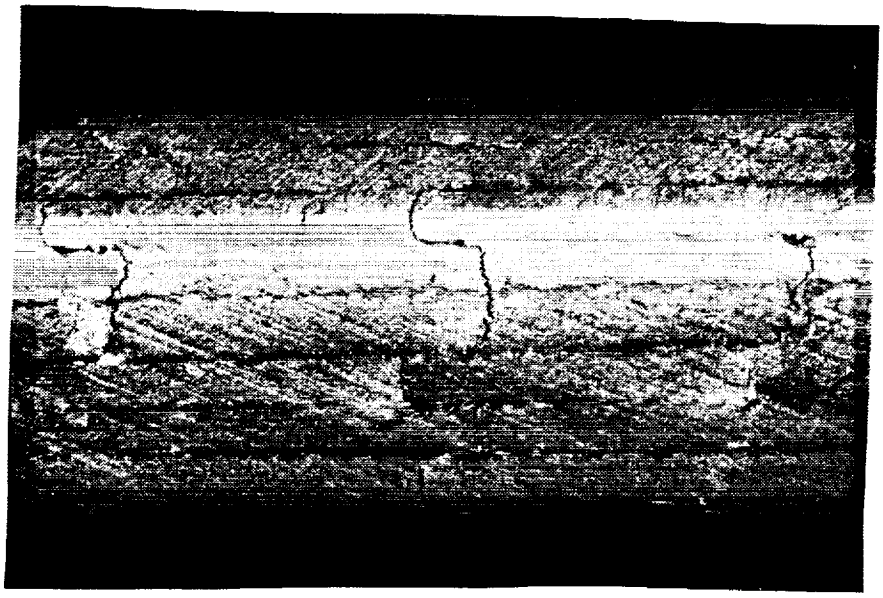

(b)

Figure 14 - Matrix Cracking in the $[45/-45]_{2s}$ IM7/5260 Composite Laminate Magnified 50x

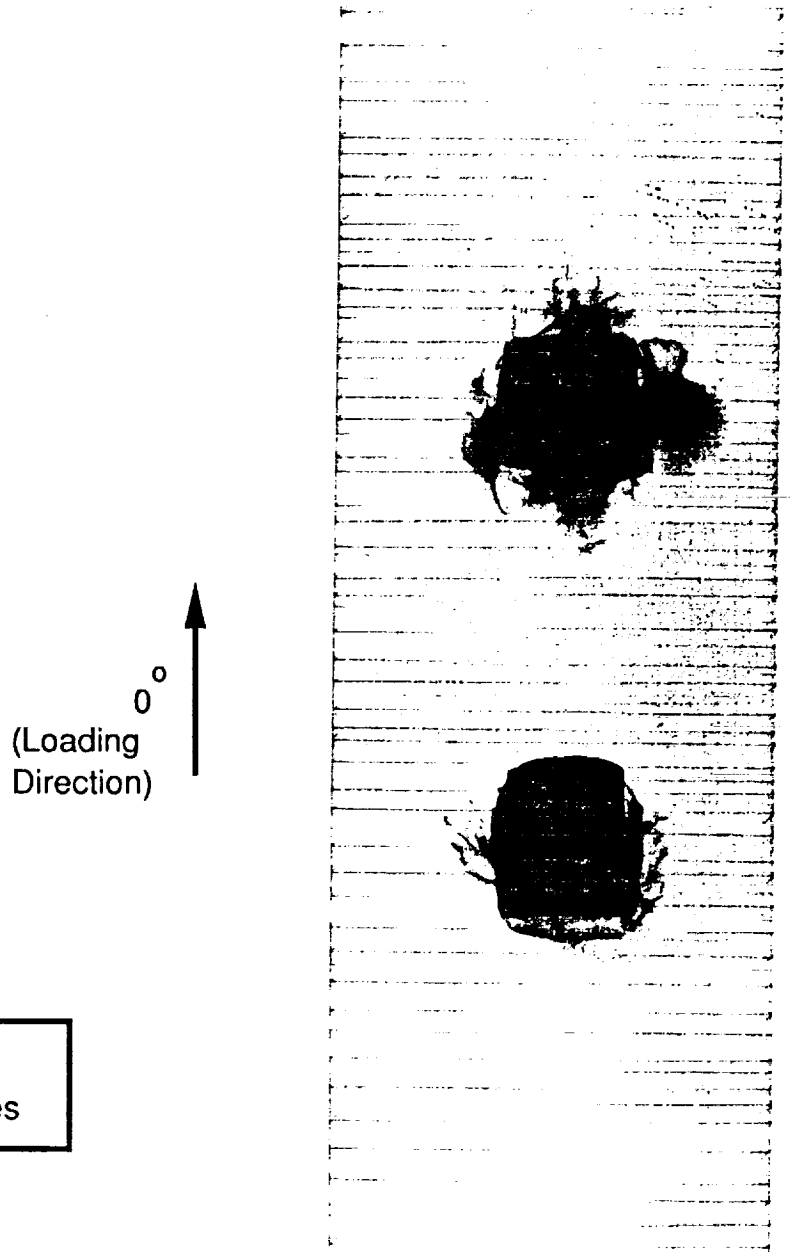

Figure 15 - X-Rays of Damaged 2.54 cm Wide $[0/45/-45/90]_s$ Laminates Subjected to Fatigue Loading. Max Stress = 494 MPa, R=0.1, f=5 Hz

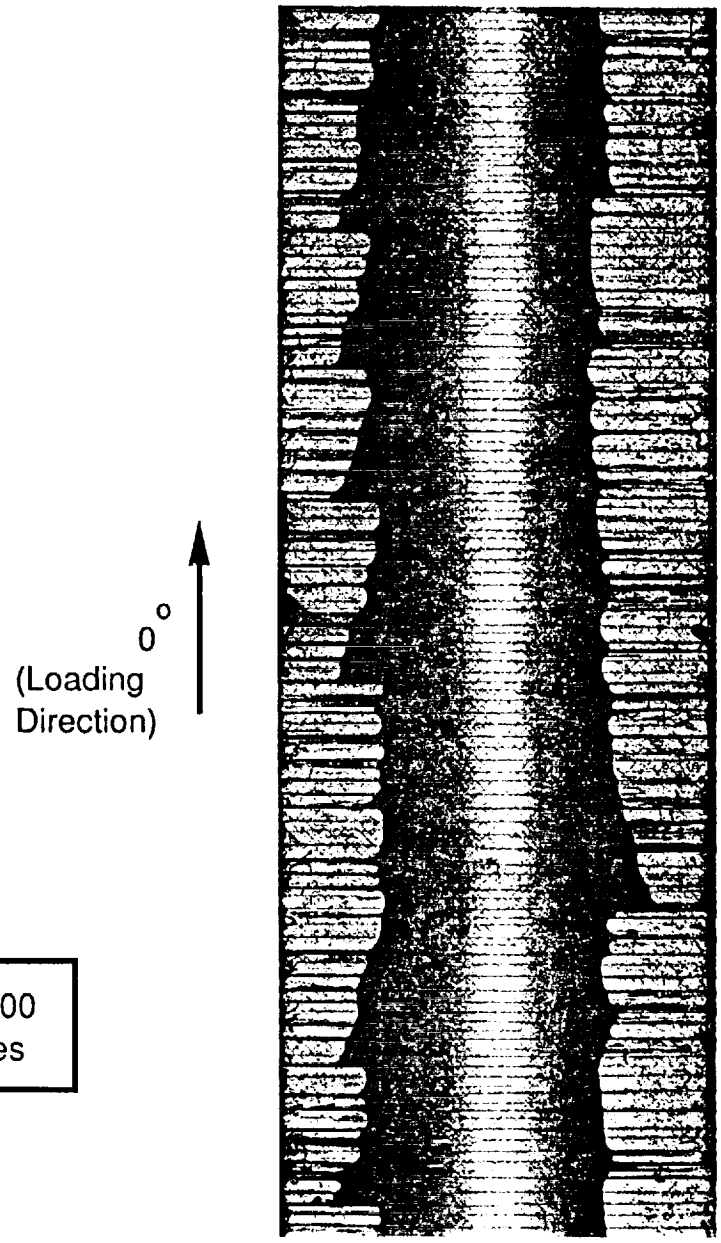

Figure 15 Cont'd

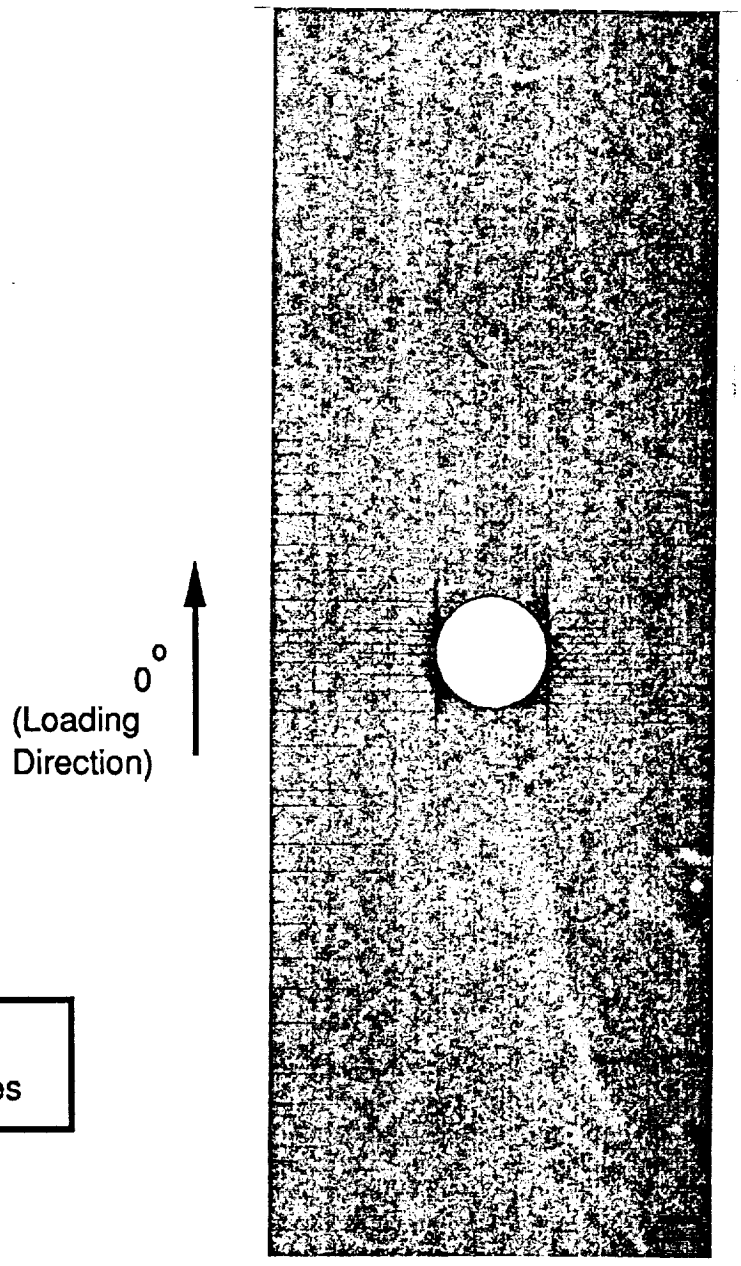

Figure 16 - X-Rays of Damaged 2.54 cm Wide $[0/45/-45/90]_s$ Centrally Notched Laminates Subjected to Fatigue Loading. Max Stress = 494 MPa, R=0.1, f=5 Hz

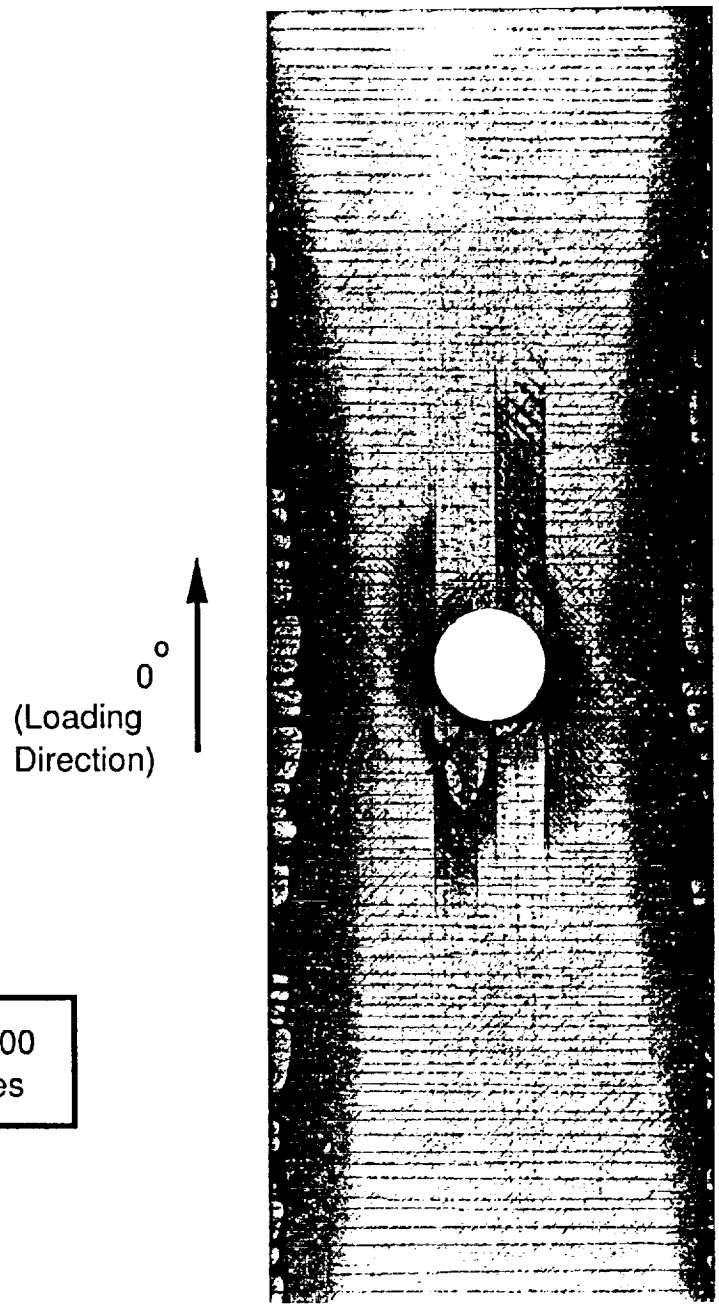

Figure 16 Cont'd

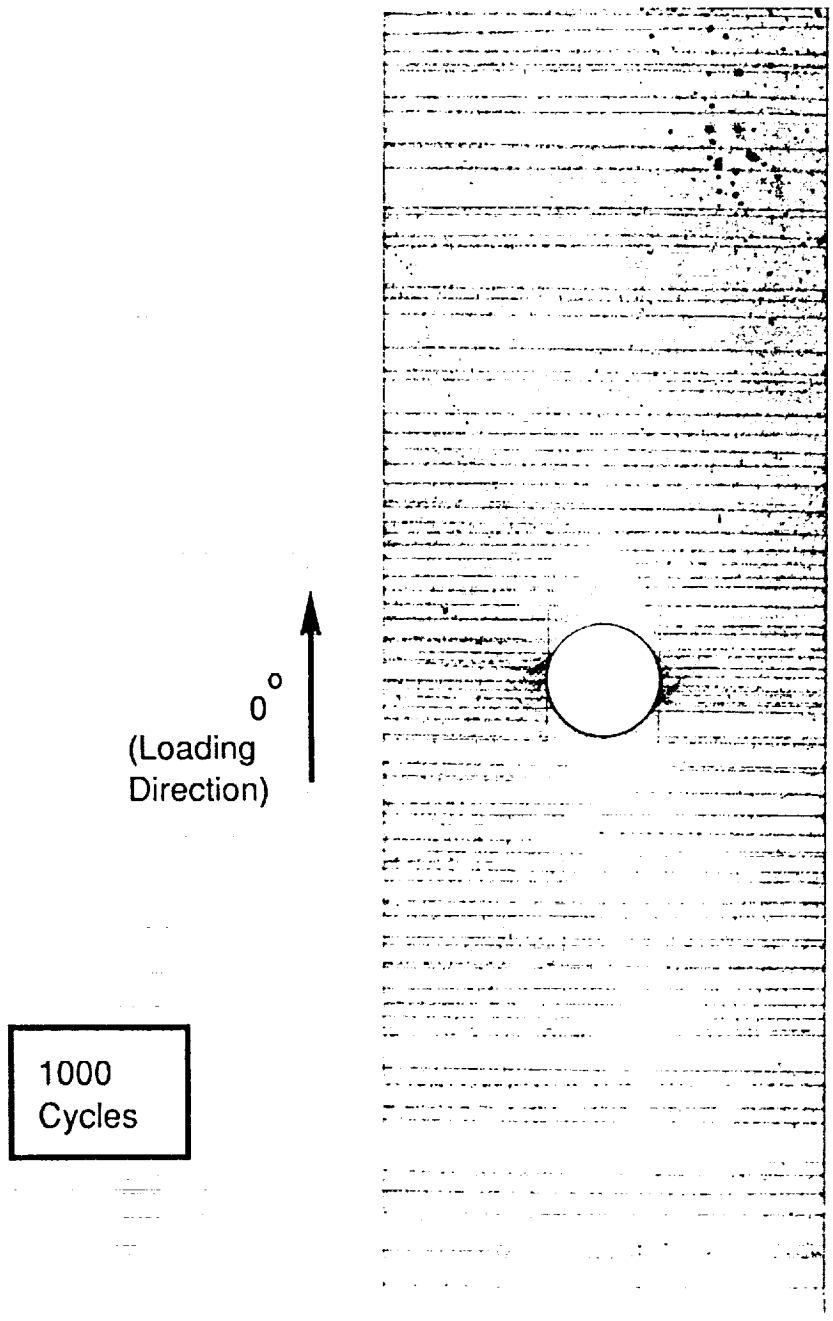

Figure 17 - X-Rays of Damaged 2.54 cm Wide $[90/-45/45/0]_S$ Centrally Notched Laminates Subjected to Fatigue Loading. Max Stress = 577 MPa, R=0.1, f=5 Hz

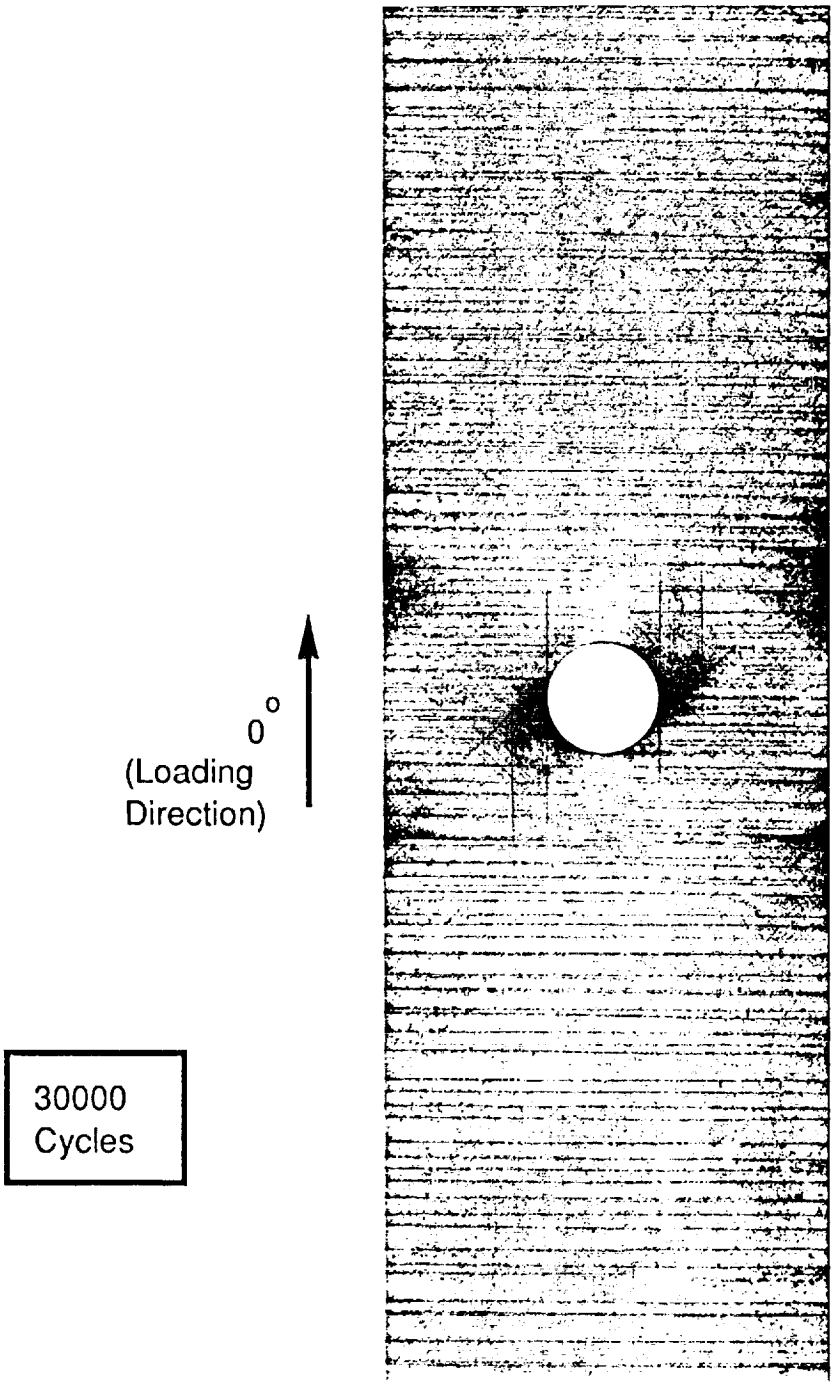

Figure 17 Cont'd

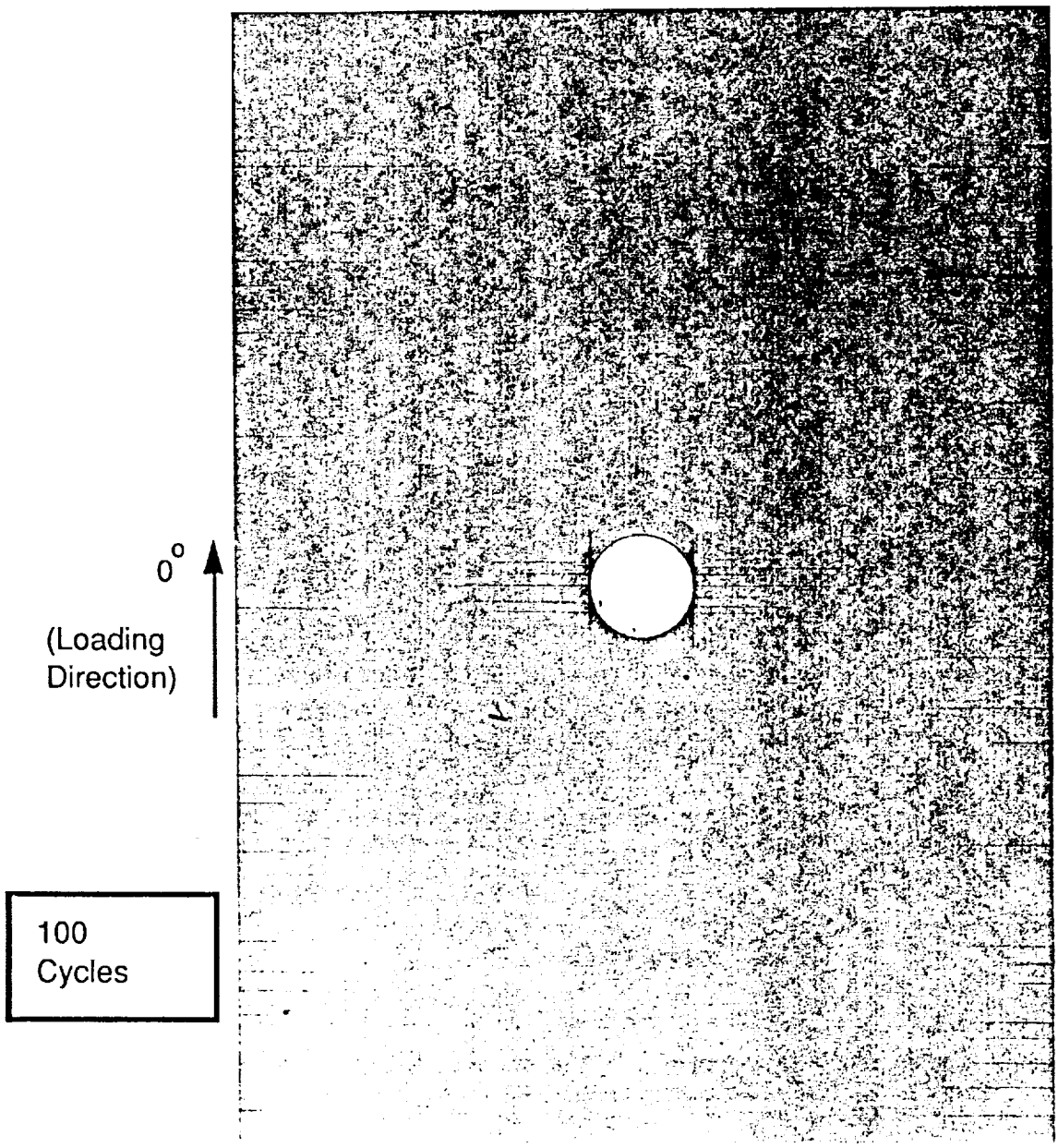

Figure 18 - X-Rays of Damaged 5.08 cm Wide $[0/45/-45/90]_s$ Centrally Notched Laminates Subjected to Fatigue Loading. Max Stress = 494 MPa, R=0.1, f=5 Hz

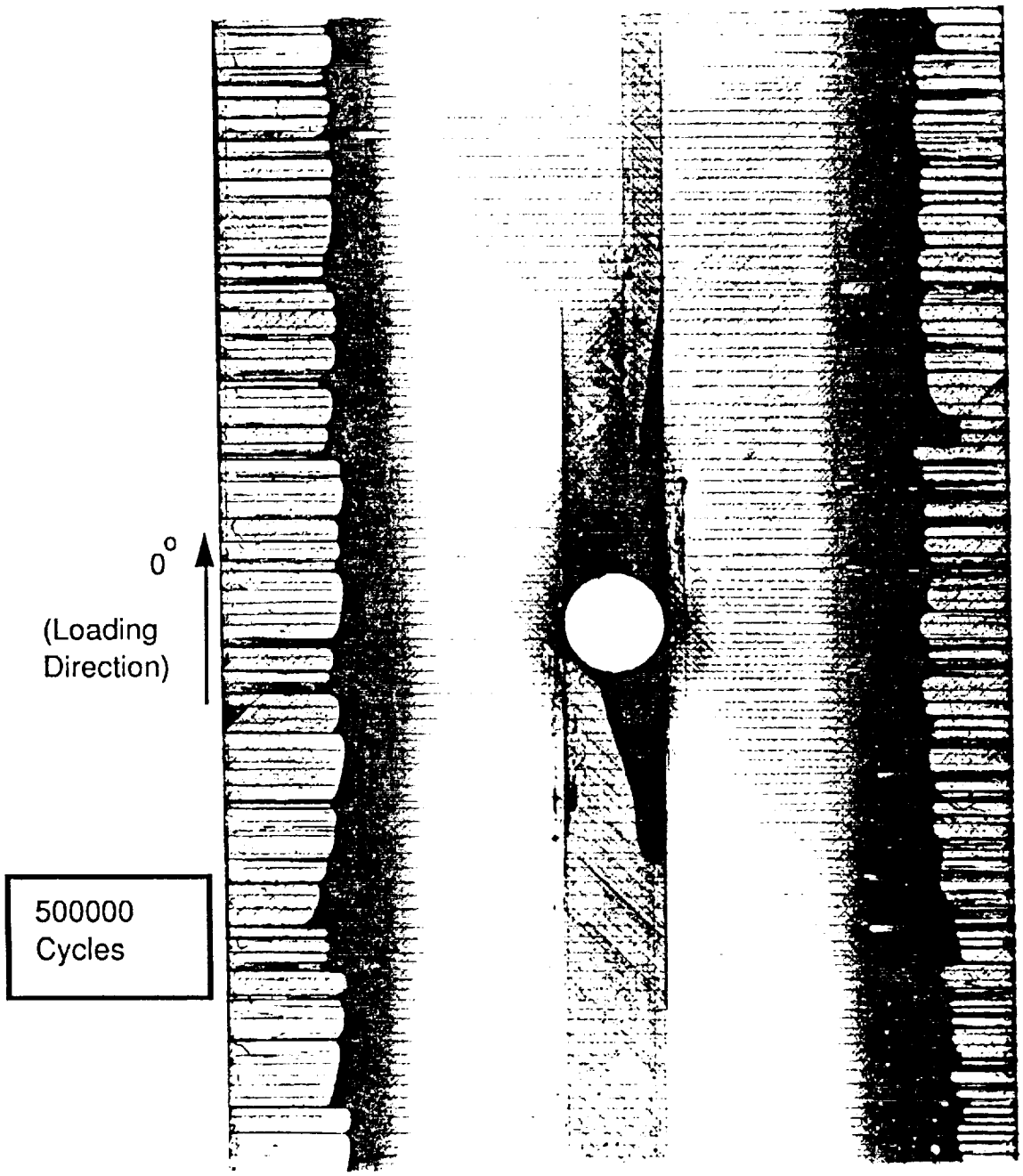

Figure 18 Cont'd

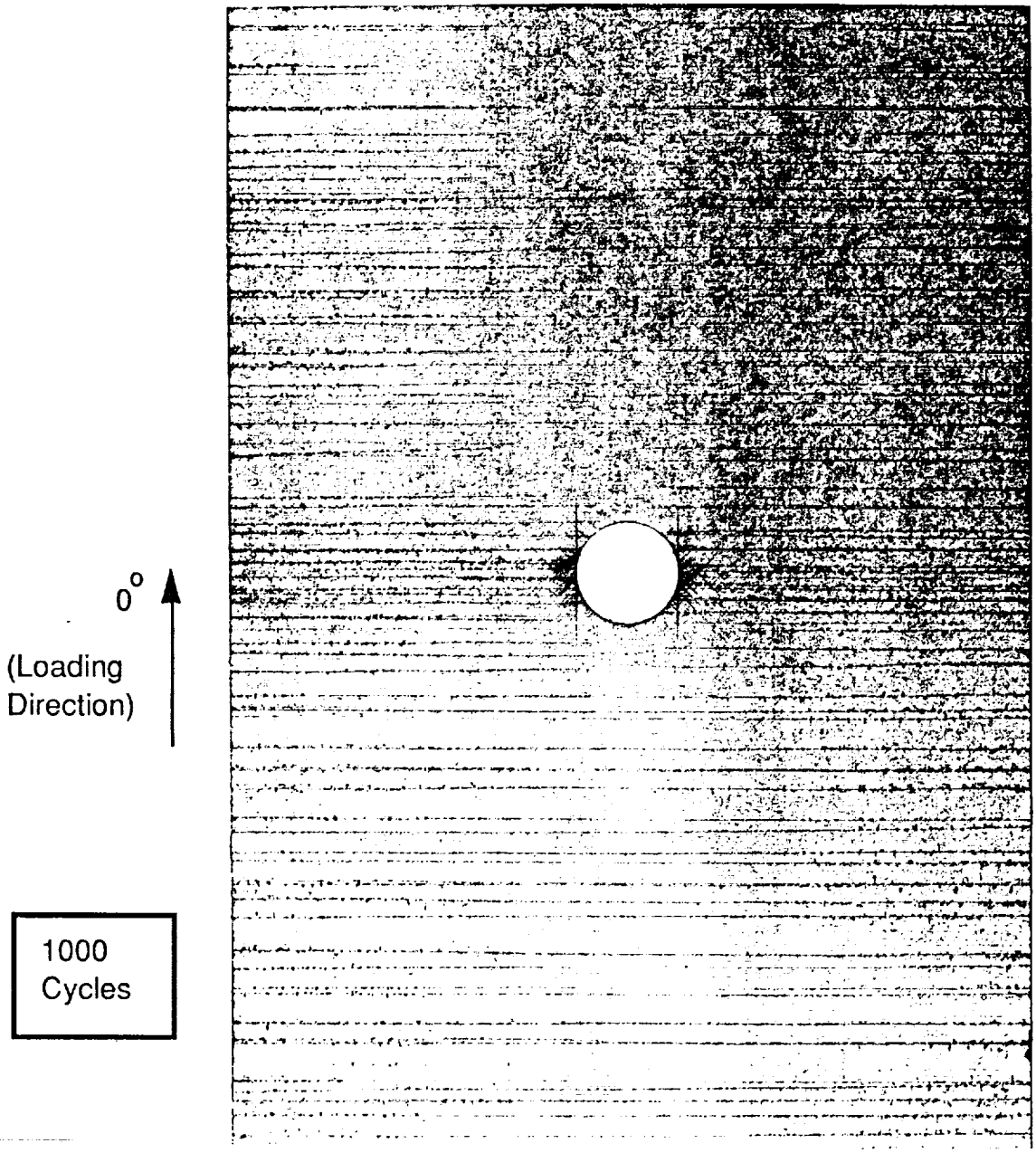

Figure 19 - X-Rays of Damaged 5.08 cm Wide $[90/-45/45/0]_s$ Centrally Notched Laminates Subjected to Fatigue Loading. Max Stress = 494 MPa, R=0.1, f=5 Hz

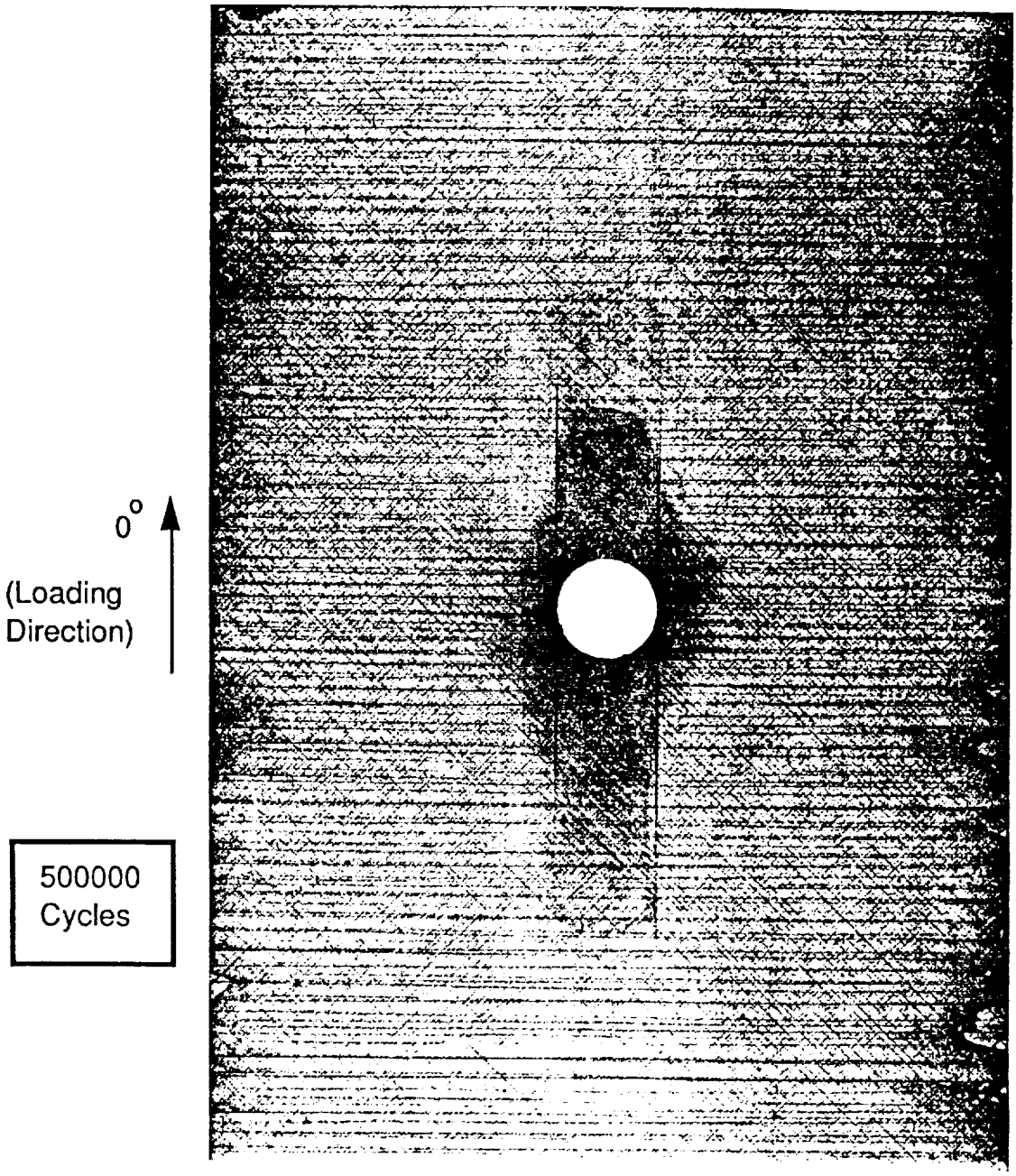

Figure 19 Cont'd

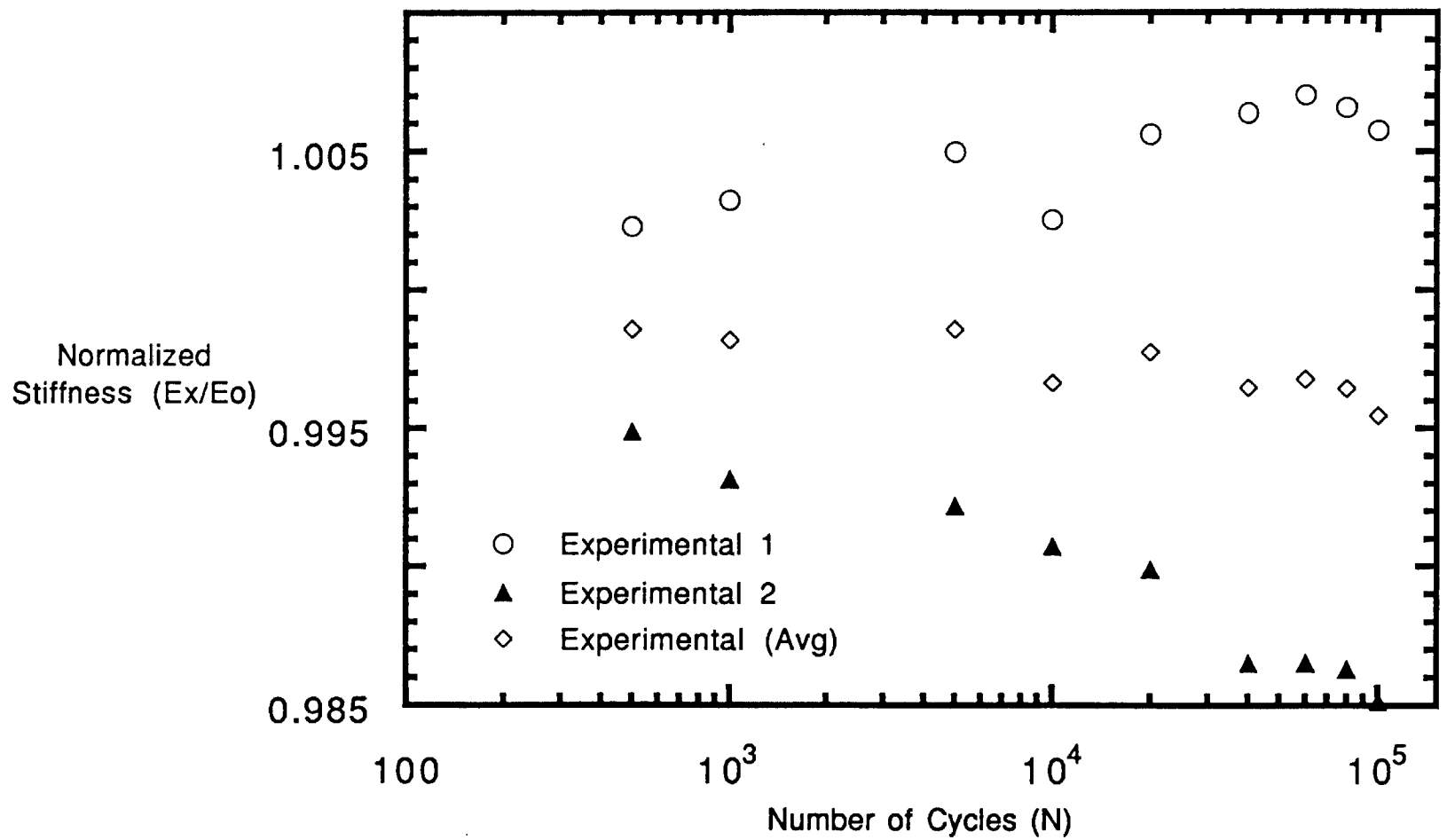

Figure 20 - Experimental Normalized Stiffness for the $[0/90/0]_s$ IM7/5260 Composite Laminates

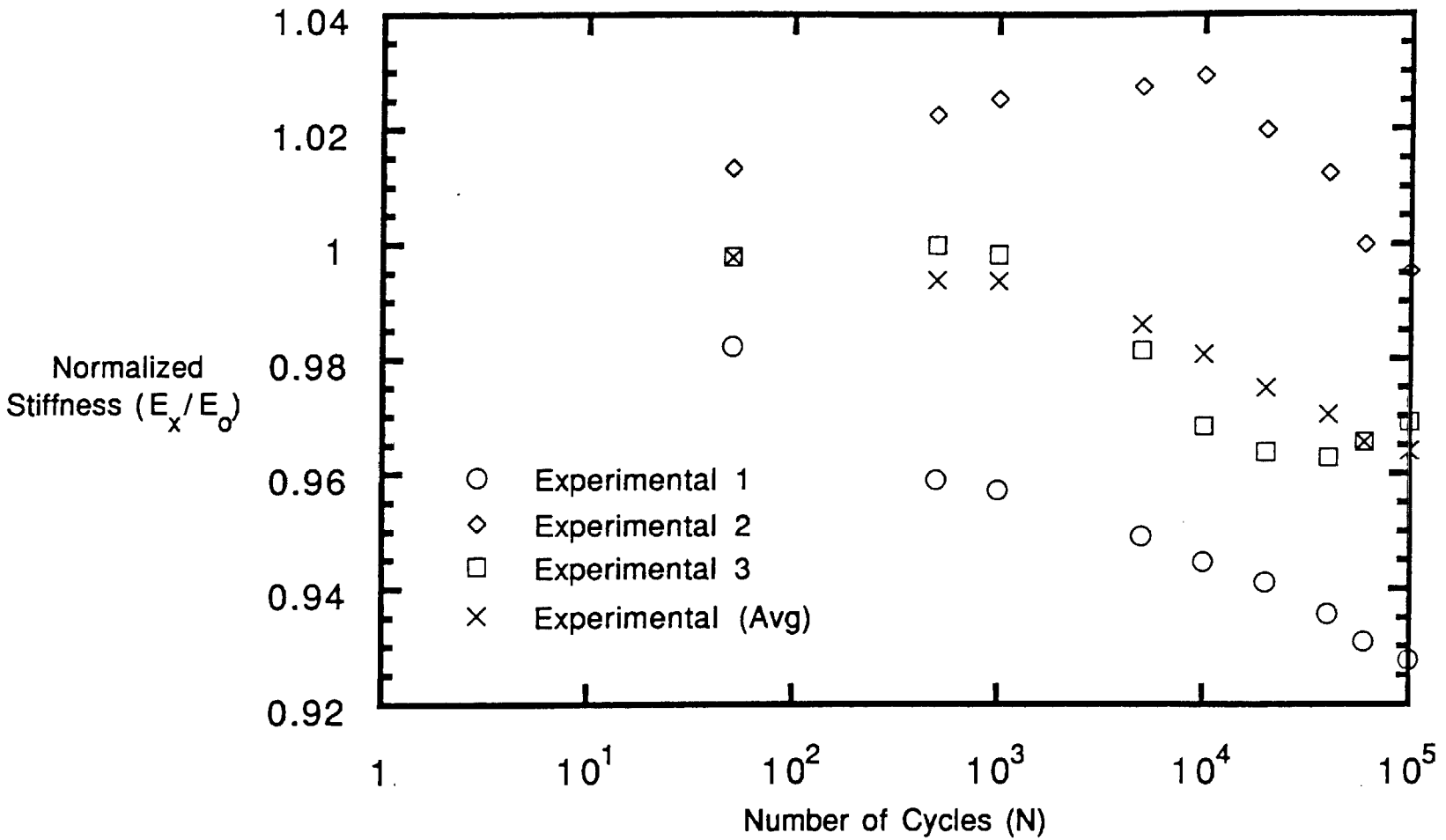

Figure 21 - Experimental Normalized Stiffness for $[0/90_2/0]_s$ IM7/5260 Composite Laminates

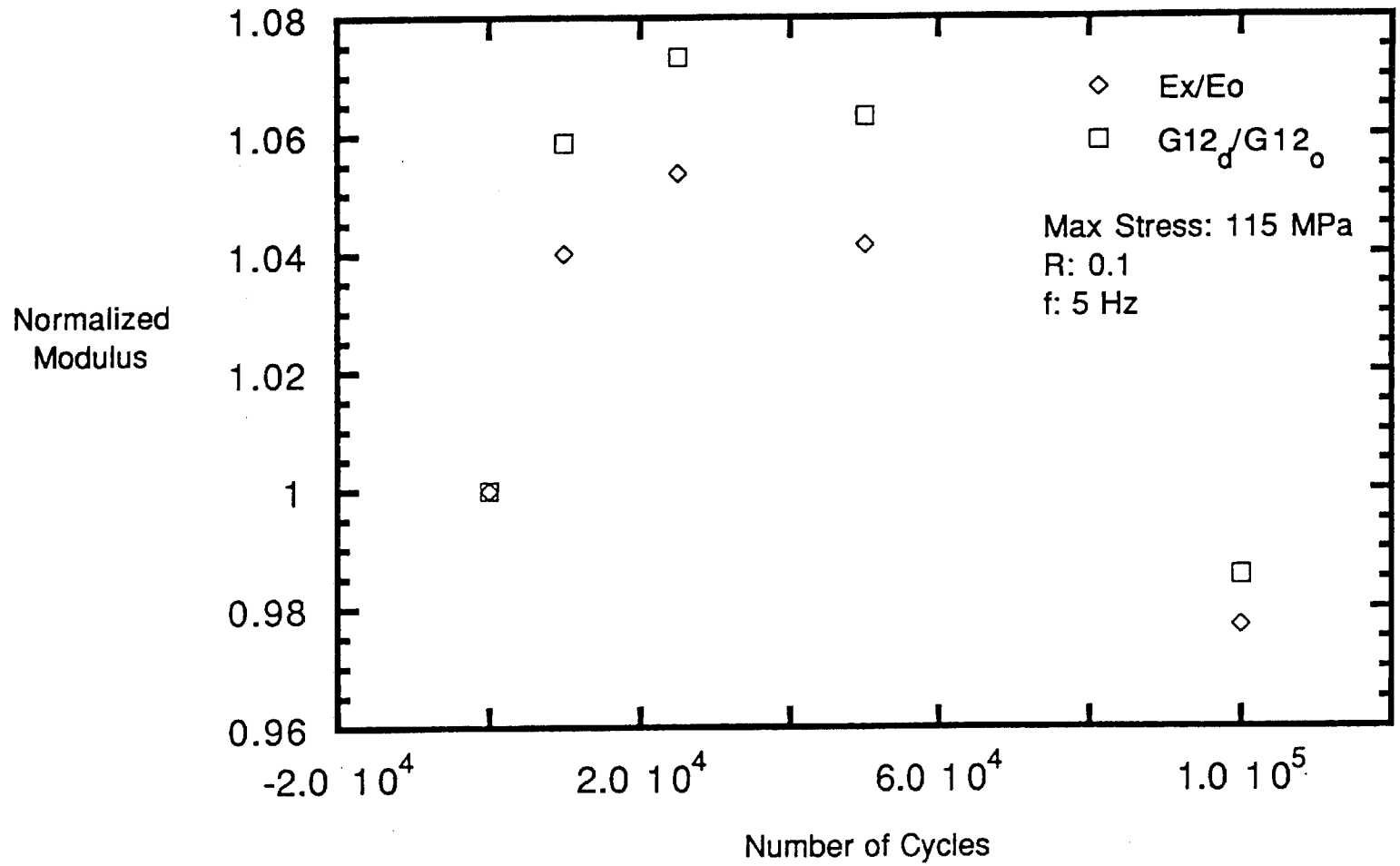

Figure 22 - Normalized Stiffness and Shear Modulus for a 2.54 cm Wide $[45/-45]_{2s}$ IM7/5260 Laminated Composite

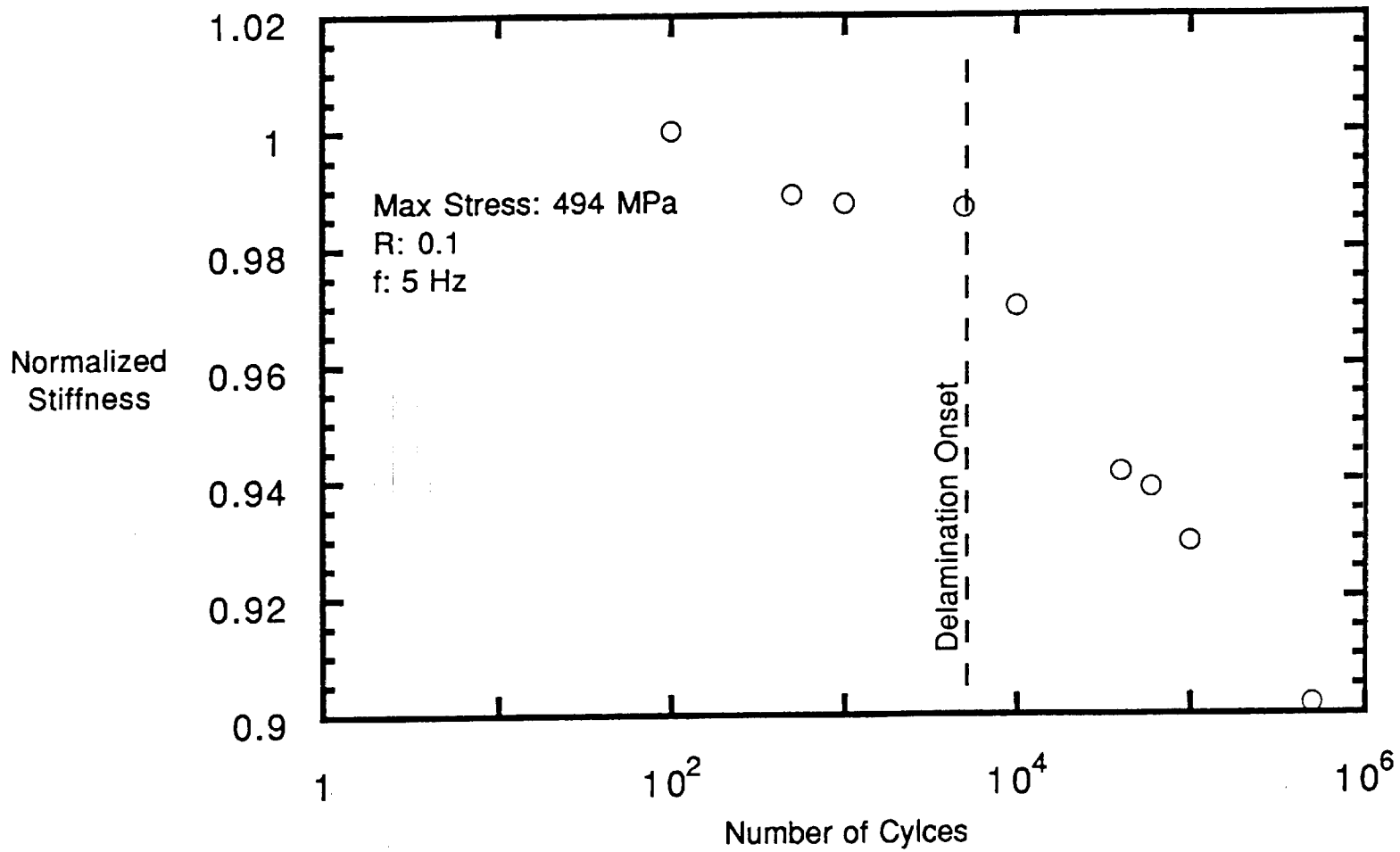

Figure 23 - Experimental Stiffness Loss of a $[0/45/-45/90]_s$ IM7/5260 2.54 cm Wide Laminated Composite

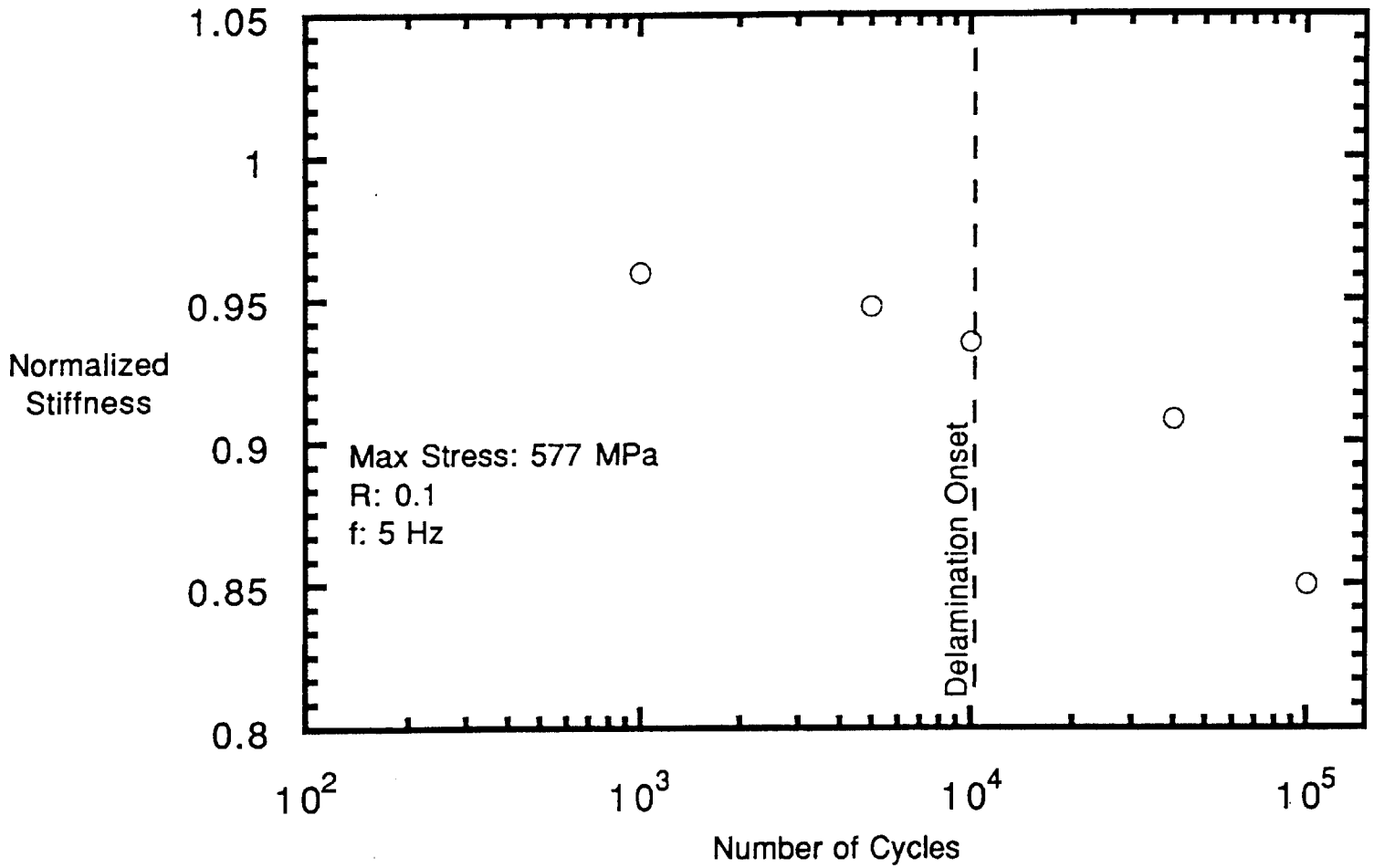

Figure 24 - Experimental Stiffness Loss of a $[90/-45/45/0]_s$ IM7/5260 2.54 cm Wide Laminated Composite

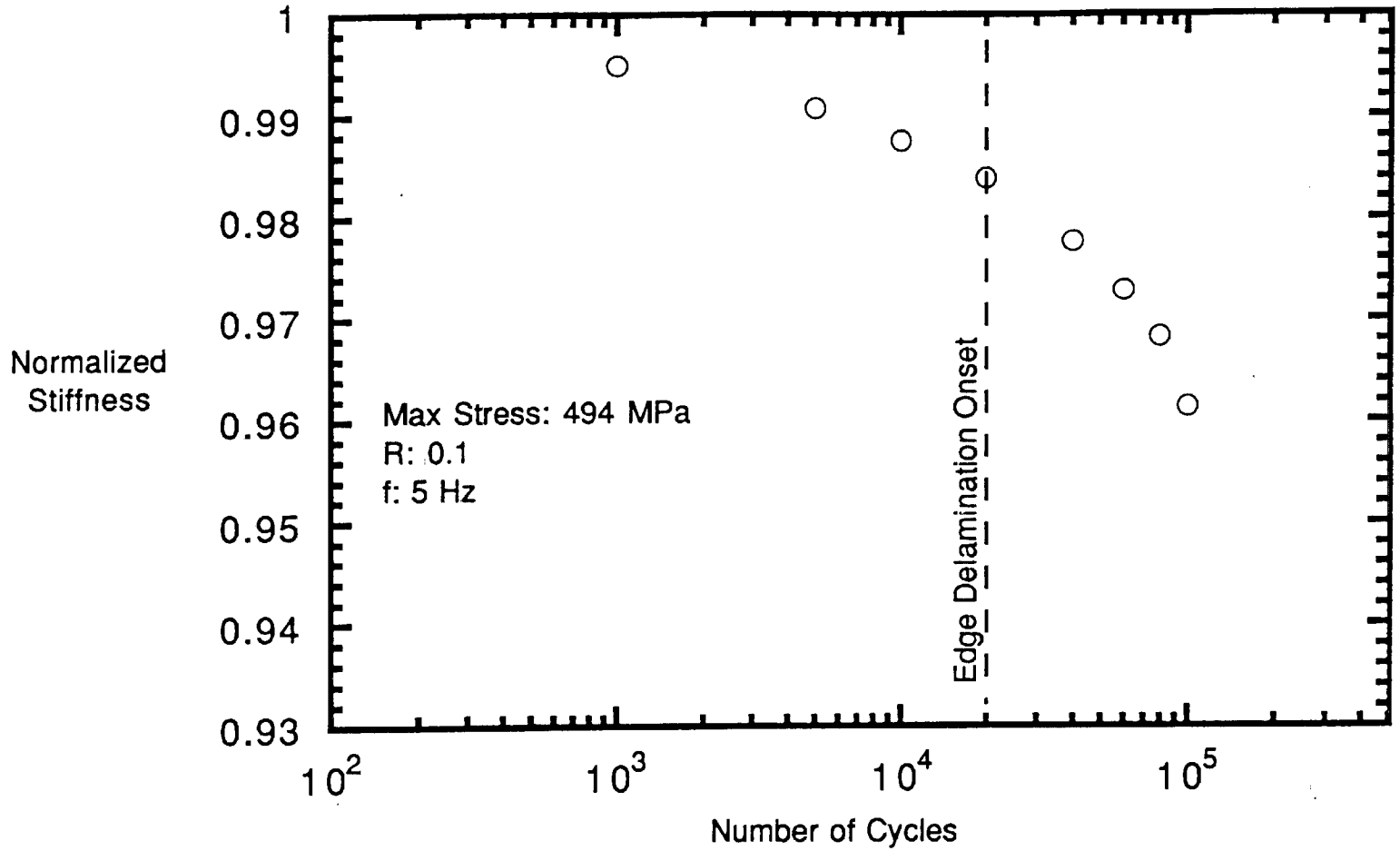

Figure 25 - Experimental Stiffness Loss of a $[0/45/-45/90]_s$ 2.54 cm Wide IM7/5260 Laminated Composite With a 6.35 mm Central Hole

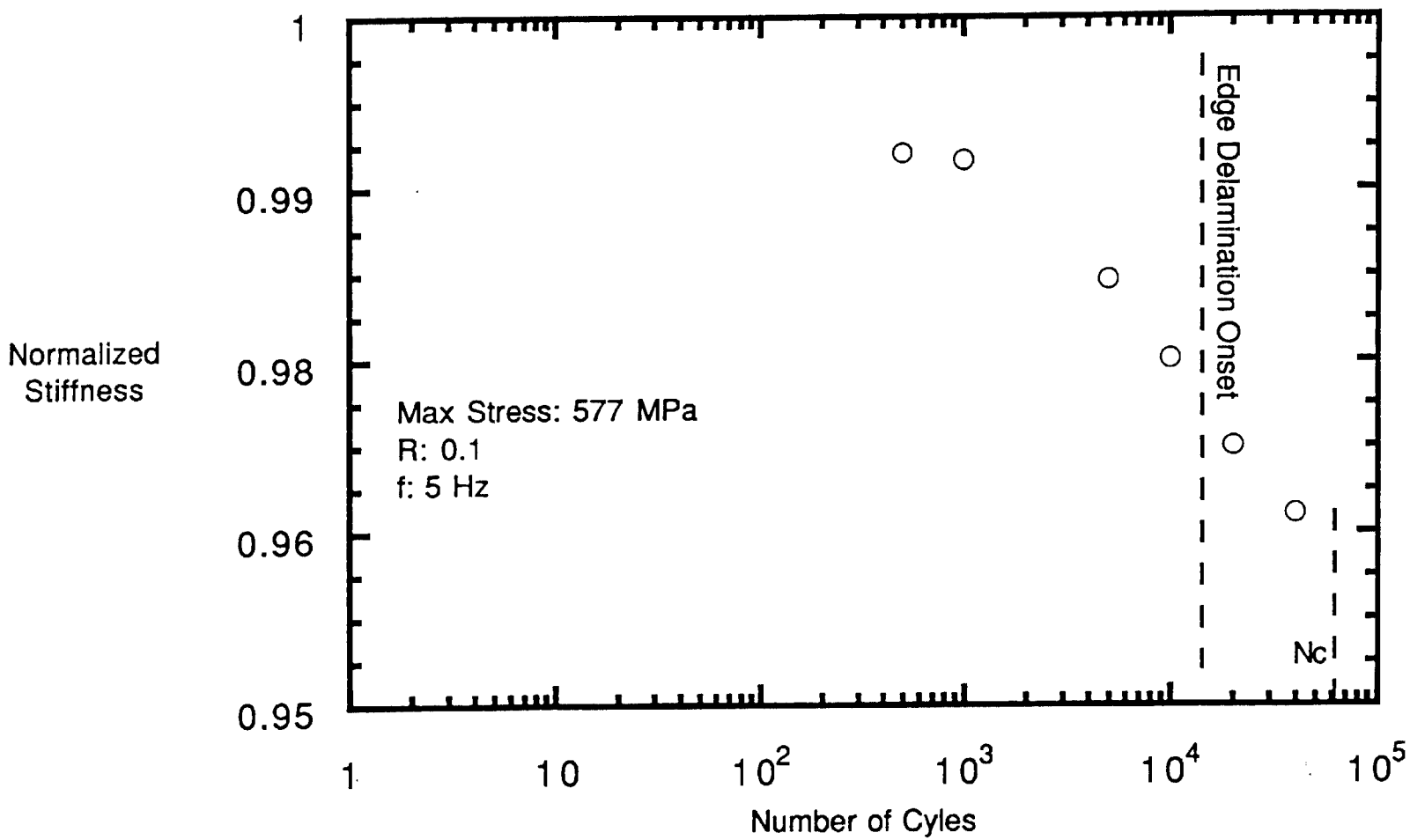

Figure 26 - Experimental Stiffness Loss of a $[90/-45/45/0]_s$ 2.54 cm Wide IM7/5260 Laminated Composite With Central 6.35 mm hole

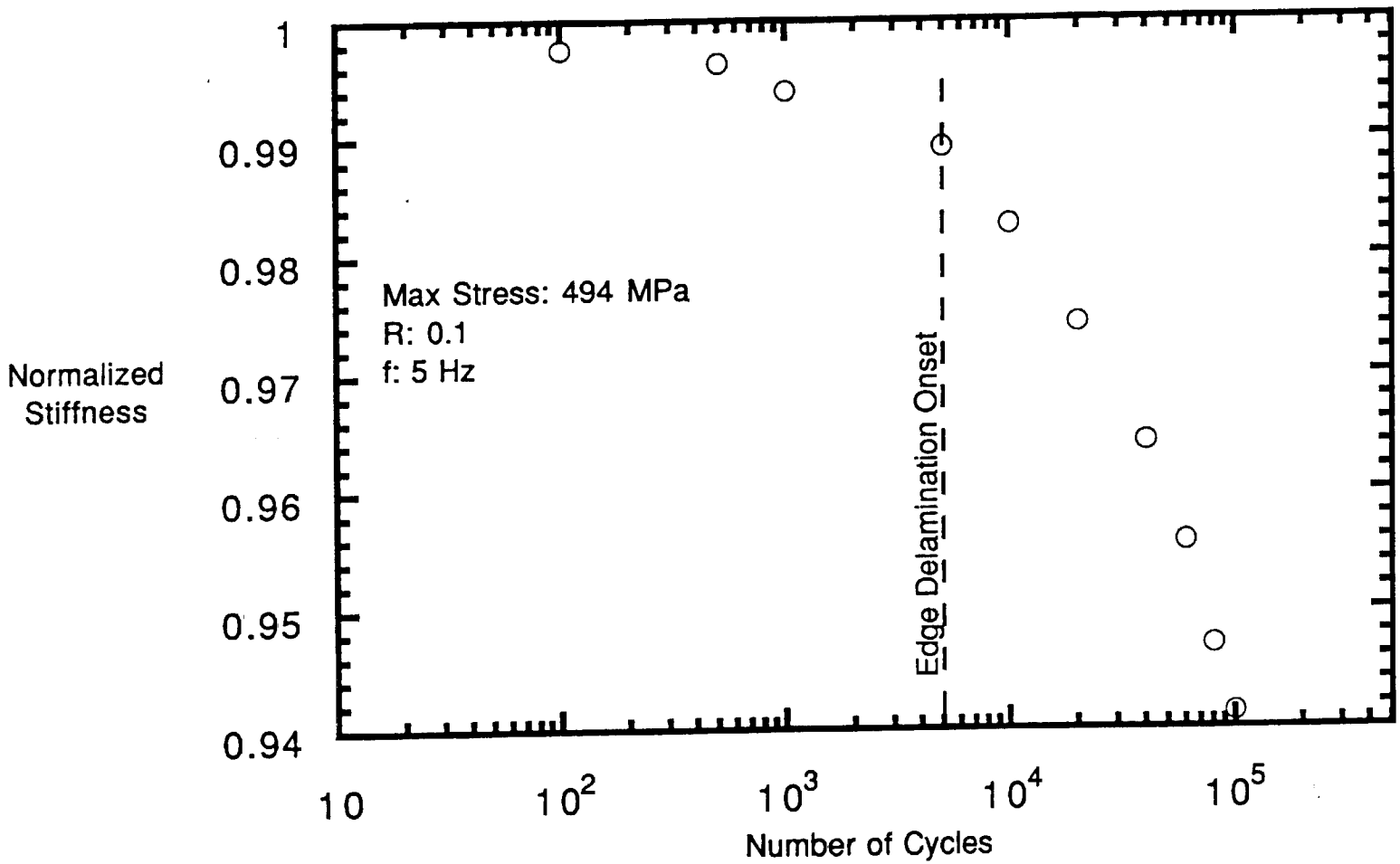

Figure 27 - Experimental Stiffness Loss of a $[0/45/-45/90]_s$ 5.08 cm Wide IM7/5260 Laminated Composite With Central 6.35 mm Hole

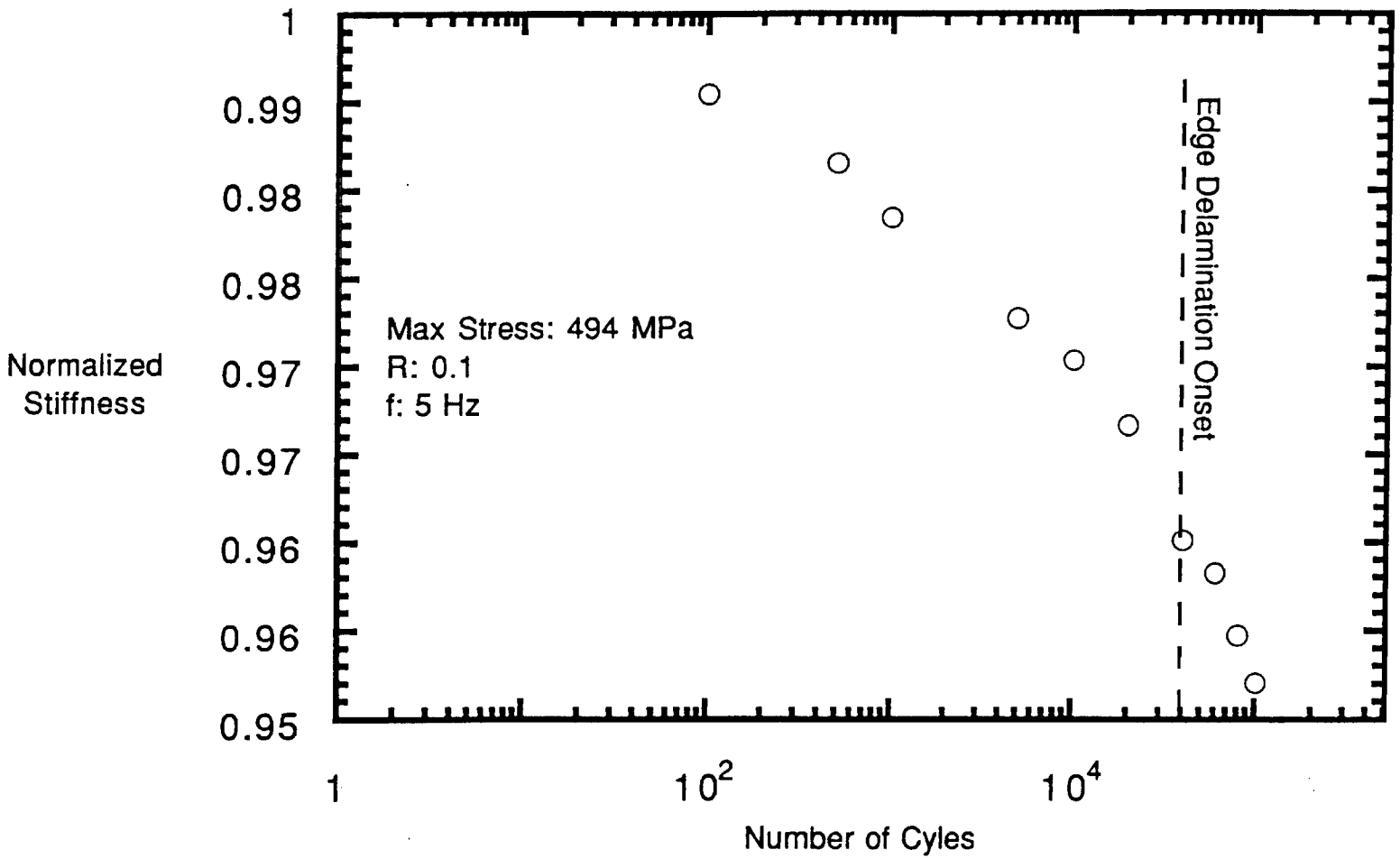

Figure 28 - Experimental Stiffness Loss of a $[90/-45/45/0]_s$ 5.08 cm Wide IM7/5260 Laminated Composite With Central 6.35 mm Hole

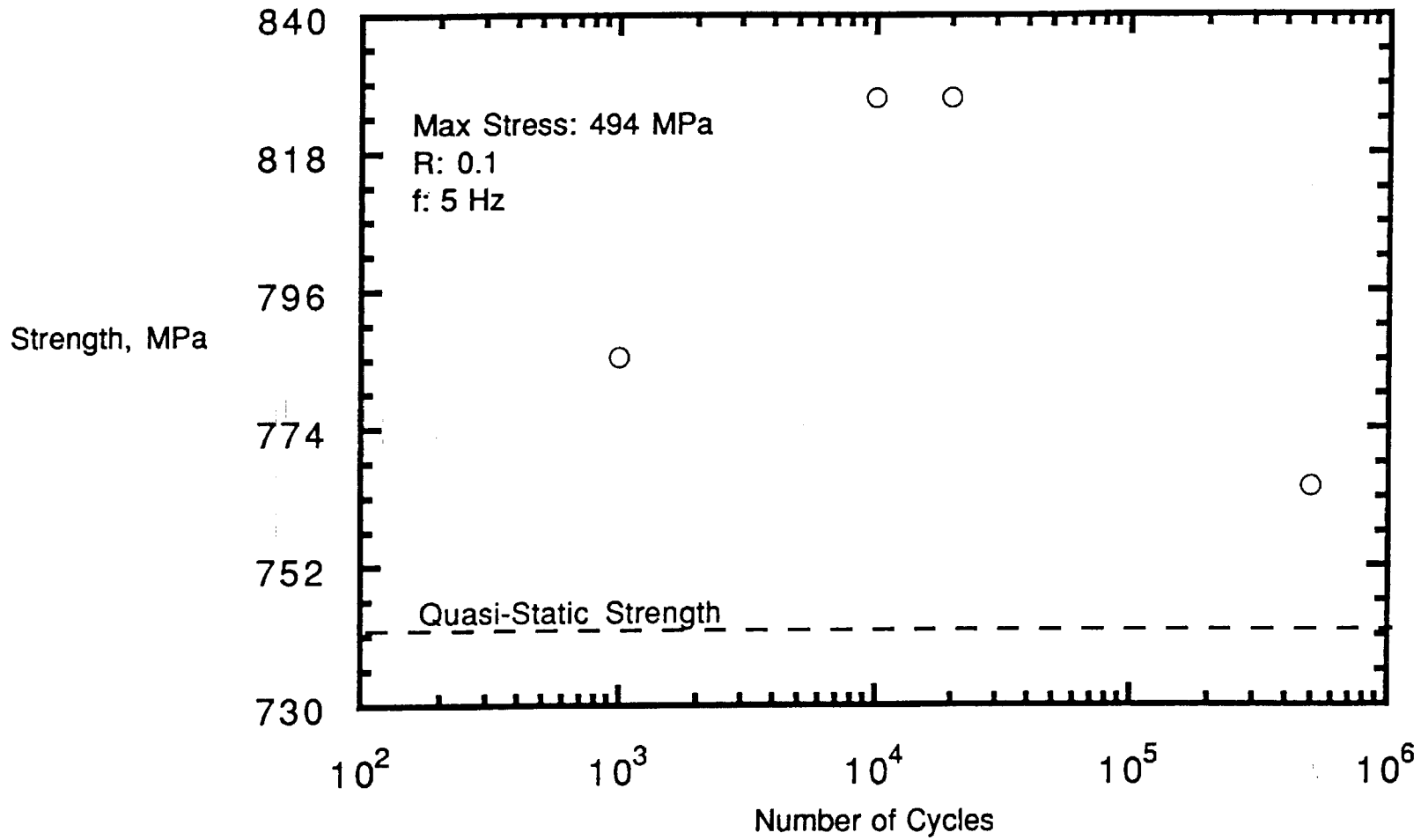

Figure 29 - Experimental Residual Strength of a $[0/45/-45/90]_s$ IM7/5260 2.54 cm Wide Laminated Composite

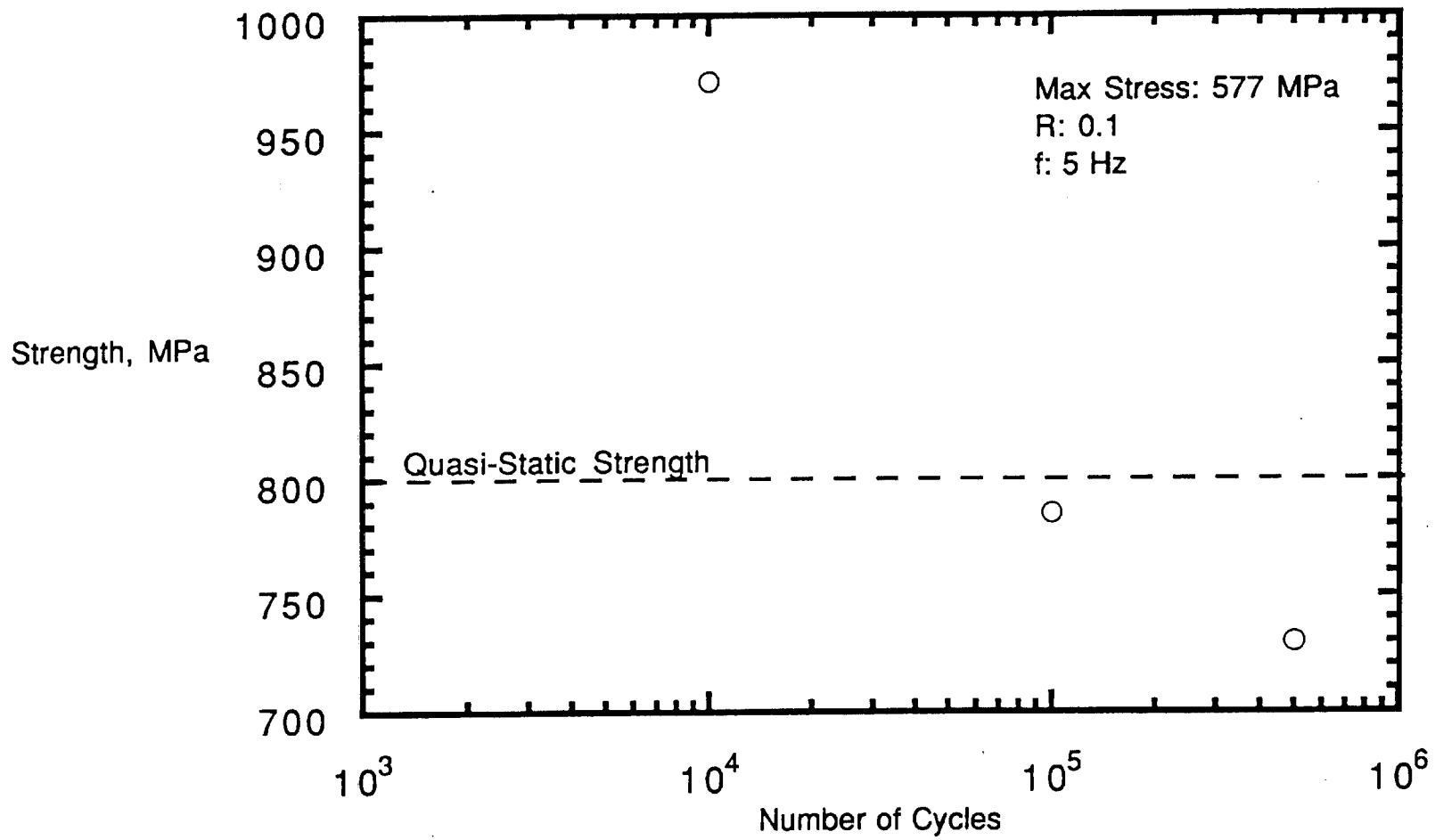

Figure 30 - Experimental Residual Strength of a $[90/-45/45/0]_s$ IM7/5260 2.54 cm Wide Laminated Composite

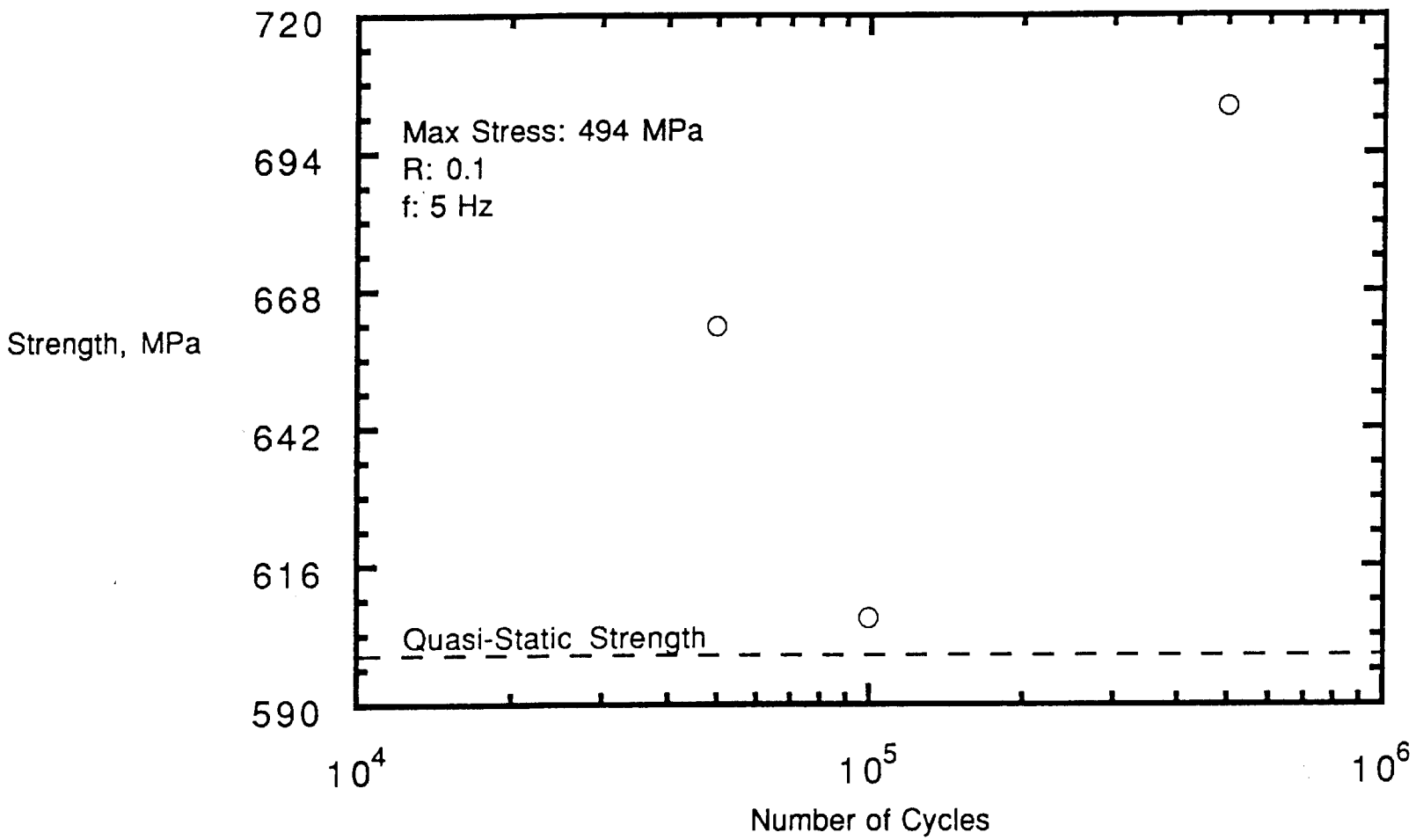

Figure 31 - Experimental Residual Strength of a $[0/45/-45/90]_s$ 2.54 cm Wide IM7/5260 Laminated Composite With Central 6.35 mm Hole

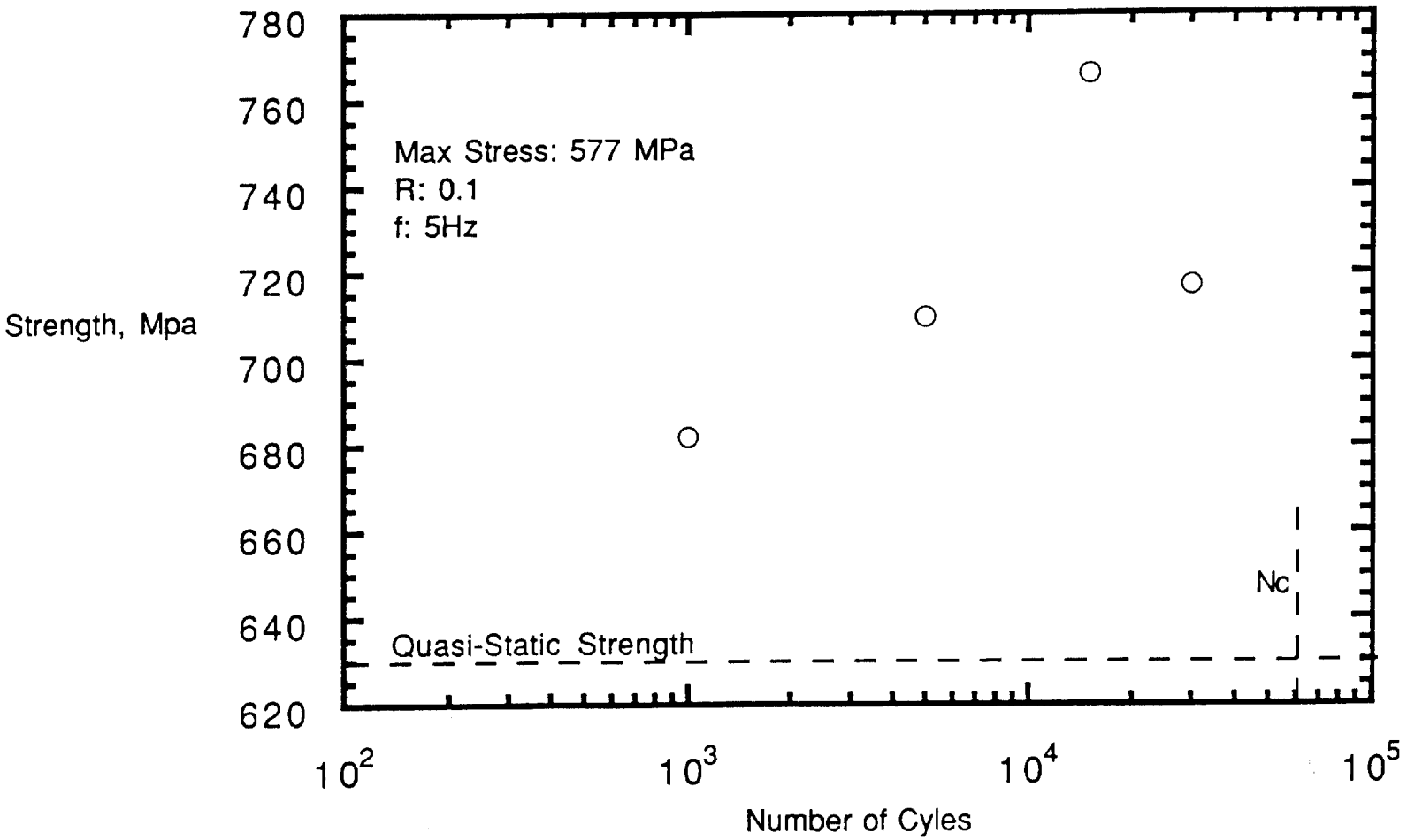

Figure 32 - Experimental Residual Strength of a $[90/-45/45/0]_s$ 2.54 cm Wide IM7/5260 Laminated Composite With a Central 6.35 mm Hole

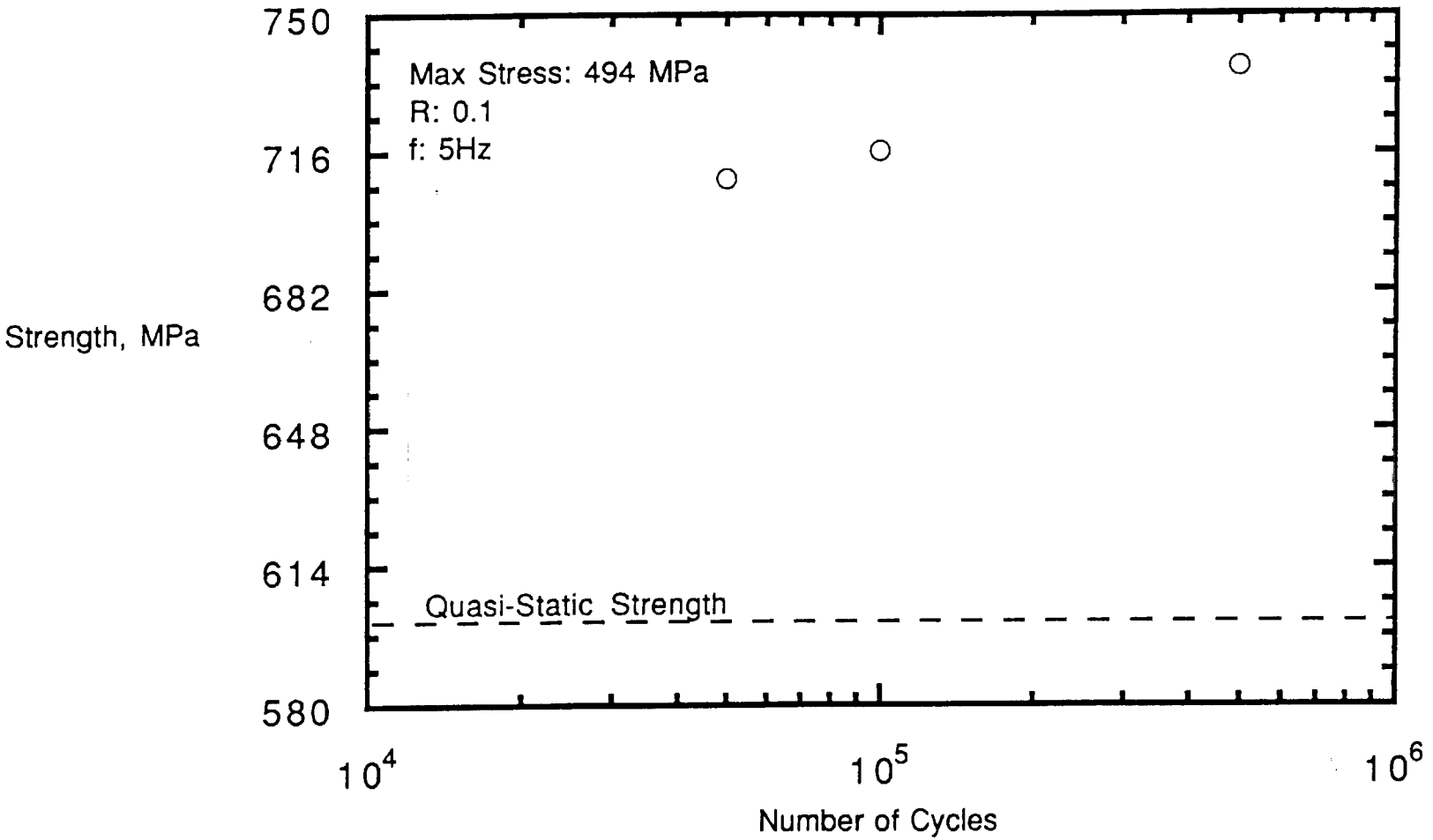

Figure 33 - Experimental Residual Strength of a $[0/45/-45/90]_s$ 5.08 cm Wide IM7/5260 Laminated Composite With Central 6.35 mm Hole

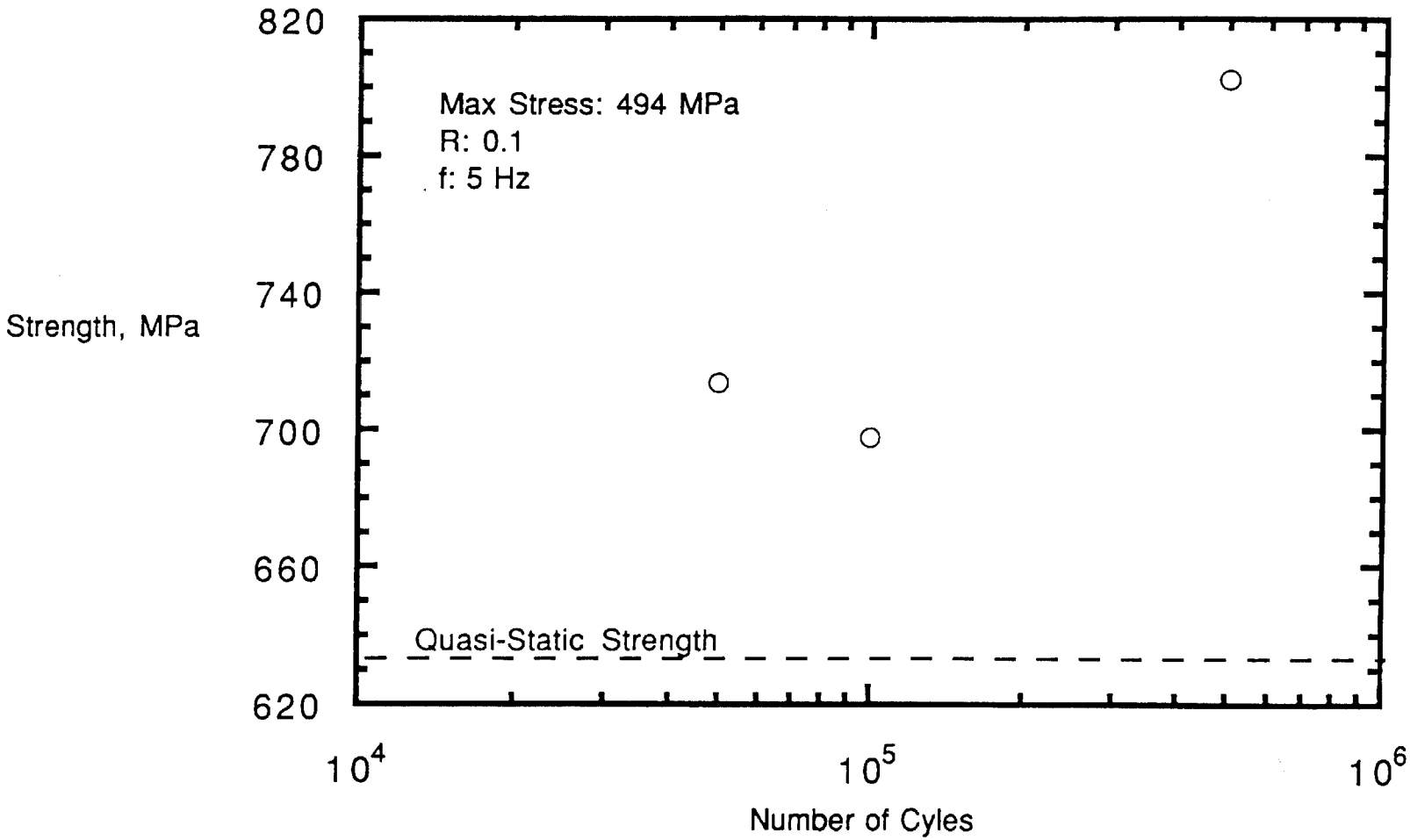

Figure 34 - Experimental Residual Strength of a 5.08 cm Wide $[90/-45/45/0]_s$ IM7/5260 Laminated Composite With Central 6.35 mm Hole

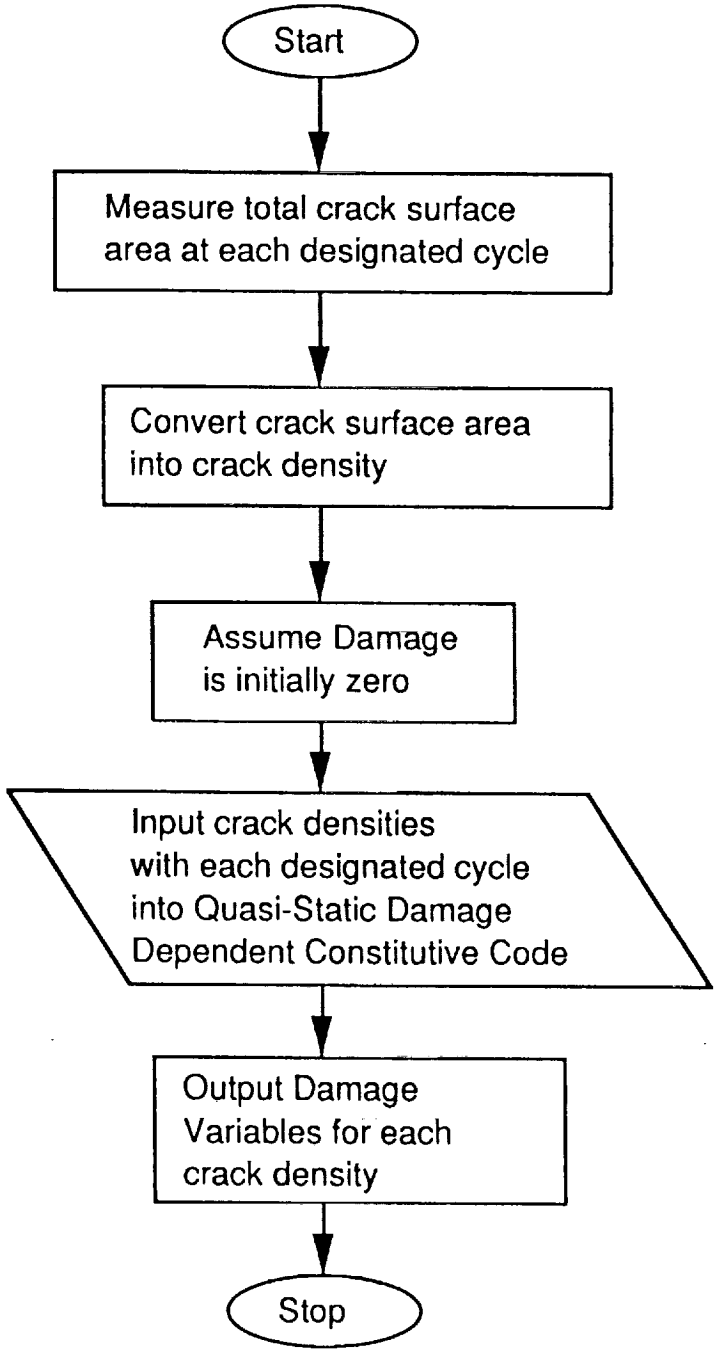

Figure 35 - Internal State Variable Calculation Scheme

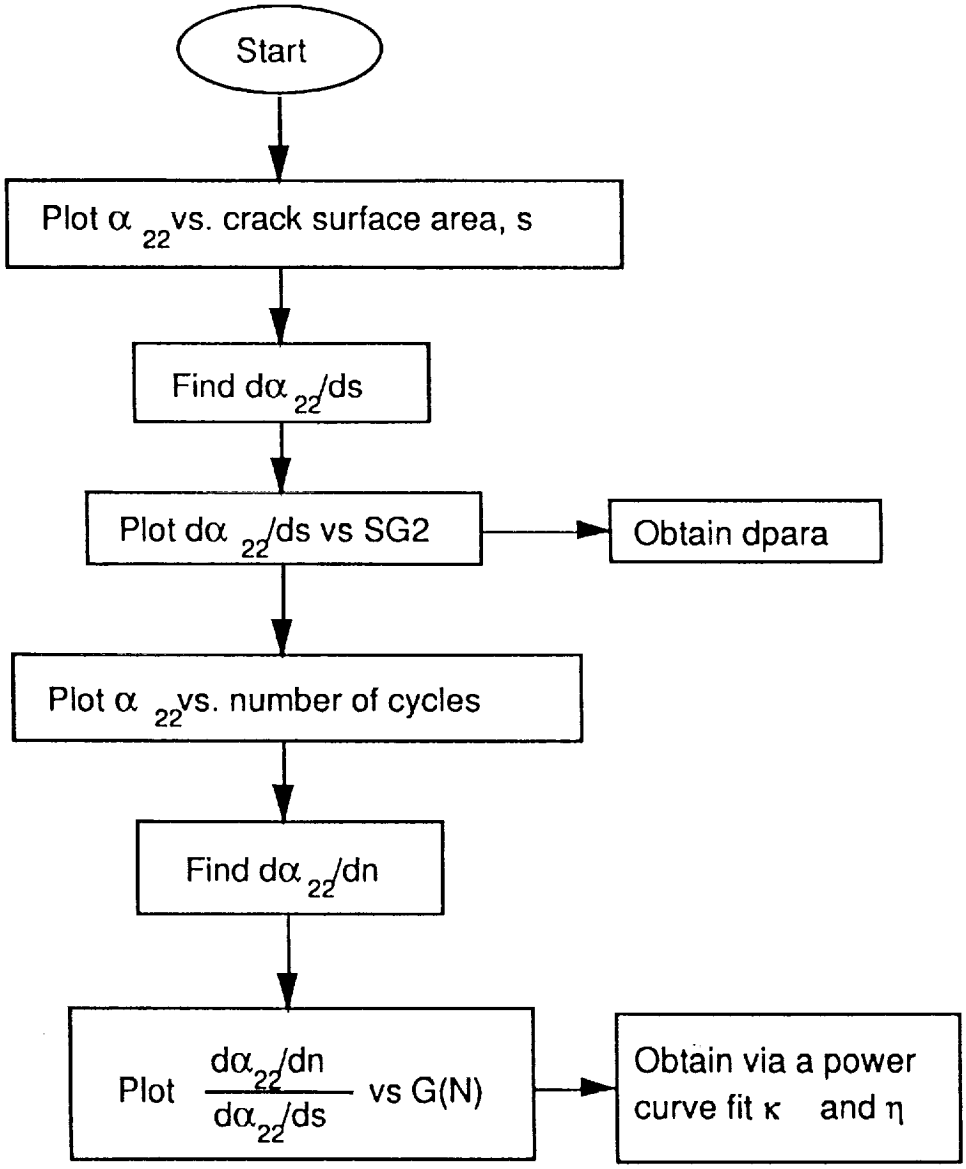

Figure 36 - Model Parameter Calculation Scheme

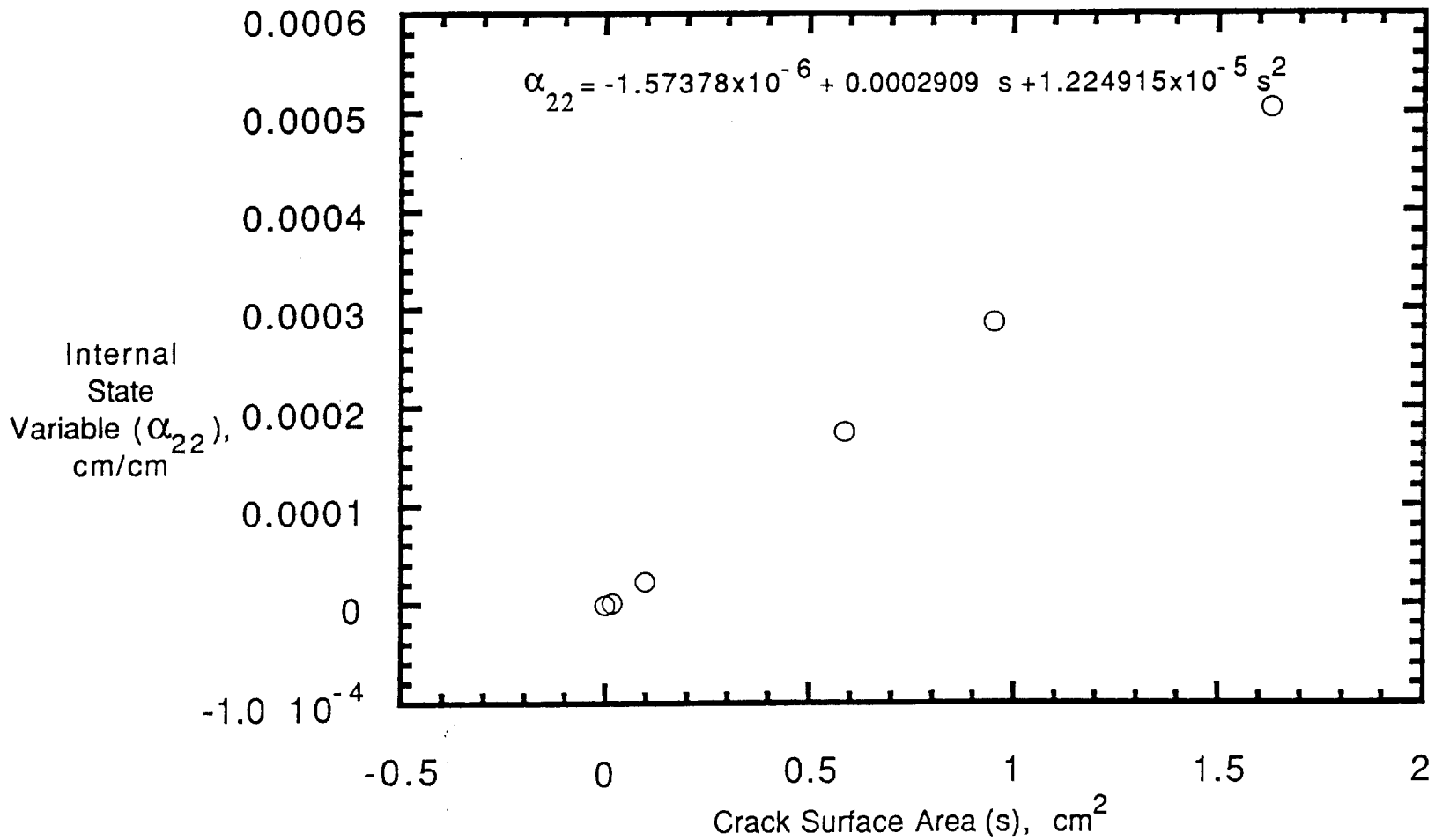

Figure 37 - Internal State Variable As a Function of Crack Surface Area for IM7/5260 Composite Laminates

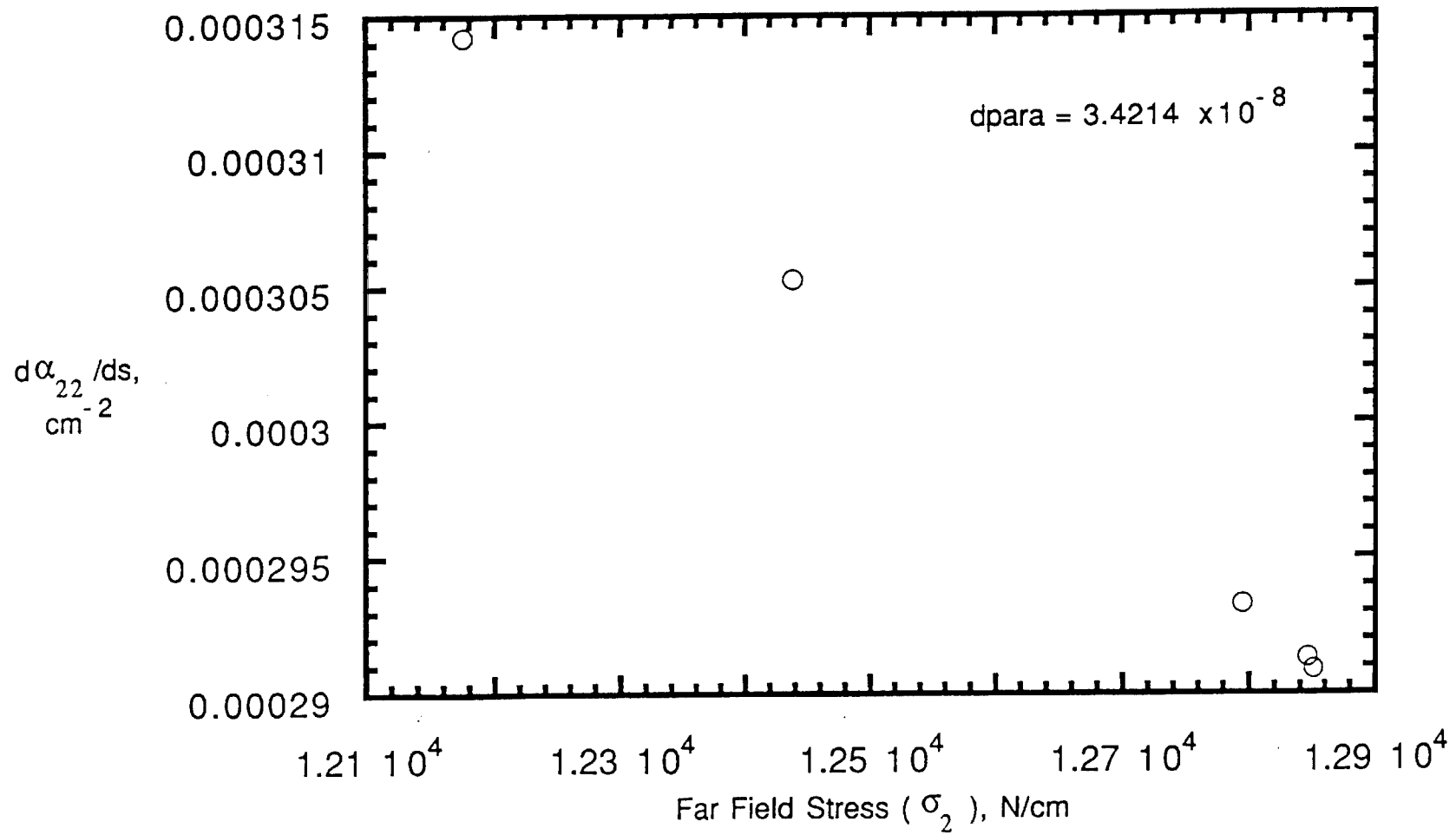

Figure 38 - dα /ds vs the Ninety Degree Ply Far Field Stress for IM7/5260 Composite Laminates

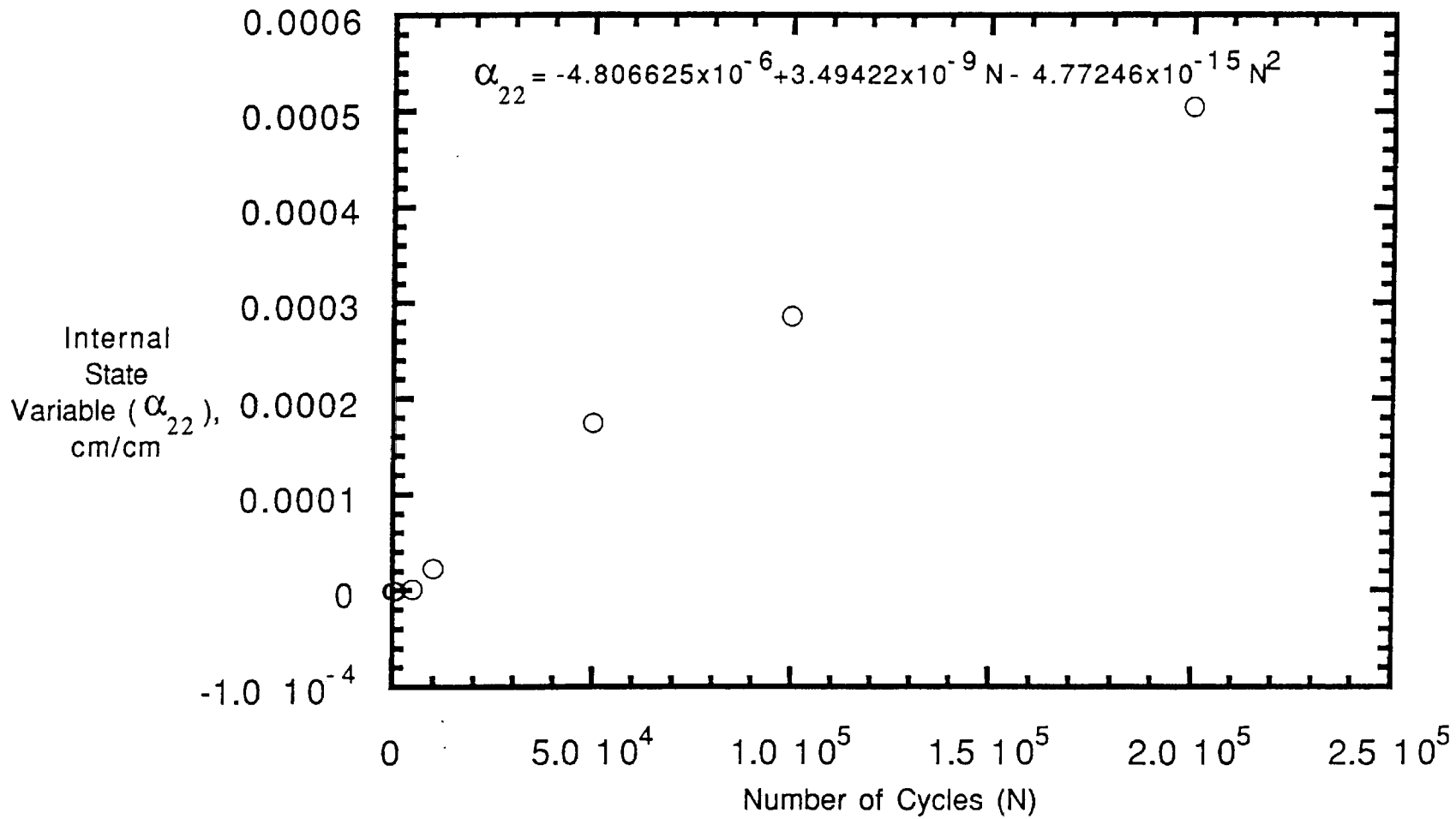

Figure 39 - Internal State Variables As a Function of Cycles for IM7/5260 Composite Laminates

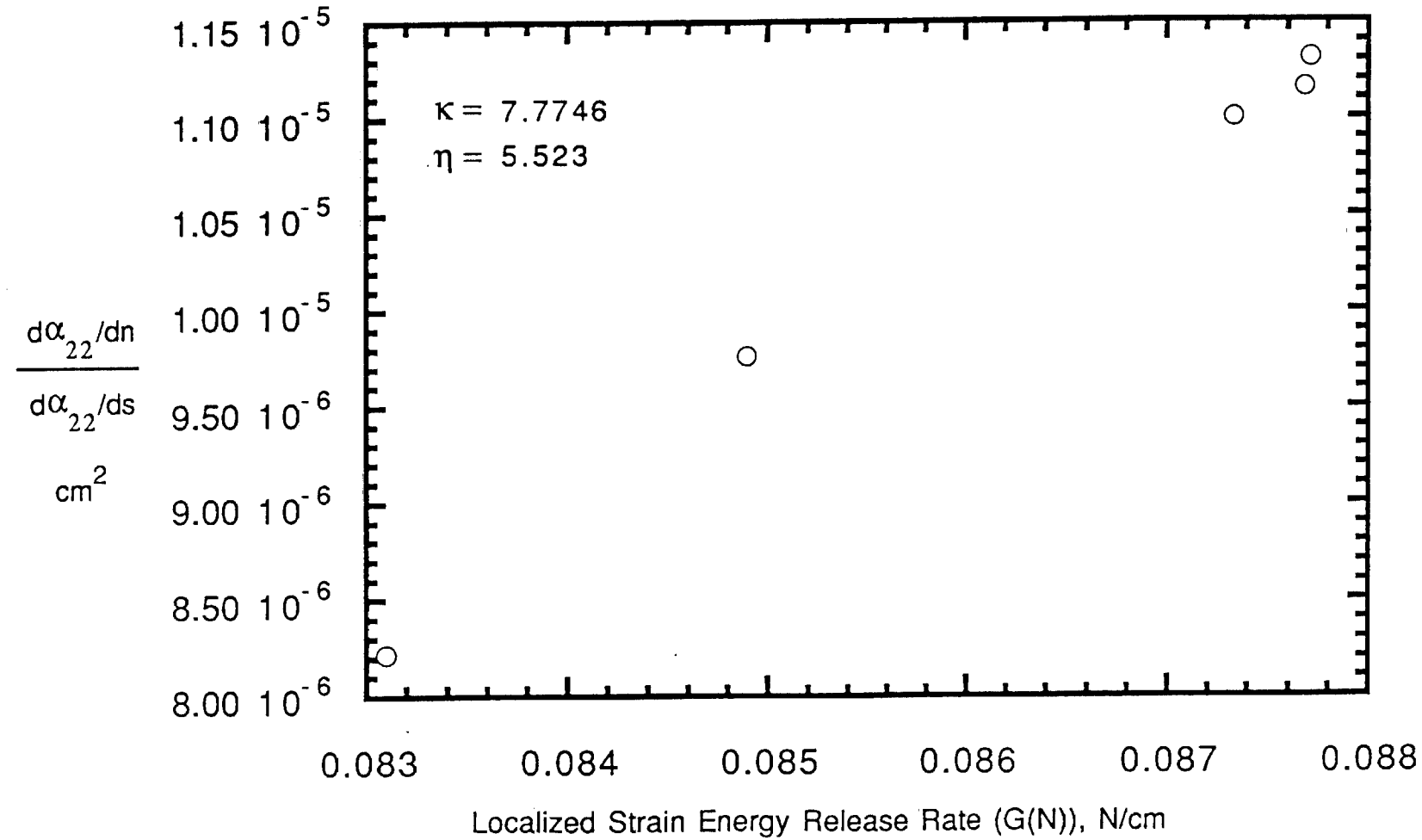

Figure 40 - $\Delta\alpha_{22}$ (N)/ $\Delta\alpha_{22}$ (s) vs the Strain Energy Release Rate

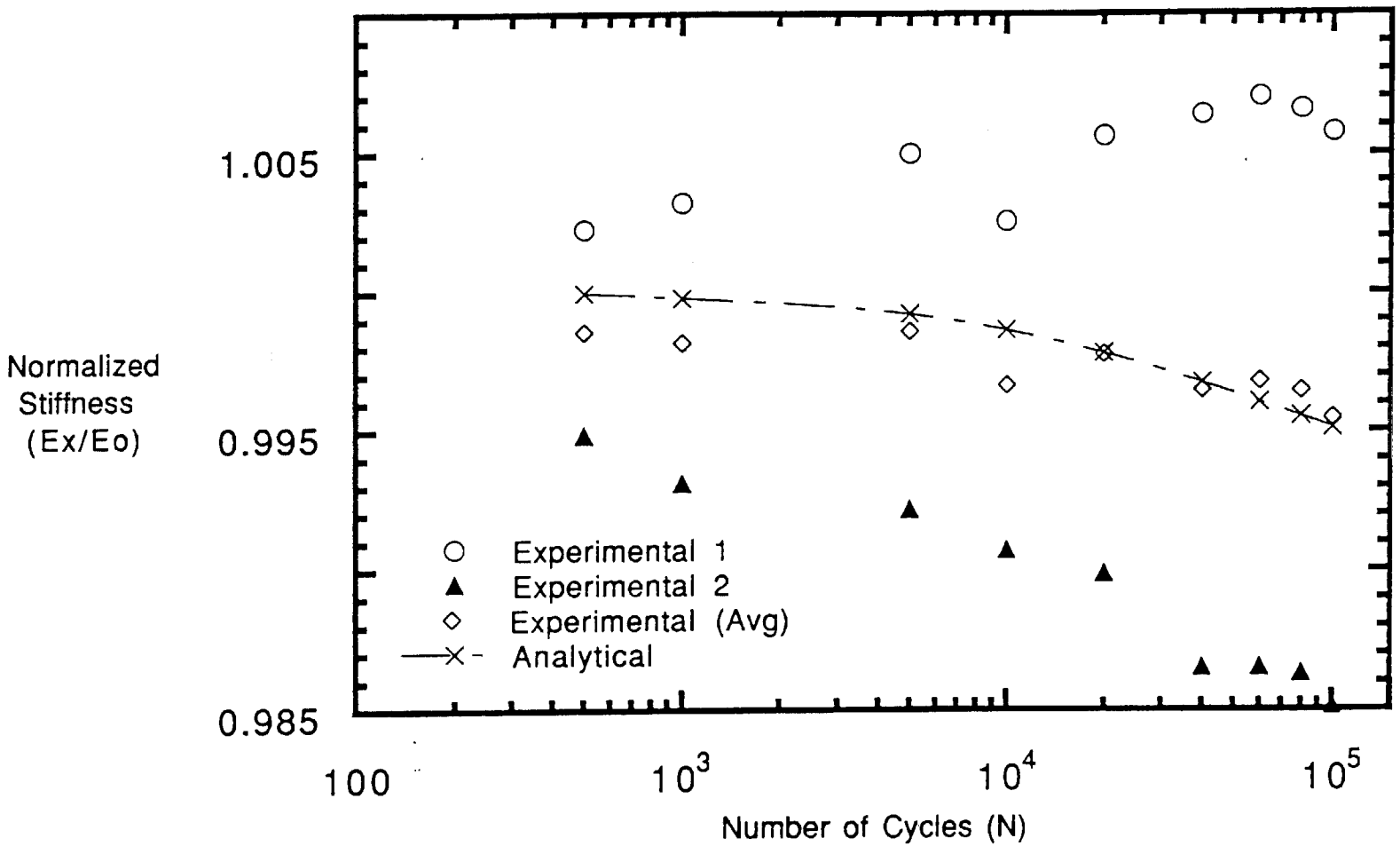

Figure 41 - Comparison of Experimental and Analytical Normalized Stiffness for the $[0/90/0]_s$ IM7/5260 Composite Laminates

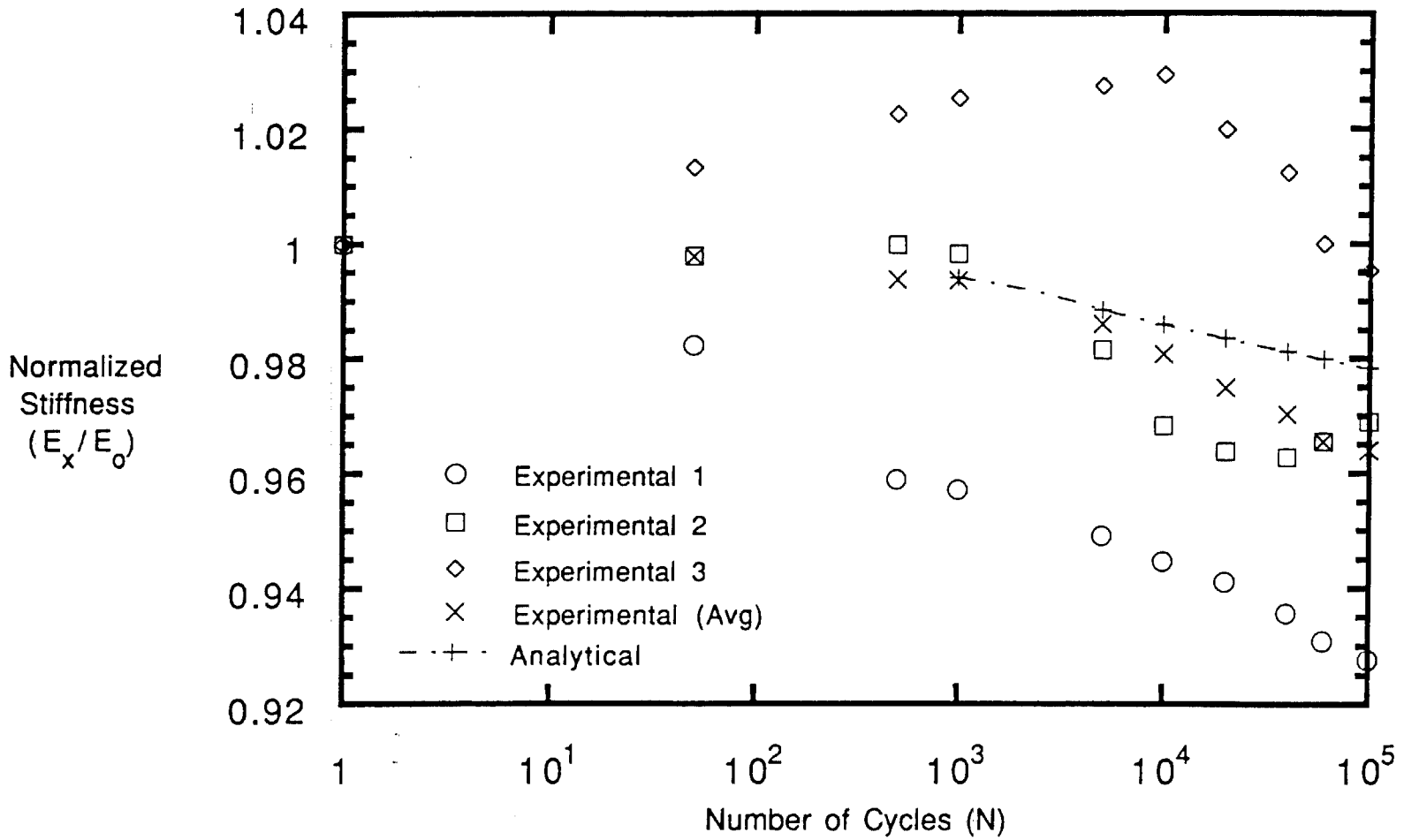

Figure 42 - Comparison of Experimental and Analytical Normalized Stiffness for $[0/90_2/0]_s$ IM7/5260 Composite Laminates

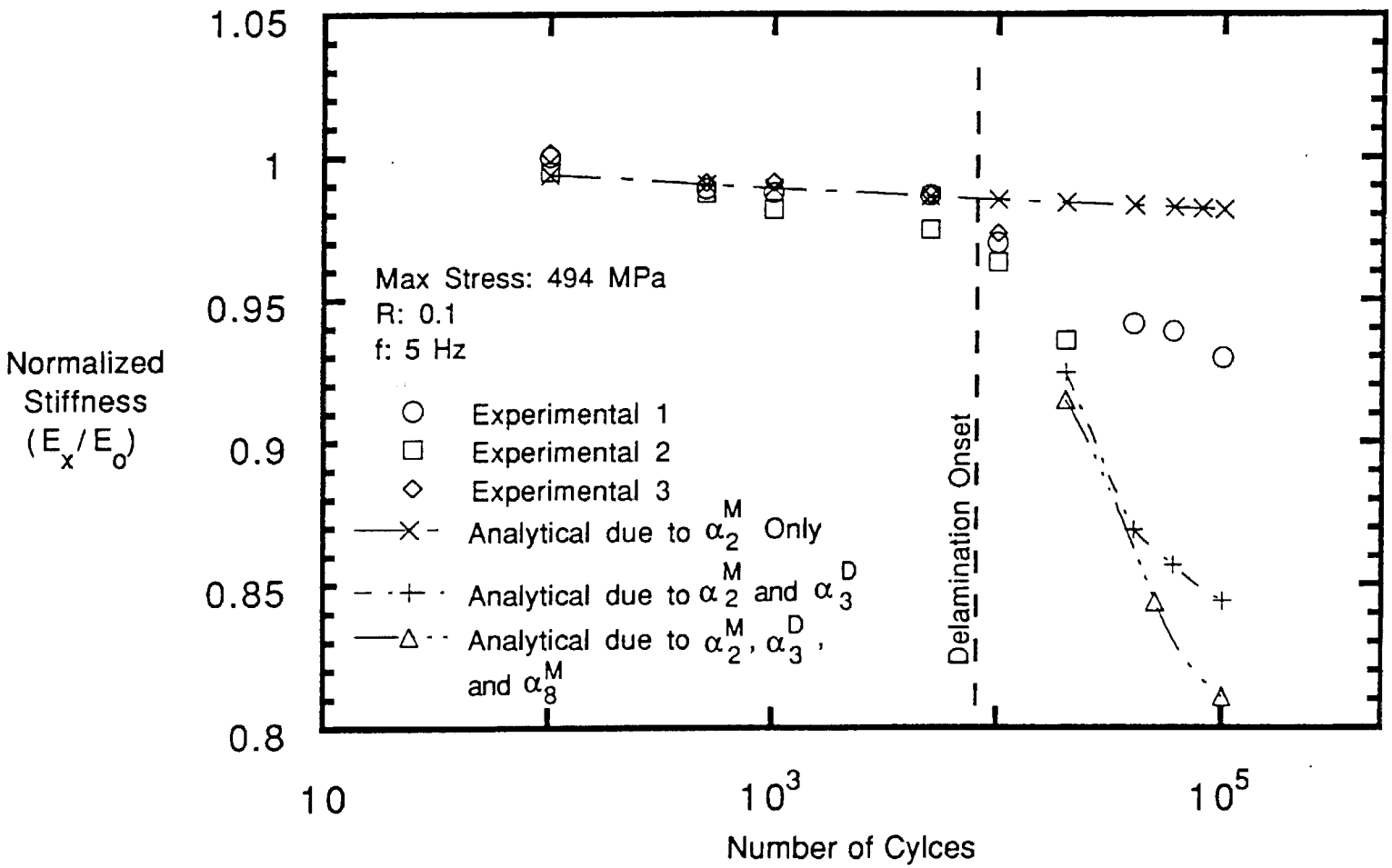

Figure 43 - Experimental and Analytical Stiffness Loss of a $[0/45/-45/90]_s$ IM7/5260 2.54 cm Wide Laminated Composite

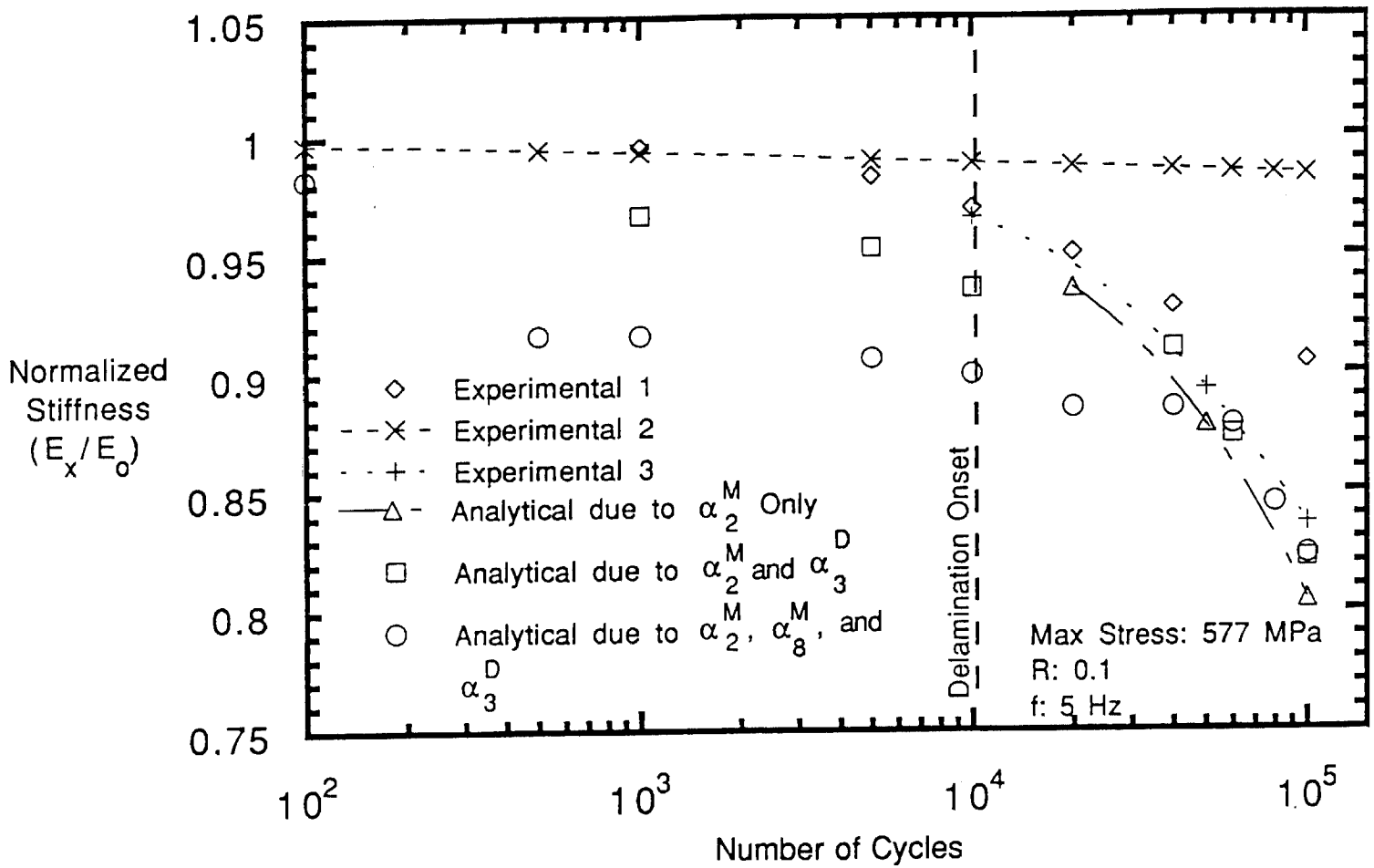

Figure 44 - Experimental and Analytical Stiffness Loss of a $[90/-45/45/0]_s$ IM7/5260 2.54 cm Wide Laminated Composite

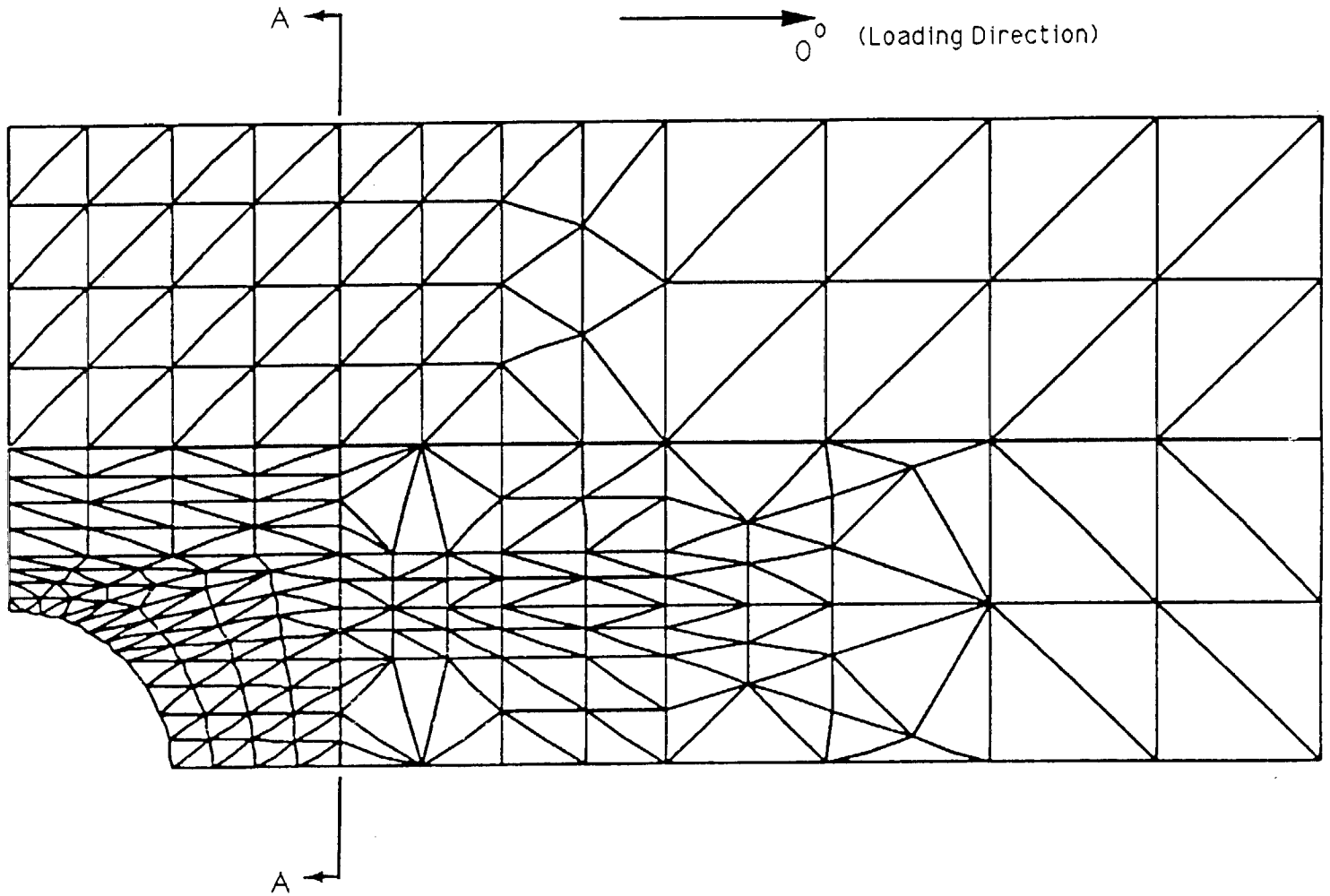

Figure 45 - Finite Element Mesh Used In Analysis

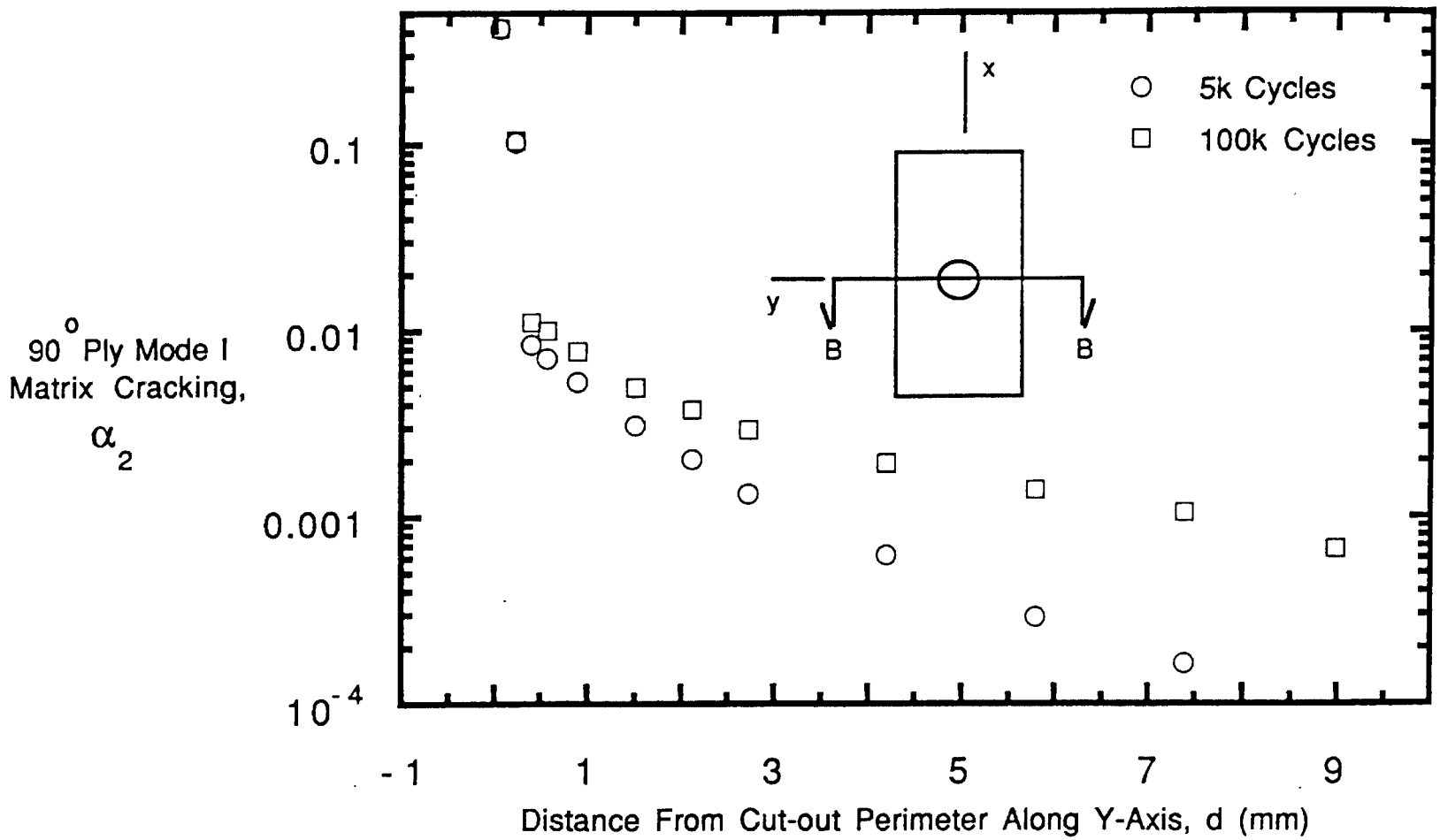

Figure 46 - Analytical Prediction of 90 Degree Ply Damage Measured Along Section BB

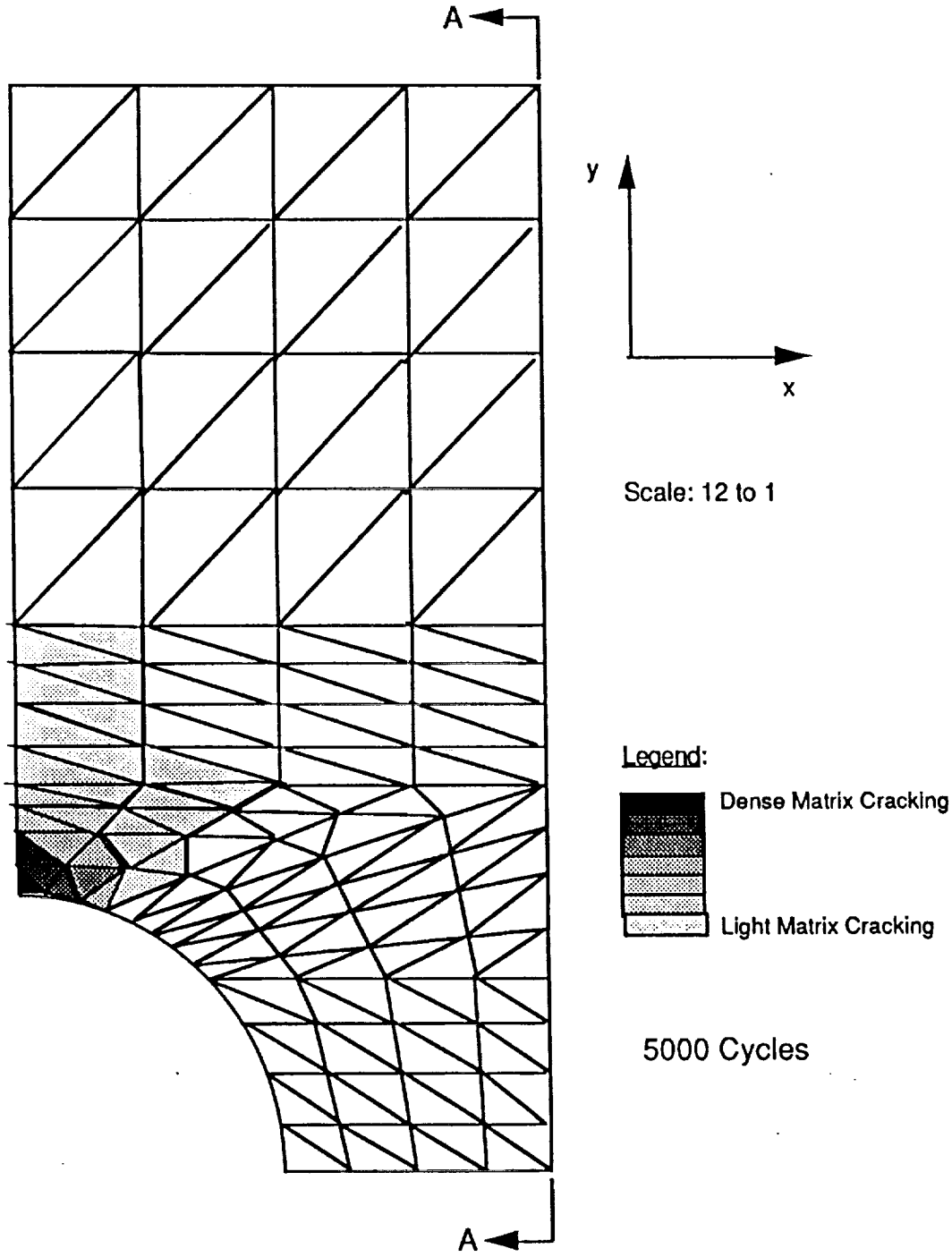

Figure 47 - Illustration of the Predicted Mode I Matrix Crack at the Circular Cut-out in the 90 Degree Plies of the $[0/45/-45/90]_s$ Composite Laminate

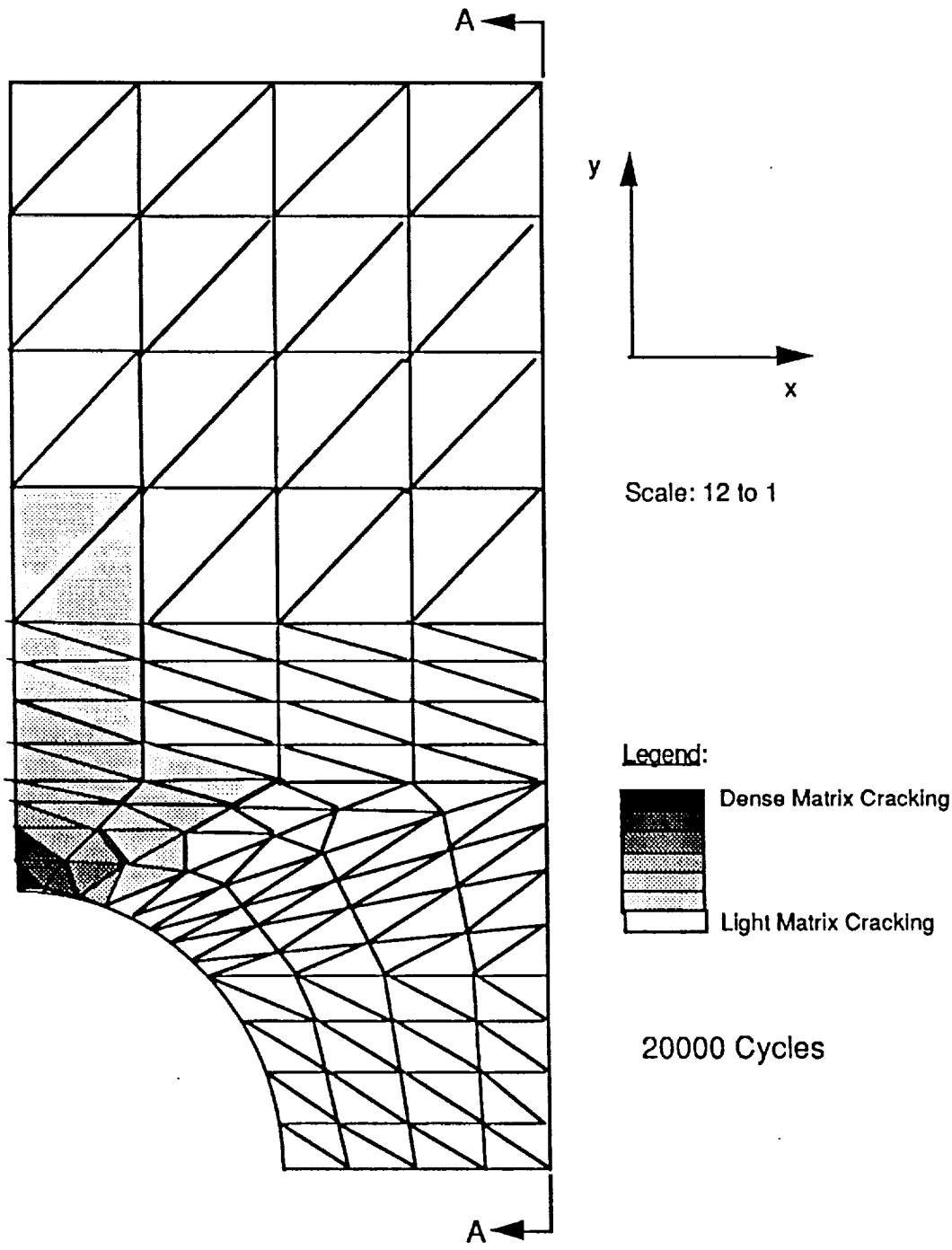

Figure 48 - Illustration of the Predicted Mode I Matrix Crack at the Circular Cut-out in the 90 Degree Plies of the $[0/45/-45/90]_s$ Composite Laminate

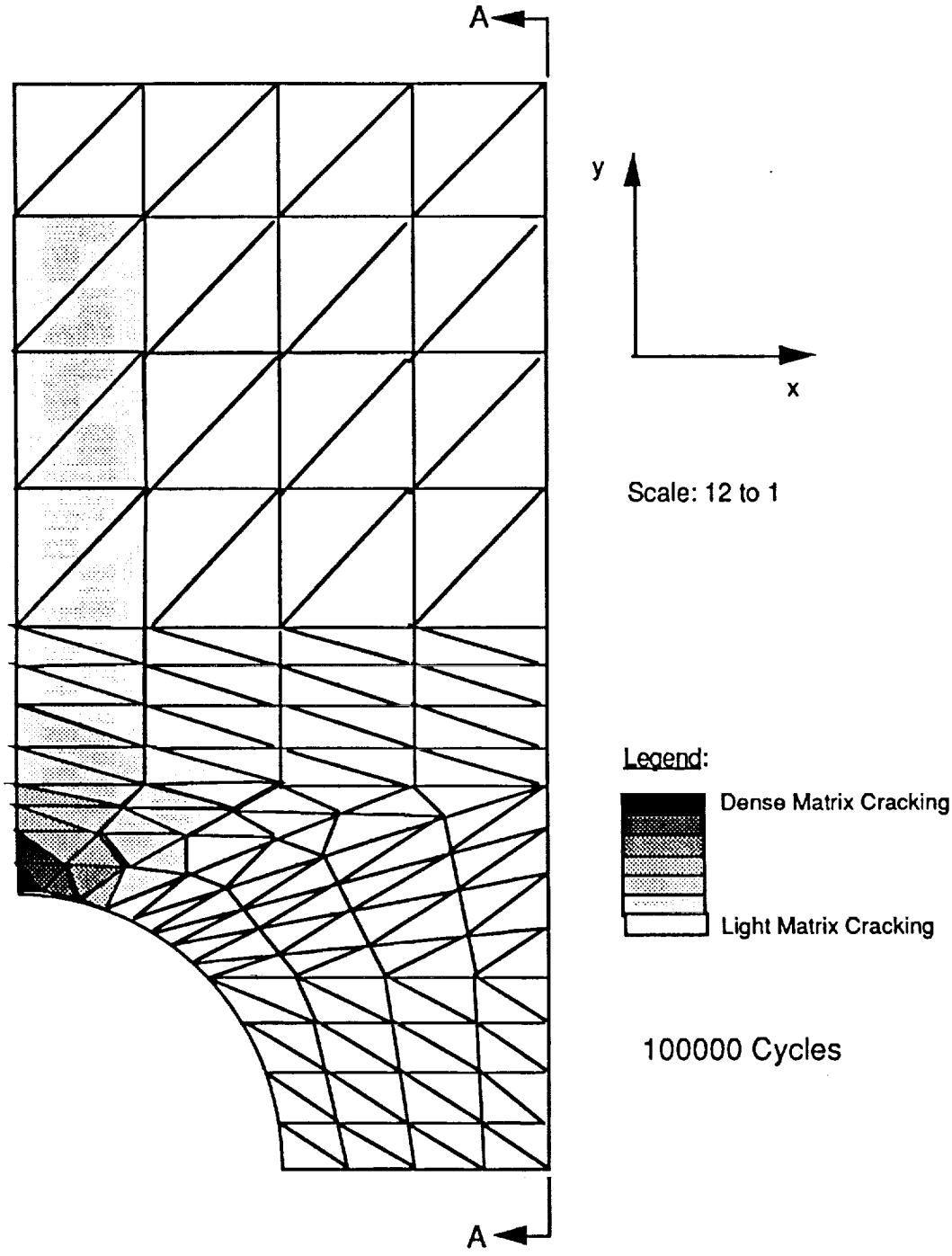

Figure 49 - Illustration of the Predicted Mode I Matrix Crack at the Circular Cut-out in the 90 Degree Plies of the $[0/45/-45/90]_s$ Composite Laminate

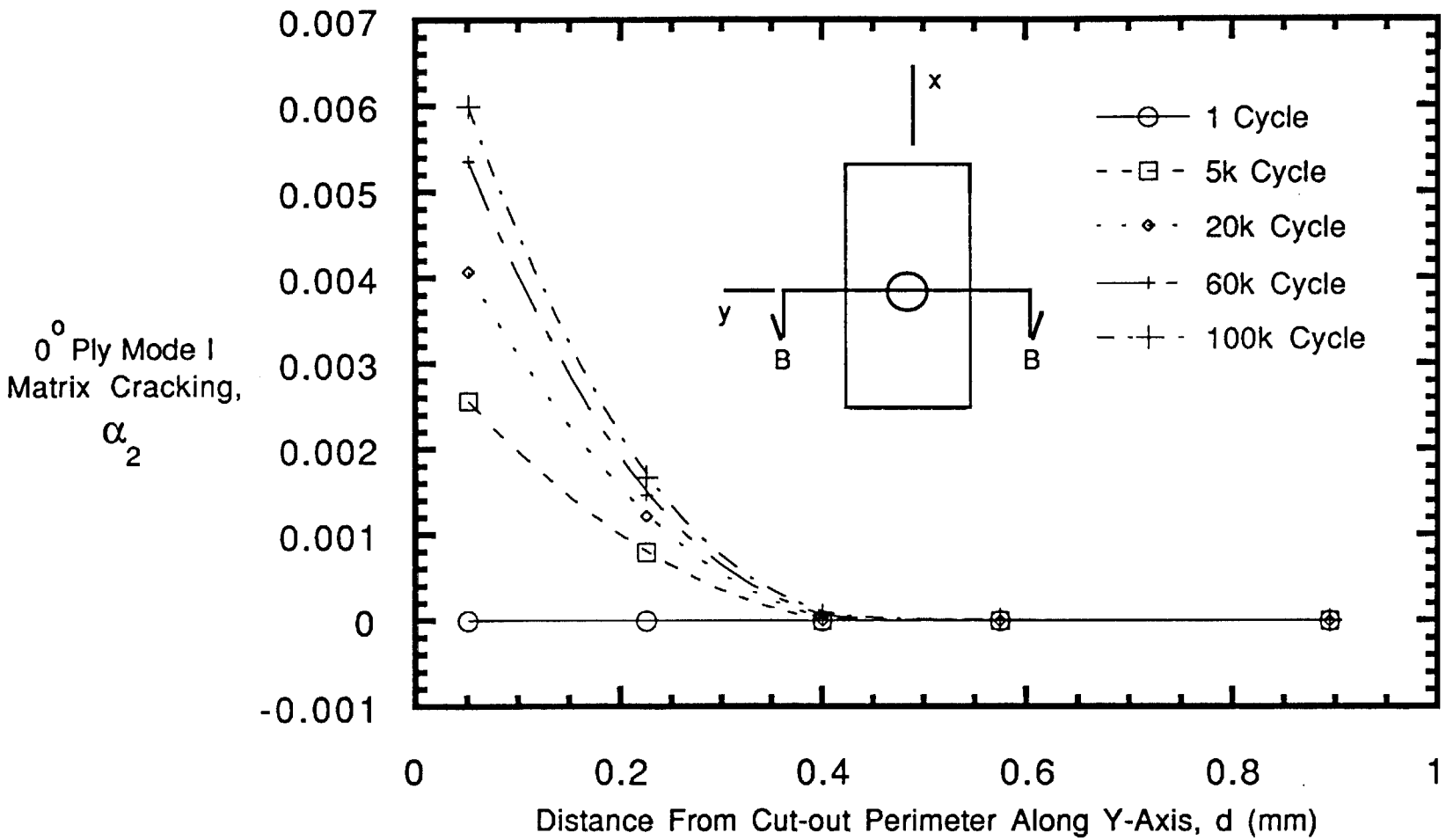

Figure 50 - Analytical Prediction of 0 Degree Ply Damage Measured Along Section BB

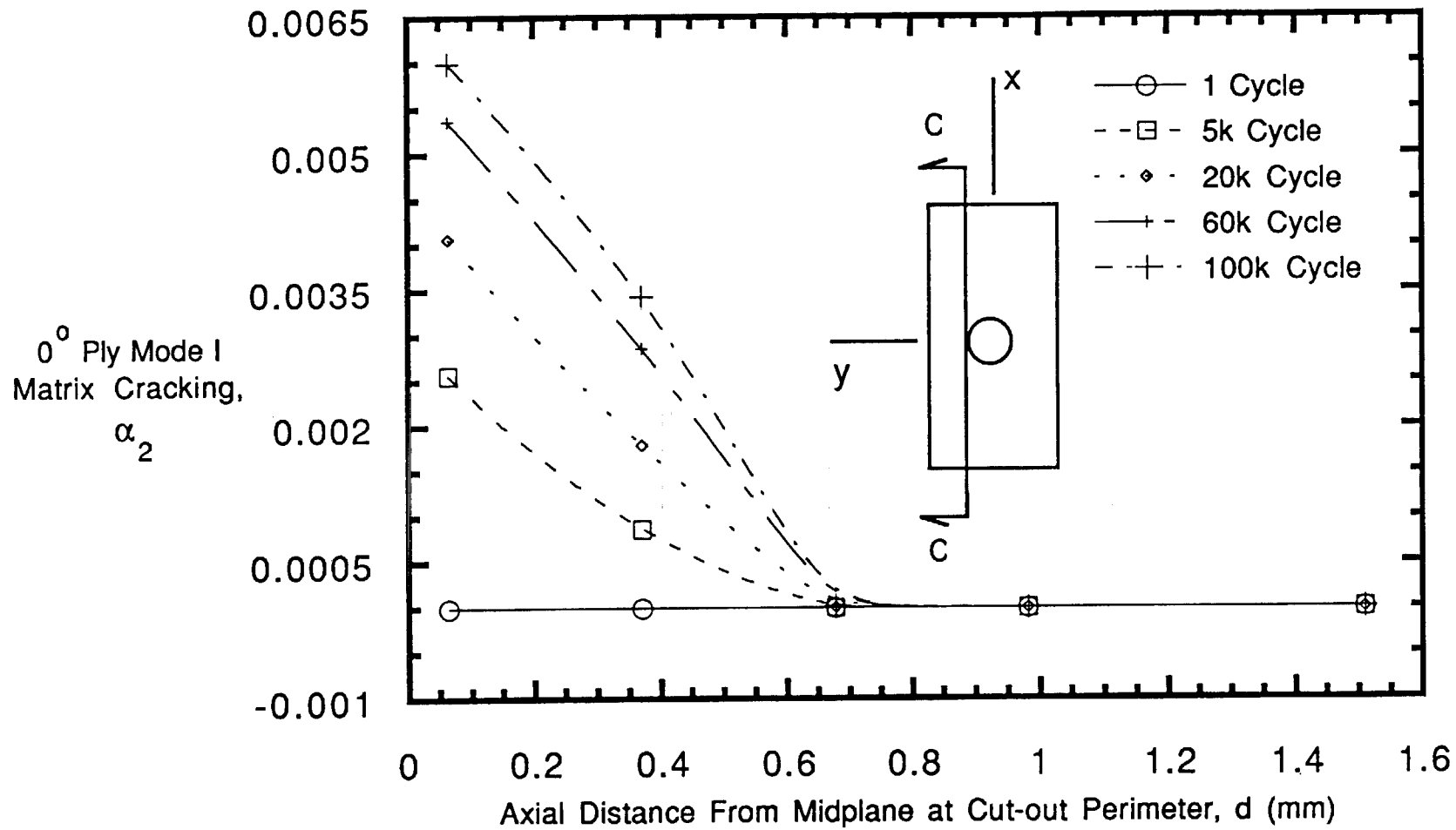

Figure 51 - Analytical Prediction of 0 Degree Ply Damage Measured Along Section CC

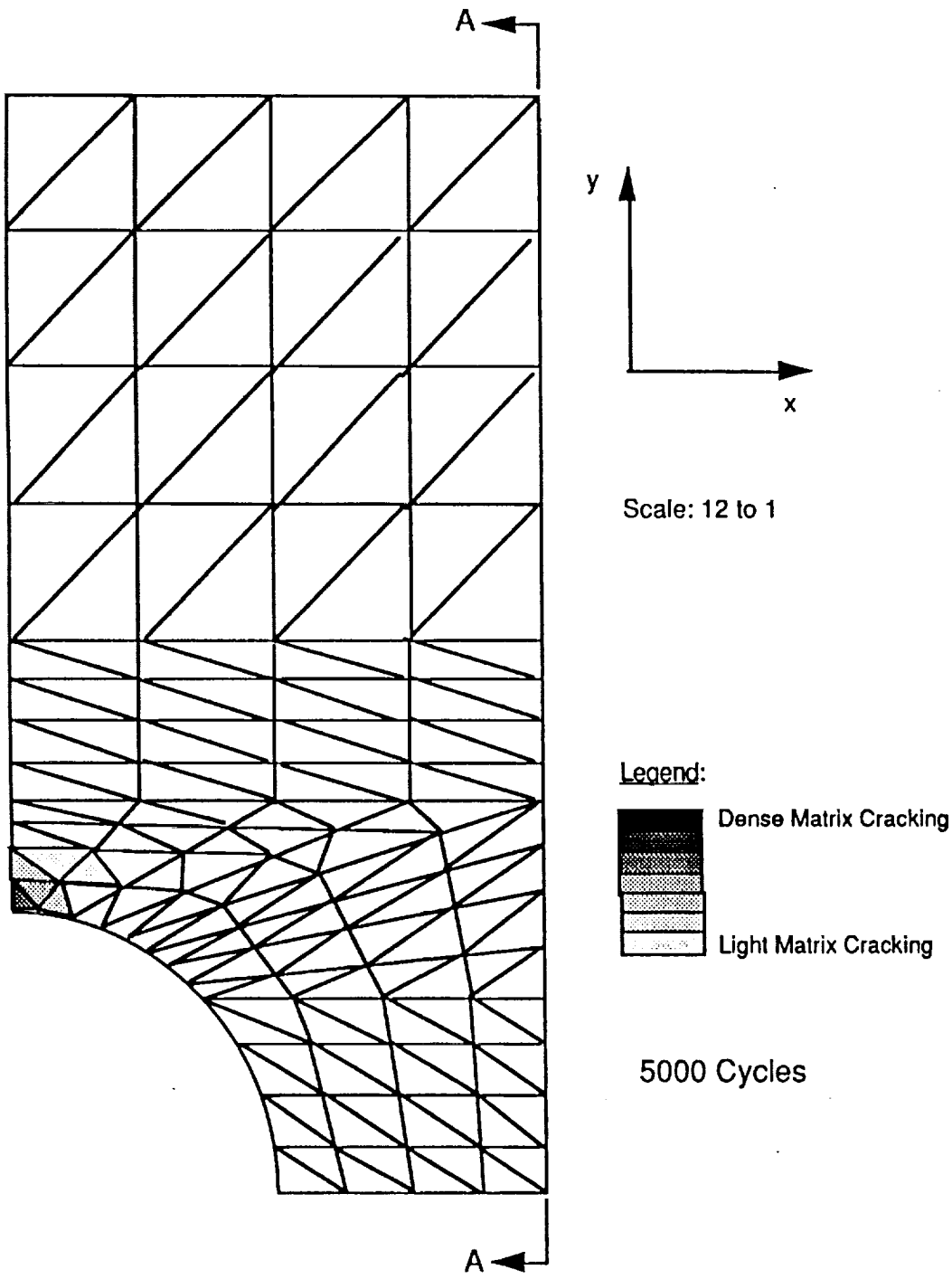

Figure 52 - Illustration of the Predicted Mode I Matrix Crack at the Circular Cut-out in the 0 Degree Plies of the $[0/45/-45/90]_s$ Composite Laminate

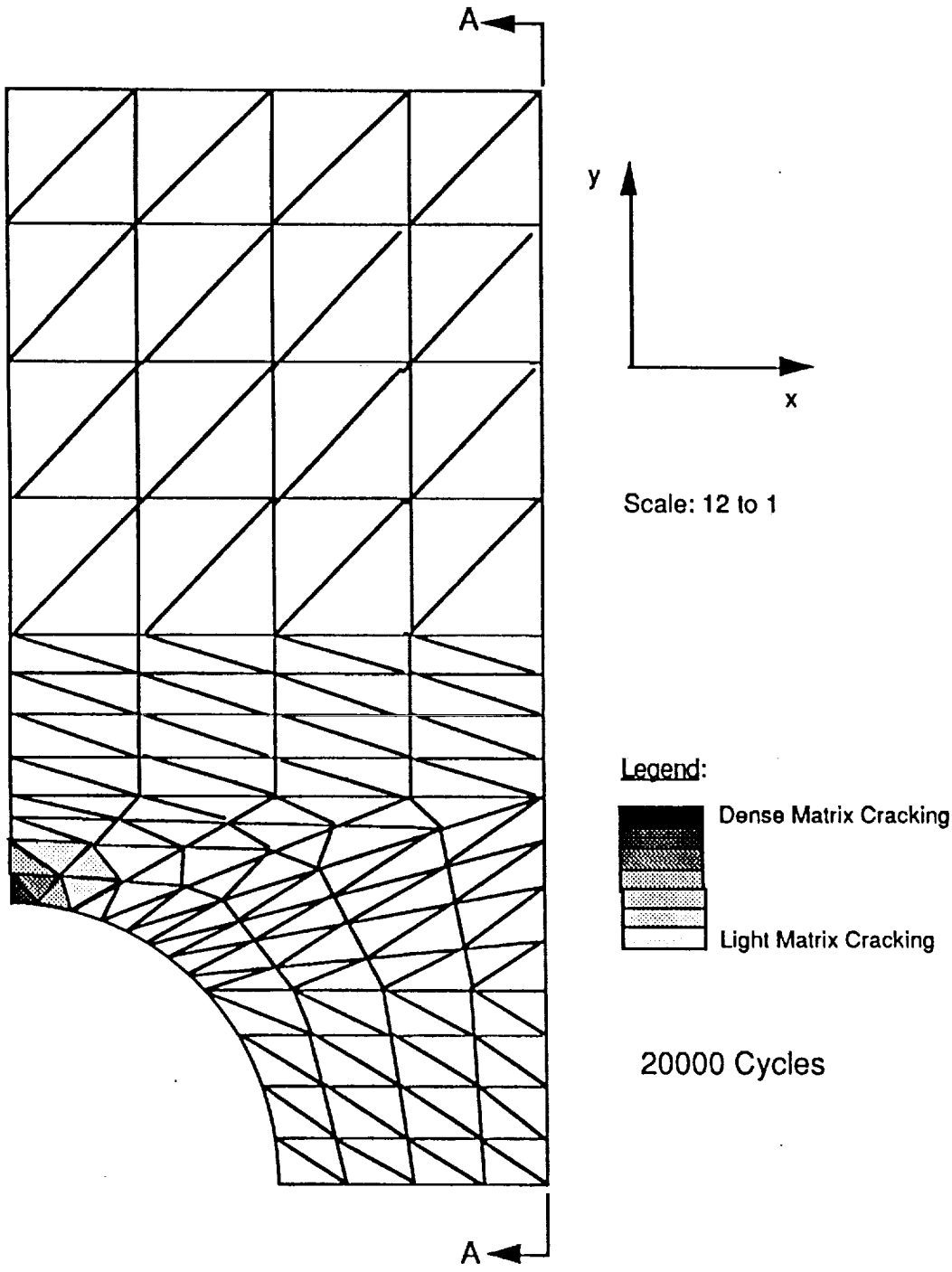

Figure 53 - Illustration of the Predicted Mode I Matrix Crack at the Circular Cut-out in the 0 Degree Plies of the $[0/45/-45/90]_s$ Composite Laminate

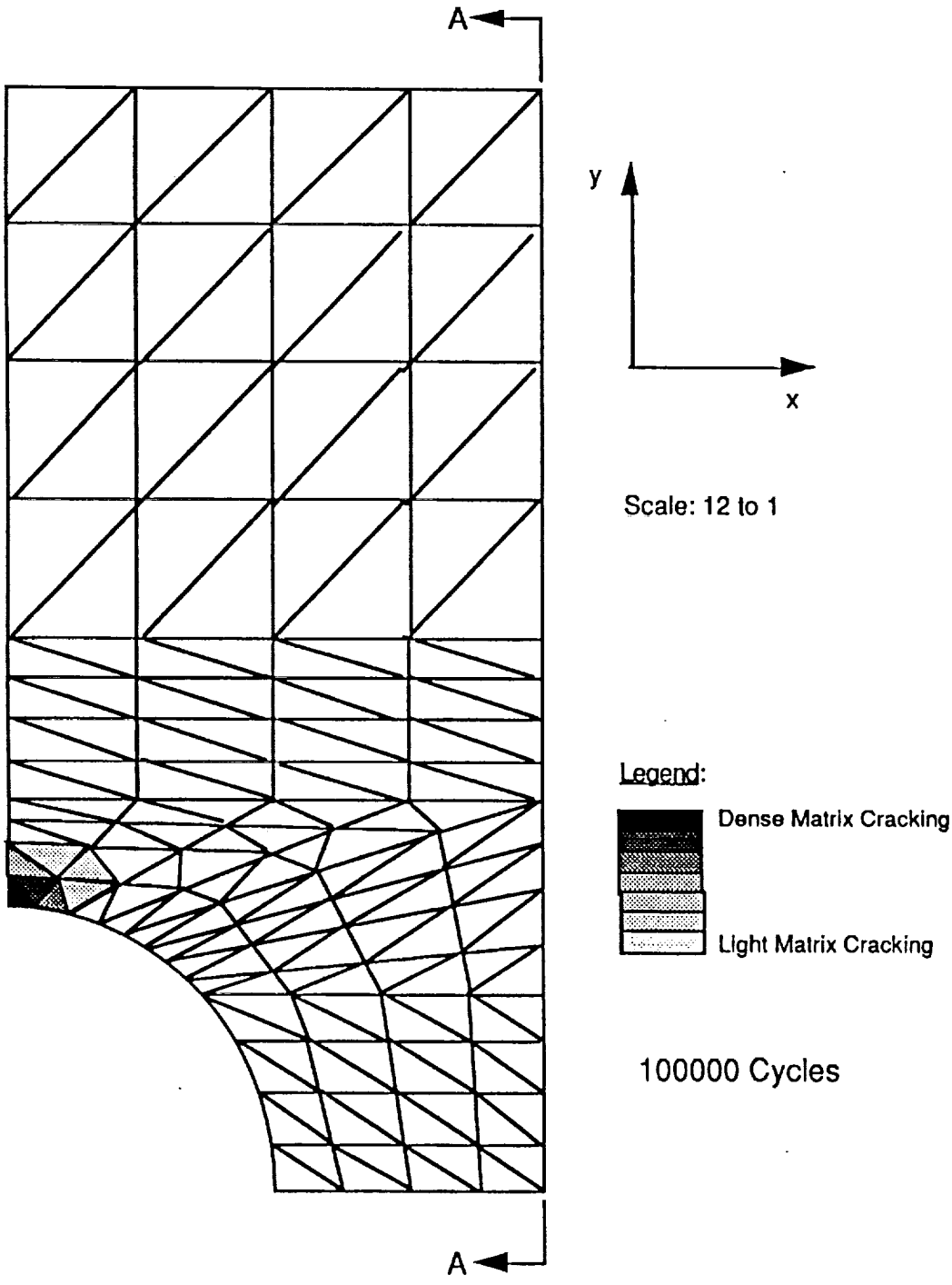

Figure 54 - Illustration of the Predicted Mode I Matrix Crack at the Circular Cut-out in the 0 Degree Plies of the $[0/45/-45/90]_s$ Composite Laminate

C-2

APPENDIX A

EXPERIMENTAL DATA

STATIC TESTS:

Specimen	Layup	Young's Modulus (GPa)	First Ply Failure Load (kN)	First Fiber Failure Load (kN)	Ultimate Strength (MPa)	Shear Modulus (GPa)
A03	[0/90/0]s	100.5	17.9	24.7	1063.5	N/A
A08	[0/90/0]s	106.3	18.0	37.0	1593.1	N/A
A05	[0/90/0]s	102.2	17.8	36.9	1588.8	N/A
I03	$[0/90_2/0]_s$	86.0	17.9	29.6	1105.8	N/A
I08	$[0/90_2/0]_s$	83.7	17.8	34.5	1114.1	N/A
B03	$[45/-45]_{2s}$	20.8	N/A	N/A	N/A	N/A
B04	$[45/-45]_{2s}$	19.9	4.5	8.9	298.2	N/A
B-1	$[45/-45]_{2s}$	23.8	N/A	N/A	N/A	6.2
B-2	$[45/-45]_{2s}$	23.5	N/A	N/A	N/A	6.2
C03	[0/45/-45/90]s	55.0	N/A	21.8	761.6	N/A
C08	[0/45/-45/90]s	51.0	N/A	21.8	819.1	N/A
F03	[90/-45/45/0]s	56.8	N/A	15.6	883.7	N/A
F08	[90/-45/45/0]s	58.7	N/A	15.6	968.5	N/A

FATIGUE TESTS: Crack Density Data From Edge Replicas (Number of Cracks/Ply/Inch)

$[0/90/0]_s$	Damage in 90 Degree Plies Only	Max Stress: 612 MPa	R: 0.1	f: 3Hz (A04,Ab03), 5Hz (Ab01)
$[0/90_2/0]_s$	Damage in 90 Degree Plies Only	Max Stress: 459 MPa	R: 0.1	f: 3Hz
$[45/-45]_{2s}$	Damage in all Plies	Max Stress: 115 MPa	R: 0.1	f: 3Hz (B01), 5Hz (B-3)

Specimen:	A04	Ab01	Ab03	I01	I09	I10	B01	B-3
Layup:	$[0/90/0]_s$	$[0/90/0]_s$	$[0/90/0]_s$	$[0/90_2/0]_s$	$[0/90_2/0]_s$	$[0/90_2/0]_s$	$[45/-45]_{2s}$	$[45/-45]_{2s}$
Cycle No.	Crack Density	Crack Density	Crack Density	Crack Density	Crack Density	Crack Density	Crack Density	Crack Density
0	0	0	0	0	0	0	0	0
100	16.833	22.667	1.000	25.667	6.667	25.833	0	0
500	17.333	40.667	11.667	37.000	21.333	37.167	0	0
1000	20.833	55.000	18.667	43.500	38.333	51.167	0	0
5000	26.000	63.333	26.167	55.833	53.333	59.500	0	0
10000	33.300	66.500	33.167	69.667	63.333	70.833	0.292	0.958
20000	40.833	71.333	37.167	71.833	N/A	73.333	N/A	4.583
40000	44.167	72.167	43.000	75.333	76.667	77.167	N/A	N/A
50000	N/A	N/A	N/A	N/A	N/A	N/A	1.167	10.667
60000	45.833	74.667	44.833	85.000	79.500	80.000	N/A	N/A
80000	50.667	75.167	45.333	88.333	83.333	83.500	N/A	N/A
100000	51.500	76.167	48.333	88.833	84.167	84.167	2.083	22.5

FATIGUE TESTS: Stiffness Loss From Extensometer and LVDT for Laminates Without Notches

Loads are the same as previously mentioned

f: 3Hz (A09, I04, I06), 5Hz (Ab07, B-1, B-2)

Specimen	A09	Ab07	Ab10	I04	I06	B-1	B-2
Layup	[0/90/0]s	[0/90/0]s	[0/90/0]s	$[0/90_2/0]s$	$[0/90_2/0]s$	$[45/-45]_{2s}$	$[45/-45]_{2s}$
Cycle No.	Ex (GPa)	Ex (GPa)	Ex (GPa)	Ex (GPa)	Ex (GPa)	Ex (GPa)	Ex (GPa)
0	91.051	122.812	106.843	74.081	91.858	23.839	23.509
50	N/A	N/A	N/A	72.772	91.665	N/A	N/A
100	91.065	122.098	106.719	72.200	92.195	N/A	N/A
500	N/A	121.884	106.561	71.043	91.837	N/A	N/A
1000	91.086	121.767	106.402	70.912	91.692	N/A	24.363
5000	90.893	121.588	106.168	70.319	90.156	N/A	24.680
10000	90.438	121.485	105.927	69.989	88.943	24.797	24.749
20000	N/A	121.071	106.223	69.727	88.530	N/A	N/A
25000	N/A	N/A	N/A	N/A	N/A	25.121	24.894
40000	89.956	120.975	105.851	69.320	88.440	N/A	N/A
50000	N/A	N/A	106.044	N/A	N/A	24.832	22.916
60000	90.080	121.092	N/A	68.969	88.695	N/A	N/A
75000	N/A	N/A	N/A	N/A	N/A	N/A	N/A
80000	89.825	121.044	N/A	68.776	N/A	N/A	N/A
100000	89.963	121.044	N/A	68.728	89.011	23.295	N/A
200000	89.963	120.906	N/A	N/A	88.344	N/A	N/A
300000	N/A	N/A	N/A	68.597	N/A	N/A	N/A
400000	89.549	N/A	N/A	68.562	87.138	N/A	N/A
500000	N/A	N/A	N/A	N/A	N/A	N/A	N/A

FATIGUE TESTS: Stiffness Loss From Extensometer and LVDT for Laminates Without Notches

Max Stress: 474 MPa R: 0.1 f: 5Hz

Specimen	C04	C07	C09	C05	C10
Layup	[0/45/-45/90]s	[0/45/-45/90]s	[0/45/-45/90]s	[0/45/-45/90]s	[0/45/-45/90]s
Cycle No.	Ex (GPa)	Ex (GPa)	Ex (GPa)	Ex (GPa)	Ex (GPa)
0	61.025	56.009	55.285	79.173	55.120
50	60.680	56.023	54.403	66.930	N/A
100	60.825	56.133	54.231	67.164	55.347
500	60.370	55.554	53.597	65.627	55.120
1000	60.026	55.554	53.411	62.368	55.754
5000	59.578	55.313			54.403
10000	58.875	54.548			53.473
20000	57.187				N/A
40000					51.896
60000					51.751
80000					51.868
100000					51.241
500000					49.711

FATIGUE TESTS: Stiffness Loss From Extensometer and LVDT for Laminates Without Notches

Max Stress: 553 MPa R: 0.1 f: 5 Hz

Specimen	F01	F04	F10
Layup	[90/-45/45/0]s	[90/-45/45/0]s	[90/-45/45/0]s
Cycle No.	Ex (GPa)	Ex (GPa)	Ex (GPa)
0	55.382	61.025	55.155
50	N/A	N/A	N/A
100	N/A	59.991	N/A
500	N/A	55.961	N/A
1000	53.439	55.940	54.817
5000	52.674	55.341	54.128
10000	51.723	54.927	53.384
20000	N/A	54.052	52.336
40000	50.311	54.038	51.083
60000	48.292	53.604	N/A
80000	N/A	51.585	51.386
100000	45.405	50.256	49.815
500000	N/A	41.788	46.184

FATIGUE TESTS: Stiffness Loss From Extensometer and LVDT for Laminates With Central Circular Cut-Outs

Specimen:	D04	G05	E03	E04	H02
Max Stress:	355 MPa	415 MPa	414 MPa	414 MPa	414 MPa

Specimen	D04	G05	E03	E04	H02
Layup	[0/45/-45/90]s	[90/-45/45/0]s	[0/45/-45/90]s	[0/45/-45/90]s	[90/-45/45/0]s
Cycle No.	Ex (GPa)	Ex (GPa)	Ex (GPa)	Ex (GPa)	Ex (GPa)
0	60.747	61.080	58.737	57.773	66.599
50	N/A	N/A	N/A	N/A	N/A
100	N/A	N/A	58.841	57.635	65.965
500	N/A	60.722	58.703	57.566	65.703
1000	59.667	60.687	58.600	57.428	65.496
5000	59.413	60.102	58.289	57.153	65.117
10000	59.220	59.716	58.117	56.774	64.959
20000	58.999	59.289	57.394	56.291	64.711
40000	58.627	58.958	56.601	55.706	64.277
60000	58.338	58.365	56.119	55.217	64.153
80000	58.062	55.926	55.602	54.714	63.919
100000	57.649		55.189	54.383	63.739
500000			50.952		62.265

FATIGUE TESTS: Strength Measurements of Laminates Without Notches

Max Stress: 474 MPa R: 0.1 f: 5Hz

Specimen	C09	C05	C07	C02	C04	C10
Layup	[0/45/-45/90]s	[0/45/-45/90]s	[0/45/-45/90]s	[0/45/-45/90]s	[0/45/-45/90]s	[0/45/-45/90]s
Cycle No.	Su MPa	Su MPa	Su MPa	Su MPa	Su MPa	Su MPa
1000	813.316	751.906				
10000			856.007	793.845		
20000					832.043	
500000						764.638

FATIGUE TESTS: Strength Measurements of Laminates Without Notches

Max Stress: 553 MPa R: 0.1 f: 5Hz

Specimen	F02	F01	F07	F04	F05
Layup	[90/-45/45/0]s	[90/-45/45/0]s	[90/-45/45/0]s	[90/-45/45/0]s	[90/-45/45/0]s
Cycle No.	Su MPa	Su MPa	Su MPa	Su MPa	Su MPa
1000	973.736				
100000		768.387	795.947		
500000				727.494	
1000000					658.291

FATIGUE TESTS: Strength Measurements of Laminates With Central Circular Cut-Outs

Max Stress: 355 MPa R: 0.1 f: 5Hz

Specimen	D09	D04	D08
Layup	[0/45/-45/90]s	[0/45/-45/90]s	[0/45/-45/90]s
Cycle No.	Su MPa	Su MPa	Su MPa
50000	494.881		
100000		454.885	
500000			527.981

FATIGUE TESTS: Strength Measurements of Laminates With Central Circular Cut-Outs

Max Stress: 415 MPa R: 0.1 f: 5Hz

Specimen	G03	G07	G10	G06	G04
Layup	[90/-45/45/0]s	[90/-45/45/0]s	[90/-45/45/0]s	[90/-45/45/0]s	[90/-45/45/0]s
Cycle No.	Su MPa	Su MPa	Su MPa	Su MPa	Su MPa
1000	526.637	496.376			
5000			532.321		
15000				574.564	
30000					537.868

FATIGUE TESTS: Strength Measurements of Laminates With Central Circular Cut-Outs

Max Stress: 414 MPa R: 0.1 f: 5Hz

Specimen	H05	H03	H01	H02
Layup	[90/-45/45/0]s	[90/-45/45/0]s	[90/-45/45/0]s	[90/-45/45/0]s
Cycle No.	Su MPa	Su MPa	Su MPa	Su MPa
50000	713.735			
100000		697.778		
500000			774.422	830.307

FATIGUE TESTS: Strength Measurements of Laminates With Central Circular Cut-Outs

Max Stress: 414 MPa R: 0.1 f: 5Hz

Specimen	E02	E04	E01	E03
Layup	[0/45/-45/90]s	[0/45/-45/90]s	[0/45/-45/90]s	[0/45/-45/90]s
Cycle No.	Su MPa	Su MPa	Su MPa	Su MPa
50000	710.400			
100000		715.961		
500000			726.571	757.473

APPENDIX B

GROWTH LAW PARAMETER CALCULATIONS

1. Calculate crack density (ρ) using 90 degree matrix cracking data from x-rays. The 90 degree matrix cracking data from x-rays was taken over 3 inches (7.62 cm) of the specimen's length.

Definition: 100% crack is a 90 degree matrix crack that traverses the entire width of the specimen.

Formulas:
- Total Cracks = (No. of 100% cracks) + (3/4)(No. of 75% cracks) + (1/2)(No. of 50% cracks) + (1/4)(N0. of 25% cracks)
- ρ = No. of cracks/ply/inch
- s = (ρ)(ply thickness)(specimen width)(2 crack faces)

Specimen : Ab02

Layup : [0/90/0]s

Cycle	100% Cracks	75% Cracks	50% Cracks	25% Cracks	Total Cracks	Crack Density, ρ	Crack Surface Area, s English	Crack Surface Area, s SI
500	0	0	0	0	0	0	0	0
1000	0	0	0	0	0	0	0	0
5000	0	0	0	5.5	1.375	0.2292	0.0028	0.0181
10000	0	0	0	30.5	7.625	1.2708	0.0153	0.0988
50000	0	6	25	114	45.500	7.5833	0.0910	0.5874
100000	11	13	48	116.5	73.875	12.3125	0.1478	0.9540

2. Calculate α_{22}^{M} (N) via formulas 12 and 13 and the static damage dependent constitutive code SLAMALPHA22.

Note: α_{22}^{M} (N) is the same in English units as it is in SI units.

Cycle	α_{22}^{M}
500	0
1000	0.00002335
5000	1.6796e-6
10000	0.00002335
50000	0.00017483
100000	0.00028645

3. Plot α_{22}^{M} vs. crack surface area to obtain a second order polynomial $\alpha_{22}^{M}(s)$.

$$\text{English: } \alpha_{22}^{M} = c+0.001877(s)+0.0005098(s)^2$$

$$\text{SI: } a_{22}^{M} = c+0.0002909(s)+1.224915 \times 10^{-5}(s)^2$$

4. Take the derivative of $\alpha_{22}^{M}(s)$ with respect to s to get $d\alpha_{22}^{M}/ds$.

$$\text{English Units: } \frac{d\alpha_{22}^{M}}{ds} = 0.001877+0.0010196(s)$$

$$\text{SI Units } \frac{d\alpha_{22}^{M}}{ds} = 0.0002909+2.44983 \times 10^{-5}(s)$$

5. Plot a(M,22) vs the number of cycles, N.

$$\alpha_{22}^{M}(N) = c+3.49422 \times 10^{-9}(N)-4.77246 \times 10^{-15}(N)$$

6. Take the derivative of $\alpha_{22}^{M}(N)$ with respect to N to get $d\alpha_{22}^{M}/dN$

$$\frac{d\alpha_{22}^{M}}{dN} = 3.49422 \times 10^{-9}-9.54492 \times 10^{-15}(N)$$

7. Plot $d\alpha_{22}^{M}/ds$ vs far field stress (σ) to get the parameter **DPARA**.

English Units:

Cycle	$d\alpha/ds$ (in/in^3)	σ (lb/in)
500	0.0018770	7334.9
1000	0.0018770	7334.9
5000	0.0018798	7332.7
10000	0.0018925	7303.5
50000	0.0019698	7099.7
100000	0.0020276	6949.5

SI Units:

Cycle	$d\alpha/ds$ (cm/cm^3)	σ (kN/cm)
5000	0.00029133	12.847
10000	0.00029331	12.796
50000	0.00030528	12.438
100000	0.00031425	12.175

English Units: DPARA = 3.8686×10^{-7}

SI Units: DPARA = 3.4214×10^{-8}

8. Plot $\frac{d\alpha/dN}{d\alpha/ds}$ vs strain energy release rate (G) to get the other parameters, κ and η where G = (ply thickness)(σ)($d\alpha/ds$).

English Units:

Cycle	$\frac{d\alpha/dN}{d\alpha/ds}$	G
1000	1.7532e-6	0.087711
5000	1.7293e-6	0.087684
10000	1.7054e-6	0.087335
50000	1.5138e-6	0.084898
100000	1.2743e-6	0.083102

SI Units:

Cycle	$\frac{d\alpha/dN}{d\alpha/ds}$	G
1000	1.1311e-5	0.056973
5000	1.1157e-5	0.057038
10000	1.1002e-5	0.057197
50000	9.7662e-6	0.057870
100000	8.2213e-6	0.058310

English Units: $\kappa = 1.2055$, $\eta = 5.5231$

SI Units: $\kappa = 7.7746$, $\eta = 5.5231$

for $d\alpha = \frac{d\alpha}{ds} \kappa G^{\eta} dN$

APPENDIX C
MODE I DELAMINATION INTERNAL STATE VARIABLE CALCULATIONS

$$\frac{\partial \alpha_3^D}{\partial \varepsilon_x} = \frac{n}{2} \frac{E_{x_o} - E^*}{Q_{15}} \frac{S_D}{S}$$

n = No. of plies in laminate

S_D/S = ratio of delamination area to total area

E_{xo} = Young's Modulus of undamaged laminate

$$E^* = \frac{1}{t} \sum_{i=1}^{d+1} E_i t_i$$

1. Calculate the delamination variables for a $[0/45/-45/90]_S$ laminate.

Delamination exists primarily between the 90 and -45 degree plies, therefore there are two delamination sites and 3 sublaminates where

t_1 = 0.018" (0.0457 cm)

t_2 = 0.012" (0.0305 cm)

t_3 = 0.018" (0.0457 cm)

Furthermore, t = (8 plies)(0.006") = 0.048" (0.1219 cm)

Concerning Q_{15}, for two delamination sites and three sublaminates,

$$Q_{15} = \frac{1}{2}(Q_{11}^A + Q_{11}^B)$$

where Q_{11}^A and Q_{11}^B are the transformed stiffnesses of the sublaminates formed by the delaminations.

Since the laminate is symmetrical,

$$Q_{11}^{A} = Q_{11}^{45^o/-45^o/0^o} = \frac{E_{11}^{45^o/-45^o/0^o}}{1-\nu_{12}\nu_{21}}$$

$$= \frac{E_{11}^{45^o/-45^o/0^o}}{0.91}$$

$$= 4610 \text{ Ksi} \quad (31.763 \text{ MPa})$$

$$Q_{11}^{B} = Q_{11}^{90^o{}_2} = \frac{E_{11}^{90^o{}_2}}{1-\nu_{12}\nu_{21}}$$

$$= \frac{E_{11}^{90^o{}_2}}{0.91}$$

$$= 1343 \text{ Ksi} \quad (9.253 \text{ MPa})$$

[0/45/-45/90]s n/2 = 4, E_{xo} = 8.033 Msi (55.347 GPa)

$$E^* = \frac{1}{0.048"}[(E_{11}^{0^o/45^o/-45^o})(0.018") + (E_{11}^{90^o{}_2})(0.012") + (E_{11}^{-45^o/45/0^o})(0.018")]$$

$$E^* = 3.462 \text{ Msi} \quad (23.853 \text{ GPa})$$

$$\text{Therefore,} \quad \alpha_3^D = 4\frac{(8.033 \text{ Msi} - 3.462 \text{ Msi})}{2.976 \text{ Msi}}\frac{S_D}{S}\varepsilon_x$$

Cycle	S_D/S (%)	ε_x	α_3^D
10000	2.0	0.0086	0.0011
20000	21.0	0.0090	0.0117
40000	40.0	0.0091	0.0224
60000	44.0	0.0092	0.0247
100000	48.0	0.0092	0.0273

2. Calculate the delamination variables for a $[90/-45/45/0]_s$ laminate.

Delamination exists primarily between the 90 and -45 degree plies as well as the 45 and -45 degree plies, therefore there are four delamination sites and 5 sublaminates where

t_1 = 0.006" (0.0457 cm)
t_2 = 0.006" (0.0305 cm)
t_3 = 0.024" (0.0457 cm)
t_4 = 0.006" (0.0457 cm)
t_5 = 0.006" (0.0305 cm)

Furthermore, t = (8 plies)(0.006") = 0.048" (0.1219 cm)

$$\frac{\partial \alpha_{3_1}^D}{\partial \varepsilon_x} = \frac{n}{2} \frac{E_{x_o} - E^*}{Q_{15_1}} \frac{S_D}{S}$$

$$\frac{\partial \alpha_{3_2}^D}{\partial \varepsilon_x} = \frac{n}{2} \frac{E_{x_o} - E^*}{Q_{15_2}} \frac{S_D}{S}$$

Concerning Q_{15}, for four delamination sites and five sublaminates,

$$Q_{15_1} = \frac{1}{2}(Q_{11}^A + Q_{11}^B)$$

$$Q_{15_2} = \frac{1}{2}(Q_{11}^B + Q_{11}^C)$$

where Q_{11}^A and Q_{11}^B are the transformed stiffnesses of the sublaminates formed by the delaminations.

Since the laminate is symmetrical,

$$Q_{11}^A = Q_{11}^{90^o} = \frac{E_{11}^{90^o}}{1 - \nu_{12}\nu_{21}}$$

$$= \frac{E_{11}^{90^o}}{0.91}$$

$$= 1387 \text{ Ksi} \quad (9.556 \text{ MPa})$$

$$Q^{B}_{11} = Q^{45^{o}}_{11} = \frac{E^{45^{o}}_{11}}{1-\nu_{12}\nu_{21}}$$

$$= \frac{E^{45^{o}}_{11}}{0.91}$$

$$= 2057 \text{ Ksi} \quad (14.173 \text{ MPa})$$

$$Q^{C}_{11} = Q^{45^{o}/0^{o}}_{11} = \frac{E^{45^{o}/0^{o}}_{11}}{1-\nu_{12}\nu_{21}}$$

$$= \frac{E^{45^{o}/0^{o}}_{11}}{0.91}$$

$$= 13.351 \text{ Msi} \quad (91.988 \text{ MPa})$$

$\underline{[90/-45/45/0]_{S}}$ $\quad n/2 = 4, \quad E_{xo} = 8.4 \text{ Msi} \ (57.876 \text{ GPa})$

$$E^{*} = \frac{1}{0.048"}[2(E^{90^{o}}_{11})(0.006")+2(E^{45^{o}}_{11})(0.006")+(E^{45^{o}/0^{o}}_{11})(0.024")]$$

$$E^{*} = 6.858 \text{ Msi} \quad (47.252 \text{ GPa})$$

$$\text{Therefore,} \quad \alpha^{D}_{3_1} = 4\frac{(8.400 \text{ Msi}-6.858 \text{ Msi})}{1.722 \text{ Msi}}\frac{S_D}{S}\varepsilon_x$$

$$\text{Therefore,} \quad \alpha^{D}_{3_1} = 4\frac{(8.400 \text{ Msi}-6.858 \text{ Msi})}{1.722 \text{ Msi}}\frac{S_D}{S}\varepsilon_x$$

Cycle	S_D/S (%)	ε_x	$\alpha^{D}_{3_1}$	$\alpha^{D}_{3_2}$
10000	3.13	0.0082	0.0011	0.0002
50000	12.50	0.0089	0.0043	0.0010
100000	20.00	0.0091	0.0068	0.0015

APPENDIX D
MODE II MATRIX CRACKING INTERNAL STATE VARIABLE CALCULATIONS

1. Calculate ρ using matrix cracking data from edge replicas of a $[45/-45]_{2s}$ specimen.

Specimen: B-3
Layup: $[45/-45]_{2s}$
Max Stress: 114 MPa R: 0.1

Specimen: B-2
Layup: $[45/-45]_{2s}$
f: 5Hz

Cycle	No. of Cracks	ρ	Cycle	G_{12} (GPa)
10000	23	0.9583	10000	
15000	64	2.6670	15000	
20000	110	4.5830	20000	
25000	154	6.4160	25000	6.656
50000	256	10.6670	50000	6.594
100000	540	22.500	100000	6.111

2. The relationship between G_{12d}/G_{12o} and ρ is linear, therefore

$$\frac{G_{12d}}{G_{12o}} = 0.9182 \text{ for } \rho_d = 22.5$$

Therefore,

$$\frac{\partial \alpha_8}{\partial \varepsilon_6} = 2[1\text{-}0.9182]\frac{\rho}{22.5}$$

$$\frac{\partial \alpha_8}{\partial \varepsilon_6} = 0.0073\,\rho$$

Furthermore,

$$\alpha_8 = (0.0073\ \rho)\varepsilon_6$$

and

$$\varepsilon_6 = \frac{\sigma_x}{2G_{12}} = \frac{114.836\ \text{MPa}}{2G_{12}}$$

Cycle	G_{12} (GPa)	ε_6	ρ	α_8
25000	0.966	0.0086	6.416	0.000403
50000	0.957	0.0087	10.667	0.000677
100000	0.887	0.0094	22.5	0.001544

APPENDIX E

STIFFNESS LOSS CALCULATIONS DUE TO SHEAR AND DELAMINATION VARIABLES

Stiffness loss due to matrix cracking and delamination:

$$\frac{E_x}{E_o} = 1 - \frac{\Delta E^M}{E_o} - \frac{\Delta E^D}{E_o} - \frac{\Delta E^S}{E_o}$$

where $\frac{\Delta E^D}{E_o}$ is defined by the following equation for any number of delamination sites as

$$\frac{\Delta E_x^D}{E_o} = \frac{1}{TE_o} \sum_{l=1}^{d} [Q_{15}]_l t_l \left\langle \frac{\partial \alpha_{3l}^D}{\partial e_{xx}} \right\rangle$$

which was reduced for two delamination sites as

$$\frac{\Delta E^D}{E_o} = \frac{1}{2}\left(1 - \frac{E^*}{E_{xo}}\left(\frac{S_D}{S}\right)\right)$$

Stiffness loss due to shear is defined as

$$\frac{\Delta E_x^S}{E_o} = \frac{1}{nE_o} \sum_{k=1}^{n} [Q_{11}]_k \left\langle \frac{\partial \alpha_8}{\partial e_6} \right\rangle$$

which for a [45/-45]2s laminate is

$$\frac{\Delta E_x^S}{E_o} = \frac{7}{8E_o}(1.872 \quad \text{Msi}) \left\langle \frac{\partial \alpha_8}{\partial e_6} \right\rangle$$

Stiffness loss for a [0/45/-45/90]s laminate with two delamination sites:

Cycle	S_D/S (%)	$\frac{\Delta E_x^M}{E_o}$	$\frac{\partial \alpha_8^M}{\partial \varepsilon_6}$	\f(ΔE_x\,E_o)
20000	21.0	0.0160	0.0468	0.9147
50000	42.0	0.0175	0.0779	0.8440
100000	48.0	0.0190	0.1643	0.8109

REPORT DOCUMENTATION PAGE

Form Approved
OMB No. 0704-0188

1. AGENCY USE ONLY *(Leave blank)*	2. REPORT DATE	3. REPORT TYPE AND DATES COVERED
	December 1994	Contractor Report

4. TITLE AND SUBTITLE
Experimental Verification of a Progressive Damage Model for Composite Laminates Based on Continuum Damage Mechanics

5. FUNDING NUMBERS
C NAS1-19858
WU 505-63-50-04

6. AUTHOR(S)
Timothy William Coats

7. PERFORMING ORGANIZATION NAME(S) AND ADDRESS(ES)
Old Dominion University
P.O. Box 6369
Norfolk, VA 23508-0369

8. PERFORMING ORGANIZATION REPORT NUMBER

9. SPONSORING / MONITORING AGENCY NAME(S) AND ADDRESS(ES)
National Aeronautics and Space Administration
Langley Research Center
Hampton, VA 23681-0001

10. SPONSORING / MONITORING AGENCY REPORT NUMBER
NASA CR-195020

11. SUPPLEMENTARY NOTES
Langley Technical Monitor: Ivatury S. Raju - Final Report
This report is the edited version of the Masters thesis written by Tim Coats.

12a. DISTRIBUTION / AVAILABILITY STATEMENT
Unclassified - Unlimited

Subject Category 24

12b. DISTRIBUTION CODE

13. ABSTRACT *(Maximum 200 words)*

Progressive failure is a crucial concern when using laminated composites in structural design. Therefore the ability to model damage and predict the life of laminated composites is vital. The purpose of this research was to experimentally verify the application of the continuum damage model, a progressive failure theory utilizing continuum damage mechanics, to a toughened material system. Damage due to tension-tension fatigue was documented for the IM7/5260 composite laminates. Crack density and delamination surface area were used to calculate matrix cracking and delamination internal state variables, respectively, to predict stiffness loss. A damage dependent finite element code qualitatively predicted trends in transverse matrix cracking, axial splits, and local stress-strain distributions for notched quasi-isotropic laminates. The predictions were similar to the experimental data and it was concluded that the continuum damage model provided a good prediction of stiffness loss while qualitatively predicting damage growth in notched laminates.

14. SUBJECT TERMS	15. NUMBER OF PAGES
Composites; Graphit/epoxy; Damage; Matrix cracks; Delamination; Internal state variables	121
	16. PRICE CODE A06

17. SECURITY CLASSIFICATION OF REPORT	18. SECURITY CLASSIFICATION OF THIS PAGE	19. SECURITY CLASSIFICATION OF ABSTRACT	20. LIMITATION OF ABSTRACT
Unclassified	Unclassified		